NASA CONTRACTOR REPORT

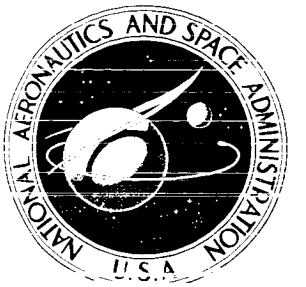

NASA CR-60

NASA CR-60

CRYOGENIC PROPELLANT FEED SYSTEMS FOR ELECTROTHERMAL ENGINES

Prepared under Contract No. NAS 8-2575 *by*
ARTHUR D. LITTLE, INC.
Cambridge, Massachusetts
for

NATIONAL AERONAUTICS AND SPACE ADMINISTRATION • WASHINGTON, D. C. • MAY 1964

CRYOGENIC PROPELLANT FEED SYSTEMS

FOR ELECTROTHERMAL ENGINES

Prepared under Contract NAS 8-2575 by
Arthur D. Little, Inc.
Cambridge, Massachusetts

NATIONAL AERONAUTICS AND SPACE ADMINISTRATION

For sale by the Office of Technical Services, Department of Commerce, Washington, D. C. 20230 -- Price $4. 00

FOREWORD

In anticipation of a flight operational thermal arc-jet engine by the mid-sixties, NASA has pursued a multi-phase program to result in the development and production of suitable propellant feed systems.

In Phase I Arthur D. Little, Inc., as one of four contractors, completed a preliminary investigation of the problems related to the storage, expulsion, metering and control of the propellant feed to these engines. The results of this work carried out under Contract No. NAS 8-1695 for the Marshall Space Flight Center, Huntsville, Alabama was documented in a final report entitled "Investigation of Propellant Feed Systems for Electrothermal Engines", October 1961.

Contract NAS 8-2575, administered by the Lewis Research Center, provides this Summary Report of following and related work in Phase II. Phase II calls for an over-all design study of systems required to support ammonia and hydrogen fed arc-jet thrustors used to transfer a communications satellite from a 500 nautical mile earth orbit to a synchronous equatorial orbit.

Technical administration of the contractors work was under the direction of Mr. Henry Hunczak, Lewis Flight Propulsion Laboratory, Lewis Research Center, National Aeronautics and Space Administration, Cleveland, Ohio.

ACKNOWLEDGEMENTS

This project was carried out as a team effort within Division 500 of Arthur D. Little, Inc. The following technical staff members were major contributors:

A. A. Fowle - Principal Investigator

R. P. Berthiaume

R. W. Breckenridge, Jr.

Mrs. E. M. Drake

H. G. Leney

R. W. Moore, Jr.

A. H. Rawdon, Jr.

TABLE OF CONTENTS

TABLE OF CONTENTS (2)

TABLE OF CONTENTS (3)

TABLE OF CONTENTS (4)

LIST OF FIGURES

LIST OF FIGURES (2)

LIST OF FIGURES (3)

LIST OF TABLES

LIST OF TABLES (2)

I. SUMMARY

A. PURPOSE AND SCOPE

This report documents the results of Phase II effort of a multi-phase program to result in the development and production of suitable propellant feed systems for operational thermal arc-jet thrustors. This Phase consists of a design study of the propellant feed systems required to service ammonia and hydrogen fueled arc-jet thrustors when used to transfer a communications satellite from a low earth orbit to a synchronous equatorial orbit. The design investigation encompasses the storage, expulsion and control elements of these systems. It is intended that the physical characteristics of these systems reflect the use of technological advances that can be anticipated in the next few years and that the nature and importance of development items be identified.

B. CONCLUSIONS AND RECOMMENDATIONS

We estimate that the take-off weight of the ammonia feed system built to service an arc-jet thrustor having a specific impulse of 750 seconds for the specified mission will be 5173 pounds. We estimate that the hydrogen feed system designed for an arc-jet thrustor of 1000 seconds for the same service will weigh 4488 pounds.

The weight figures cited for the ammonia and hydrogen feed systems refer to designs calling for widely different amounts of technological development. The ammonia feed system incorporates state-of-the-art technology and can be built with relatively little component development.

The nature of the developments required will be to tailor the existing technology, to modify hardware of conventional type for specific purposes and to demonstrate satisfactory performance, particularly in respect to reliability. On the other hand, the hydrogen feed system design while calling for developments of the type required by the ammonia system, in addition, calls for a technologically advanced thermal protection system - a protection system whose efficacy is yet to be proven by test. This is the major and critical development item in the hydrogen system. It is recognized that a great deal more experimentation with the application and performance of super insulations on spaceborne cryogenic containers is needed before a final specification of the thermal protection system can be made. We believe that the development of a thermal protection system that will achieve the goals specified will entail costs measured in millions of dollars.

On the other hand, it is worth noting that other elements of our national space program depend upon the successful development of suitably insulated cryogenic tanks having service requirements similar to those called for in this program. Therefore, it appears reasonable to project the necessary expenditure of effort to develop the technology of thermal protection systems to the state required by the design set forth herein for the hydrogen feed system.

Full information pertaining to the characteristics of the boost vehicle, the SNAP-8 power plant and payload is needed for purposes of integrating the feed system with these components for a well balanced

over-all system design. The value of further design investigations of an over-all feed system is questionable until such time as this information is available.

Lack of information on the meteoroid environment and on the behavior of meteoroid protection systems based on the bumper concept make the specification of meteoroid protective design very tenuous at this time. The proposed meteoroid protective system must be accepted in this light. Nevertheless, our interpretation of the available information leads us to believe that adequate meteoroid protection can be provided for both the hydrogen and the ammonia tanks without a large weight penalty.

II. HYDROGEN FEED SYSTEM

A. INTRODUCTION

The high specific impulse attainable with the use of hydrogen as a propellant in an electrothermal engine accounts for this preoccupation with the hydrogen feed system. Although a higher specific impulse may be achieved with hydrogen, it has long been recognized that the low density and temperature of liquid hydrogen are characteristics that detract from the advantages derived from its higher specific impulse. Most importantly, the need to preserve the liquid hydrogen supply, stored at temperatures near $20^{\circ}K$, demands an extremely effective and light-weight thermal protection system.

B. BASIS FOR DESIGN

The mission chosen as a basis for the design of the hydrogen storage and expulsion system is one in which the arc-jet engine is used to propel an 8500-pound active communications system from a 500 nautical mile parking orbit to a 22,400 nautical mile synchronous orbit. The arc-jet vehicle will be launched into parking orbit and will remain in this orbit for forty-eight hours while the SNAP-8 power reactor is turned on and the system checked out. The arc-jet engine will then be activated and will transfer the vehicle in a spiral path to its final orbit.

Other design criteria are a hold time of six hours on the ground prior to launch, a maximum steady acceleration of 6.5 g's in the longitudinal direction and 1.5 g's in the transverse direction during boost and a

maximum tank diameter of ten feet. Other mission parameters, specified by NASA, are shown in Table I.

TABLE I

MISSION PARAMETERS FOR HYDROGEN SYSTEM

Power Available to Arc-Jet Engine	30 kw
Engine Specific Impulse	1000 sec.
Propellant Weight Flow	5×10^{-4} lb/sec.
Pressure at Engine Inlet	1 to 2 atmos.
Weight Flow and Pressure Tolerance	$\pm$10%
Propulsion Time	85 days
Stay Time	115 days
Propellant Reserve at the end of Propulsion Time	5 weight %

Some things important to the design of a well-integrated and balanced over-all vehicle (e.g., weight and configuration of the payload and location of radiators) are not known at present, therefore the design was made independent of these factors insofar as possible. This approach yields an over-all vehicle which is somewhat heavier than would result from an integrated design since it does not permit using components to perform dual functions. In cases where the nature of adjacent components was not known, reasonable assumptions have been made. These assumptions are mentioned where they are applicable.

C. SYSTEM DESCRIPTION

The schematic flow sheet of the system is shown in Figure 1. The system consists of the hydrogen storage tank, the expulsion and metering

Figure 3. At the aft end of the tank there is another penetration. The one shown in the over-all assembly is the alternate system which contains the rotary phase-separating heat exchanger. This penetration is shown in more detail in Figure 4. If the rotary phase-separating heat exchanger is not necessary, the after penetration becomes considerably simpler as may be seen from Figure 5.

The tank shell is shown in Figure 6. This shell is supported at only one place - the junction between the cylindrical shell and the hemispherical head at the after end of the tank. The support is a thin walled cylinder made of a thermally insulating material and joins the cylindrical skirt-like extension of the tank wall to the main structure of the vehicle. This support is shown in more detail in Figure 7. The entire tank is covered by a thermal and meteoroid protection system which is shown in Figure 8. The propellant metering system as well as all the control elements of the over-all system are supported around the inside of the main structure of the vehicle which has been assumed to be a continuous cylindrical shell.

The over-all system weight is 741 pounds if the system uses the rotary phase-separating heat exchanger, and 603 pounds, if it uses an internal tank heater only. The break-down of these weights is shown in Table II.

D. THE STORAGE VESSEL

1. Capacity Requirement

The amount of propellant required for propulsion is 3670 pounds, and 193 pounds is required for the five percent usable reserve. About 12 pounds of hydrogen gas will remain in the tank when it is drained as much

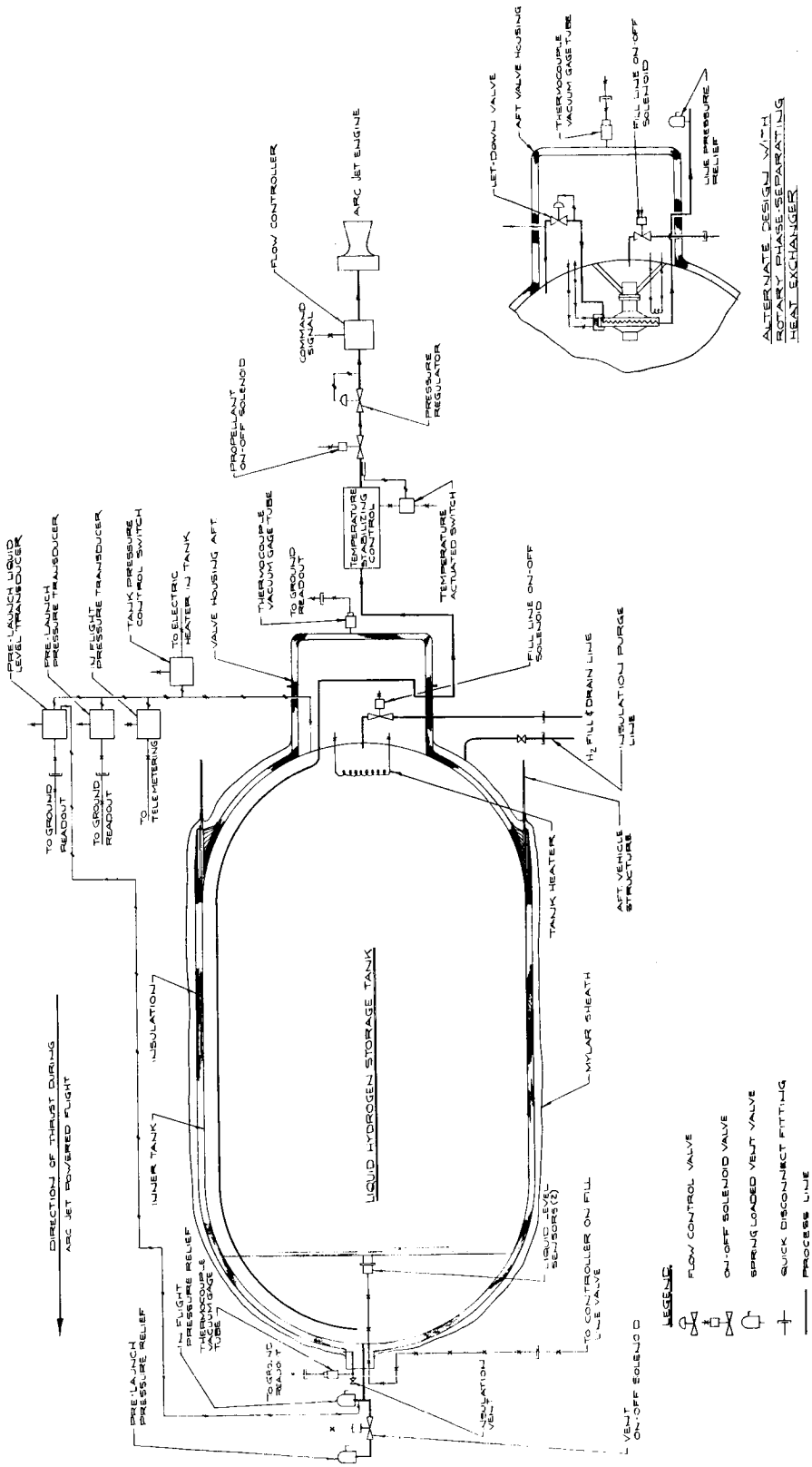

FIGURE 1 SCHEMATIC FLOWSHEET - HYDROGEN SYSTEM

system, and auxiliary instrumentation and controls. Referring to Figure 1 and tracing the flow circuit: gaseous hydrogen, saturated at tank pressure, is withdrawn from the tank and is heated to approximately room temperature in the temperature-stabilizing control. It then passes through an on-off solenoid valve and a pressure regulator to the flow controller. From the flow controller the propellant is fed directly to the engine.

As discussed more fully in a succeeding section (Section II-E), this flow system may be used if enough is known about the location of the liquid and vapor phases in the tank so that the withdrawal pipe inlet can be placed in the vapor phase. From our present knowledge of the mission we expect this to be the case. However, in recognition of the fact that there may be some uncertainty as to the location of the liquid and vapor phases in the tank, a positive phase-separating system may be provided to assure that only vapor is withdrawn. Such a system is shown as the alternate design in Figure 1. It includes a rotary phase-separating heat exchanger as its principal component. With this system, either liquid, vapor, or a mixture of the two may be taken into the withdrawal pipe. This fluid is then throttled through the let-down valve where it comes to equilibrium at a lower pressure and temperature than the bulk of the fluid in the tank. It is then piped back to the tank where it passes through the rotary phase-separating heat exchanger. In this exchanger, heat is transferred from the bulk fluid in the tank to the fluid in the tube, vaporizing any liquid in the tube, and assuring that only vapor is withdrawn from the tank. This vapor then goes to the temperature-stabilizing control, from which point

it is handled as previously. This alternate system requires that the liquid hydrogen be stored at a higher pressure than in the system first presented because there must be a pressure differential maintained across the let-down valve. This differential must be great enough so that the corresponding saturated temperature differential is enough to transfer heat across the heat exchange surface in the rotary phase-separating heat exchanger. This higher pressure system requires a heavier tank in addition to introducing the complications of an internal heat exchanger.

The electric heater inside the tank is used to keep the tank pressure from falling below the operating level during withdrawal of the vapor feed. This heater is controlled by a pressure-actuated switch which turns the heater on as tank pressure falls below a pre-set value and turns the heater off when the pressure rises to a pre-set value.

The liquid level sensors are used to control a valve on the hydrogen fill line during filling and topping of the tank prior to launch. The fill and drain line has a solenoid valve in it to assure positive shut-off of this line at launch. At the forward end of the tank (the end which is up prior to launch) there are two safety relief valves and a solenoid valve. The pre-launch pressure relief valve is used to control the tank pressure at launch and is sized to handle the large boil-off rates which will result from the high heat leakage into the tank prior to launch. This valve is more in the nature of a control valve to set the pressure of the hydrogen in the tank at launch rather than to protect the tank from failure, since its setting is considerably below the tank's maximum allowable

working pressure. Immediately prior to launch, the vent on-off solenoid valve is closed, removing the pre-launch pressure relief valve from service. From this point on, the tank is protected by the in-flight pressure relief valve which is set at the tank's maximum allowable working pressure.

There are three pressure transducers in the system. The pre-launch liquid level transducer is a differential pressure indicator and is used to monitor the filling operation. The pre-launch pressure transducer is used to monitor tank pressure prior to launch. The in-flight pressure transducer is used to monitor tank pressure during flight.

The entire tank is insulated with layer of foam-type insulation next to the tank wall covered by a layer of multi-foil reflective insulation. This insulation system is enclosed in a Mylar sheath which serves as a vacuum jacket prior to launch, protection for the fragile multi-foil insulation during ascent, and a meteoroid bumper in space. This sheath has a purge line leading into it and vent line leaving it. Prior to launch the pressure between the sheath and the tank wall is monitored by a thermocouple vacuum gage at each end of the tank.

The over-all assembly of the system is shown in Figure 2. As may be seen from this figure, the tank is cylindrical with hemispherical heads. Its over-all length is 19 1/2 feet and is just under 10 feet in diameter. At the forward end there is a penetration assembly which contains the liquid level sensors, the pre-launch pressure relief valve with its solenoid valve, the in-flight pressure relief valve, the insulation vent valve, and a thermocouple vacuum gage tube. This penetration is shown in more detail in

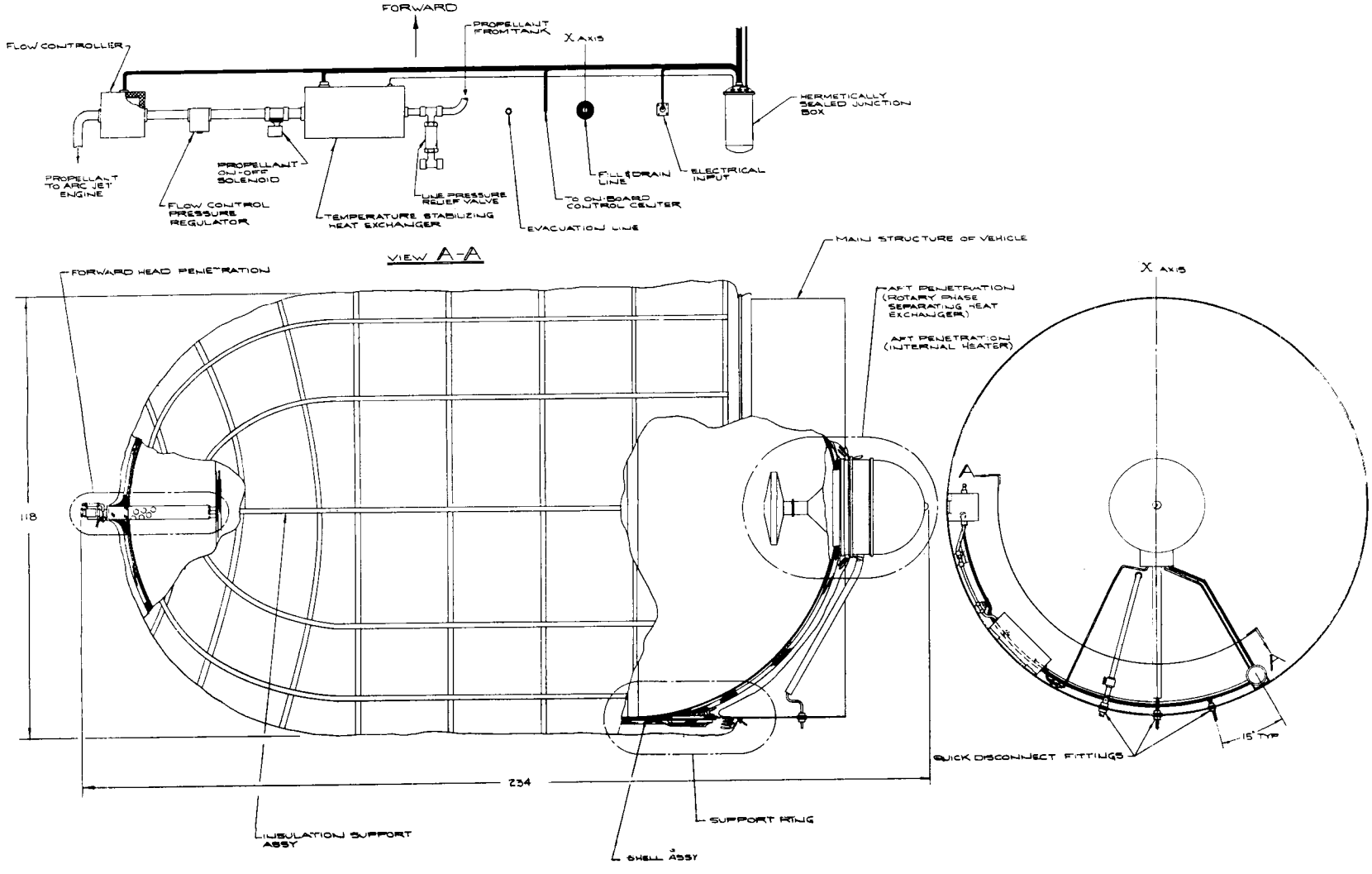

FIGURE 2 OVER-ALL ASSEMBLY - HYDROGEN SYSTEM

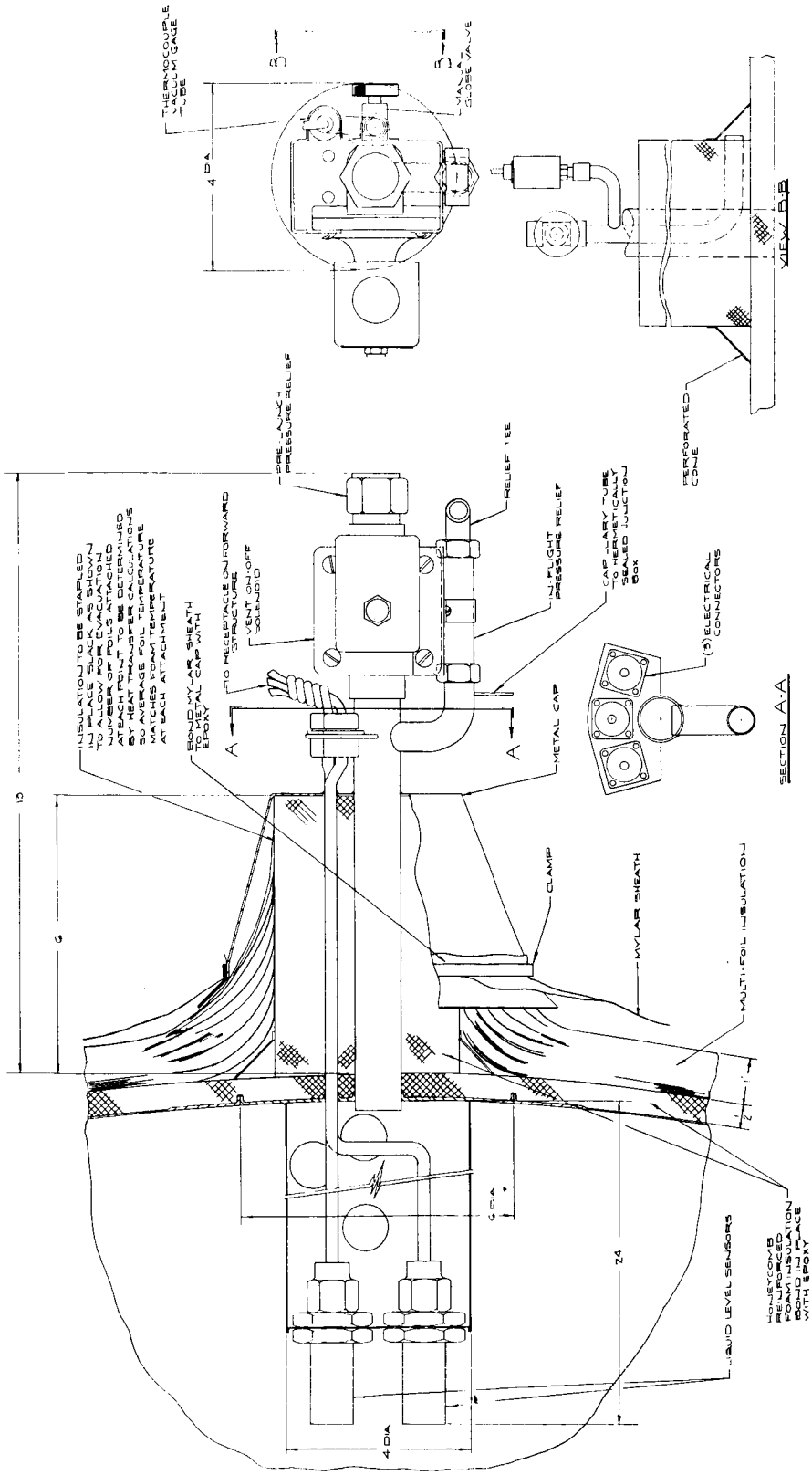

FIGURE 3 FORWARD HEAD PENETRATION - HYDROGEN TANK

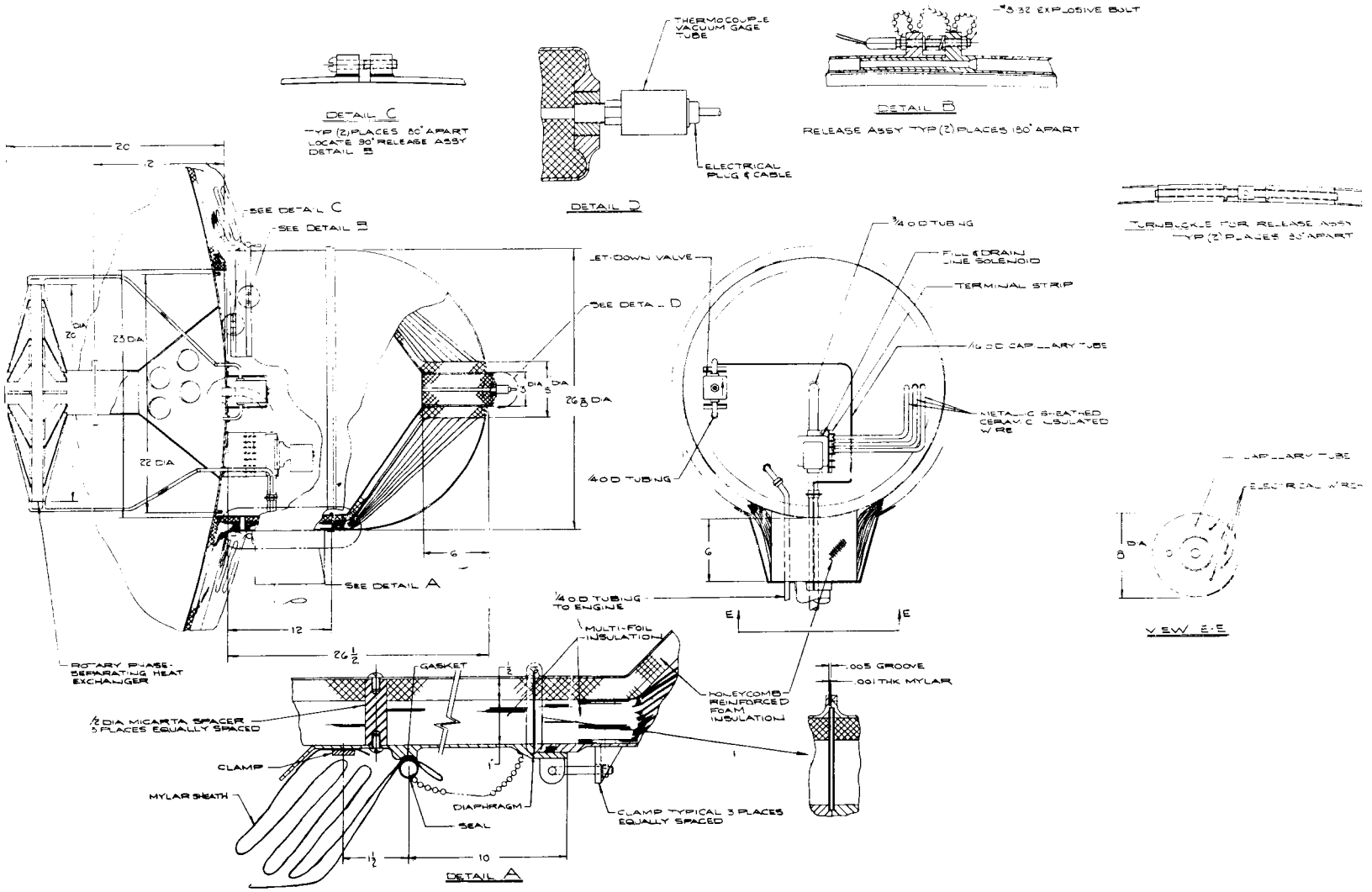

FIGURE 4 AFT HEAD PENETRATION - HYDROGEN TANK (WITH ROTARY PHASE-SEPARATING HEAT EXCHANGER)

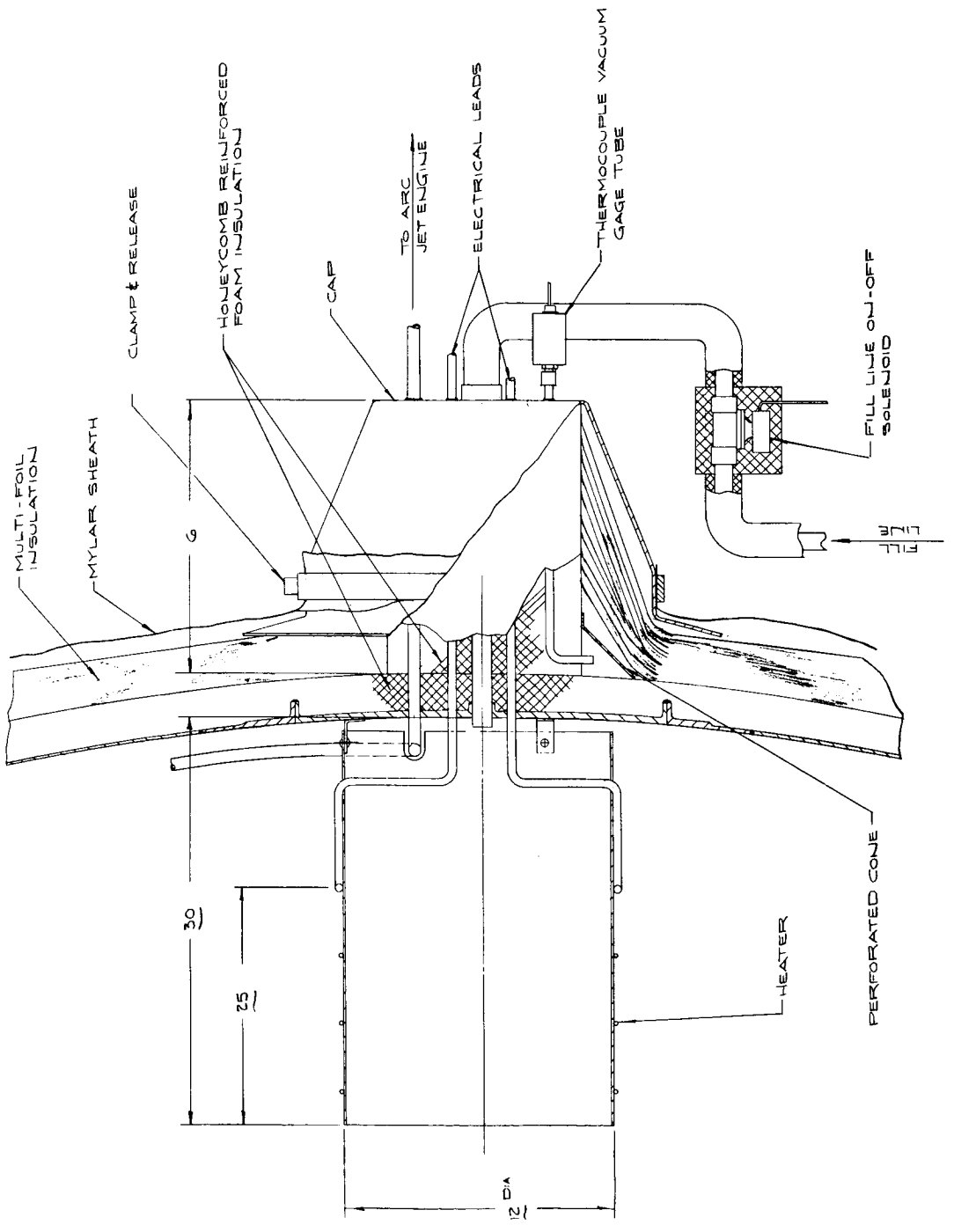

FIGURE 5 AFT HEAD PENETRATION-HYDROGEN TANK (WITH INTERNAL HEATER)

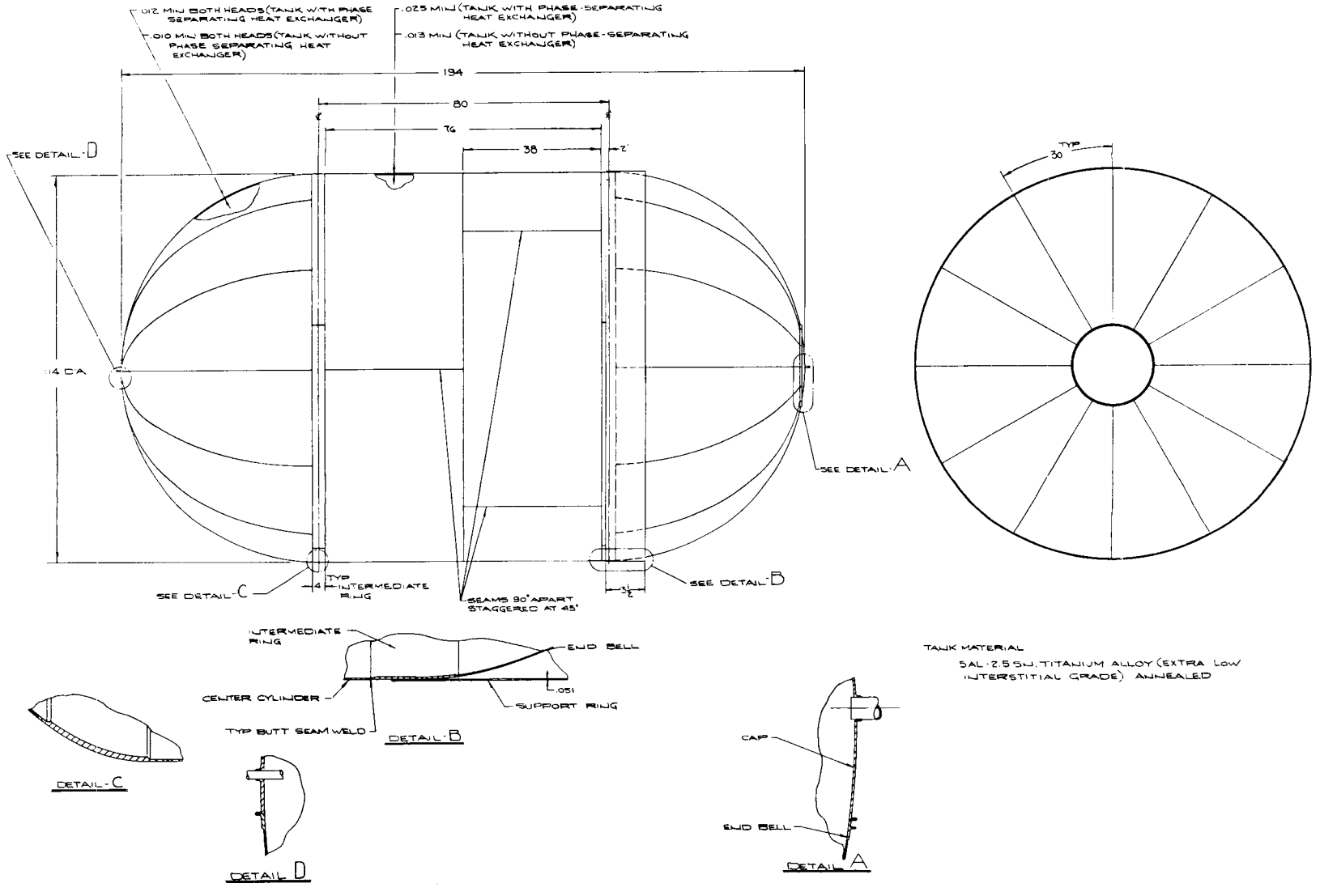

FIGURE 6 SHELL ASSEMBLY - HYDROGEN TANK

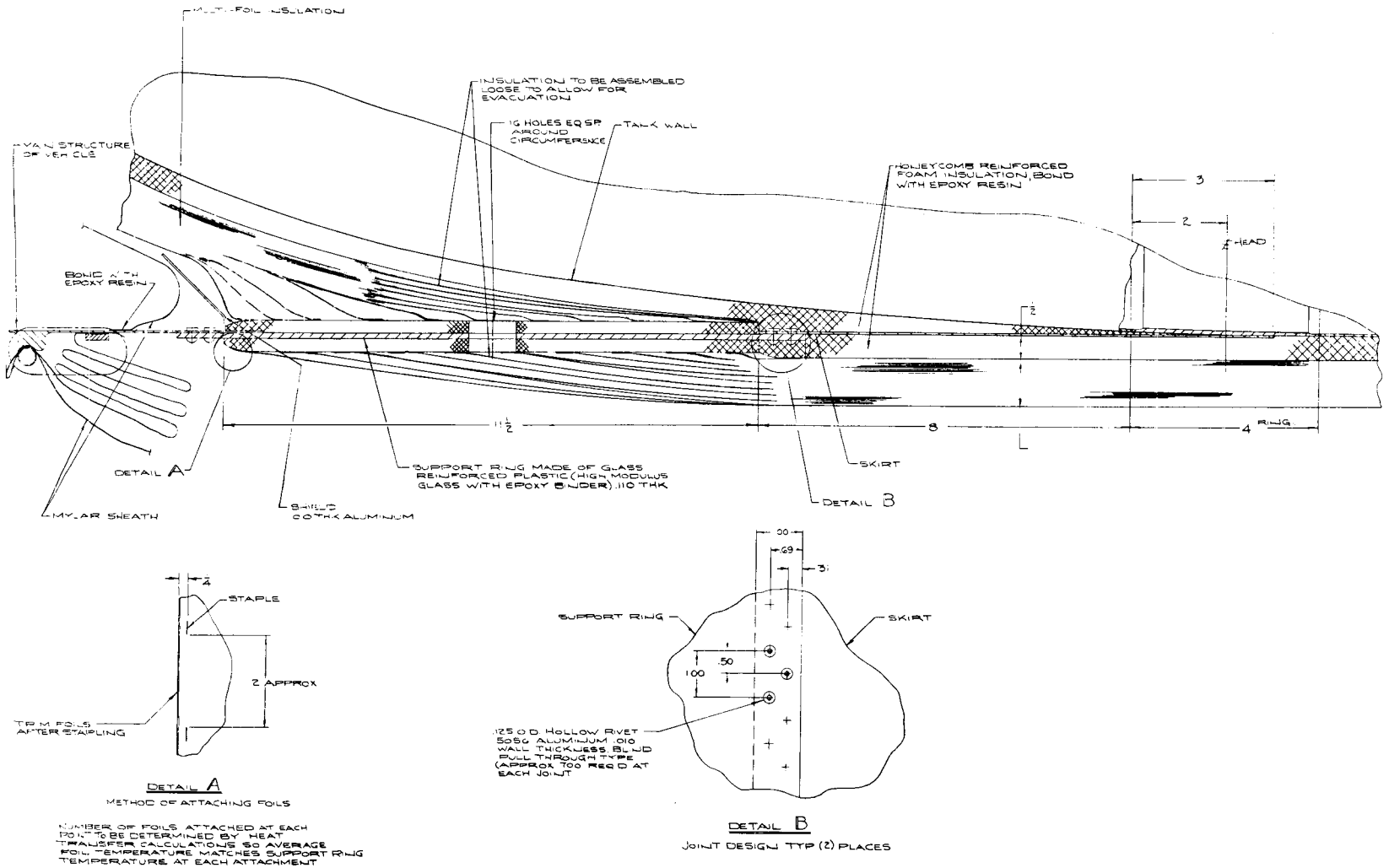

DETAIL A
METHOD OF ATTACHING FOILS

NUMBER OF FOILS ATTACHED AT EACH POINT TO BE DETERMINED BY HEAT TRANSFER CALCULATIONS SO AVERAGE FOIL TEMPERATURE MATCHES SUPPORT RING TEMPERATURE AT EACH ATTACHMENT

DETAIL B
JOINT DESIGN TYP (2) PLACES

FIGURE 7 SUPPORT RING - HYDROGEN TANK

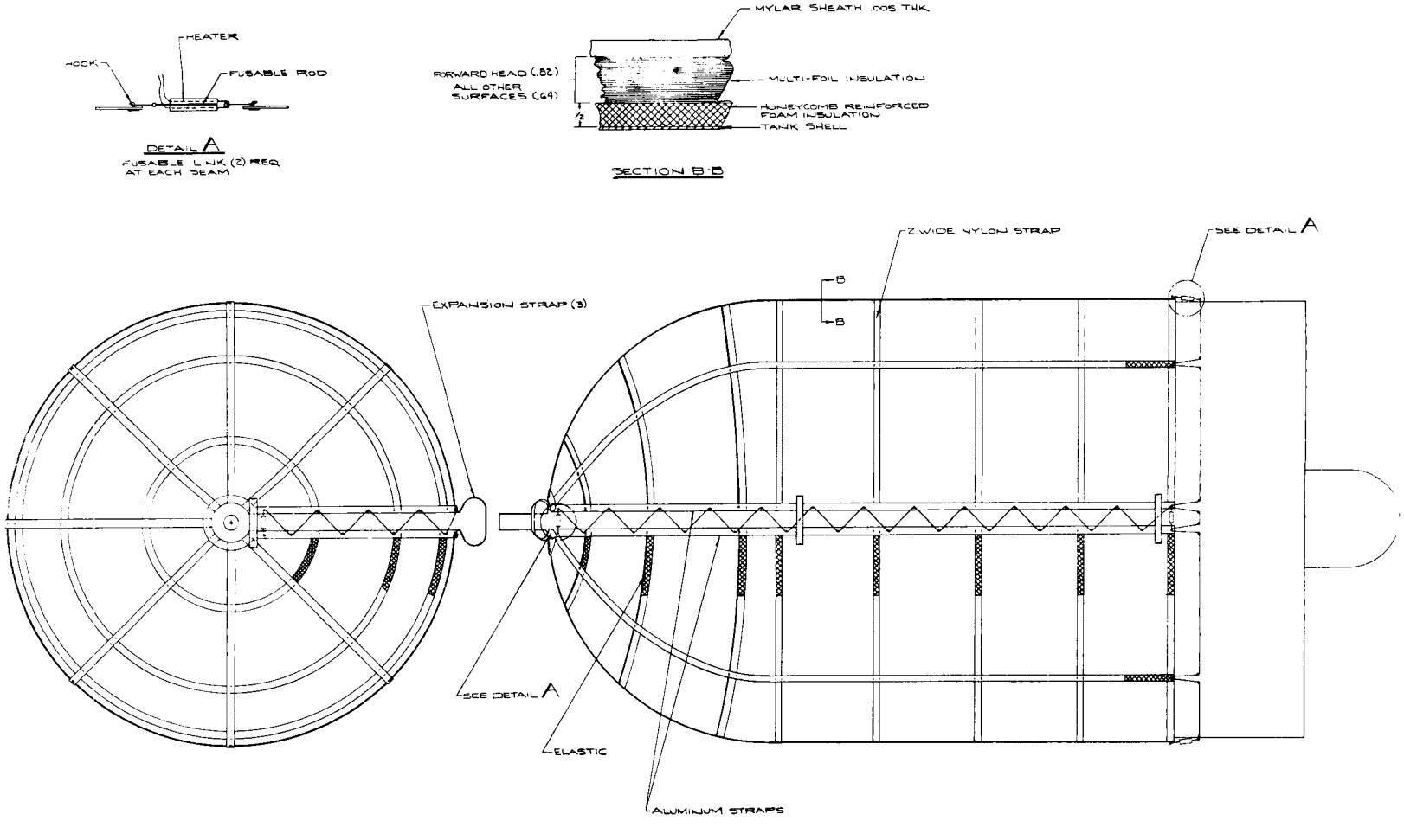

FIGURE 8 THERMAL AND METEOROID PROTECTION SYSTEM ASSEMBLY - HYDROGEN SYSTEM

TABLE II

HYDROGEN SYSTEM WEIGHT BREAKDOWN

ITEM	WEIGHT	
	SYSTEM WITH TANK HEATER ONLY	SYSTEM WITH ROTARY PHASE-SEPARATOR
Hydrogen Tank	146 lbs.	241 lbs.
Support Skirt	35	35
Thermal Isolating Support Ring	41	41
Rotary Phase-Separating Heat Exchanger	-	25
Miscellaneous Structure	9	25
Piping and Valving	8	9
Instrumentation and Controls	15	15
Meteorite Bumper	30	30
Insulation System	320	320
Total Tank and Expulsion System	603 lbs.	741 lbs.
Hydrogen in Tank at Lift-Off	3885 lbs.	3885 lbs.
Total System at Lift-Off	4488 lbs.	4626 lbs.

as is practical and 10 pounds have been allowed for leakage loss through valves, etc. Thus, the amount of propellant which must be in the tank at launch is the sum of these quantities, or 3885 pounds. Taking an ullage volume of five percent and a tank pressure of 45 psia at launch, 3873 pounds of liquid and 12 pounds of vapor will be in the tank at lift-off and the required tank volume is 919 cu. ft.

The selection of the tank capacity and geometry is discussed in more detail in Appendix A.

2. Tank Shell Design

The tank shell assembly is shown in Figure 6. As may be seen, it is a cylindrical tank with hemispherical heads. The capacity requirement and envelope restriction dictates a vessel that is 114 inches in diameter and 194 inches long. The cylindrical portion of the tank is built for a maximum allowable working pressure of 109 psi (system with phase-separating heat exchanger) is 0.025-inch thick, and the hemispherical heads are 0.0125-inch thick. These dimensions become 0.013 and 0.010-inch respectively, for the tanks without the positive phase-separating device. There are two girth rings which act as transition pieces between the cylindrical and hemispherical portions of the shell. These rings are thickened slightly over the shell thickness to accommodate the discontinuity stresses at this juncture. The girth ring at the after head-to-shell junction, also withstands the stresses imposed by the tank support at this location.

The tank is designed as a stressed membrane, requiring internal pressure to give it rigidity. It is made entirely of 5 Al - 2.5 Sn titanium

alloy with extra low interstitial content. This alloy has a tensile strength of 276,000 psi and a yield strength of 273,000 psi at liquid hydrogen temperature. The tank design is based on the use of these low-temperature properties. The selection of this material is discussed in more detail in Appendix B.

The tank is fabricated of rolled sheet in sizes which will be commercially available in the near future. The shell of the tank is made by rolling the sheet into a cylinder, and the heads are built up of "orange peel" segments which will be stretch-formed to the spherical contour prior to welding into the head. The girth rings will be hot rolled in sections and welded together to form a complete ring, and the penetrations will be made of specially forged or machined sheet. Shell areas adjacent to the two penetrations in the heads have been thickened to accommodate discontinuity and bending stresses at these points. A cylindrical strip-like extension of the tank support skirt is rolled out of sheet and welded to the after girth ring.

A few comments on fabrication techniques are appropriate at this point. The tank has been designed to use fabrication techniques which are presently used in the aerospace industry. These techniques are fairly advanced and require extensive use of jigs and fixtures, since the tank wall is not capable of supporting its own weight during fabrication. Additionally, special machinery and equipment must be used to handle, weld, and form the thin sheets without damaging them. And finally, extreme care must be taken in making all welds to insure sound, vacuum-tight joints.

This latter requirement is novel to propellant tank construction.

3. Tank Support

The tank support ring is shown in Figure 7 and its design is discussed in Appendix C. It is a cylinder made of glass reinforced plastic, and is designed to transmit the tank loads from the tank wall to the main structure of the vehicle and also to isolate the tank thermally from the rest of the vehicle. It is riveted to the main structure of the vehicle at one end. It is covered by a layer of foam insulation to which the multi-foil insulation is stapled at various points. The support cylinder itself is 13 1/2 inches long, .110-inch thick, weighs 37 pounds, and has heat leak through it of 7 watts.

4. Thermal Protection System

The allowable heat addition to the propellant (101 watts) is determined by the propellant withdrawal rate. If heat is added at greater rate, tank pressure will rise, and if heat is added at a lesser rate, tank pressure will fall. Approximately half of the required heat will be taken as uncontrolled heat leak and the other half will be supplied by the internal tank heater in a controlled manner. A breakdown of the heat leak through the various components is shown in Table III.

TABLE III

BREAKDOWN OF TANK HEAT LEAK

Heat Leak Through:	
Insulation	20 watts
Tank Support	7
Piping and Other Penetrations	9
Gamma Heating	16
Total Heat Leak During Transfer:-	52 watts

A section through the insulation on the tank shell is shown in Figure 8. It may be seen from this detail that the thermal protection system is a composite made up of a half-inch layer of honeycomb reinforced foam insulation next to the tank wall followed by a layer of perforated multi-foil super insulation. The multi-foil insulation thickness on the forward head is 0.82-inch and 0.64-inch on all other surfaces. The multi-foil insulation is held in place by a net which, in turn, is covered by a Mylar sheath. The Mylar cover is held in place with Nylon netting and strapping until the vehicle is in parking orbit. The basis for the design of the thermal protection system and the state-of-the-art as it pertains to such systems is discussed in Appendices E and F.

The tank support penetration through the multi-foil insulation is shown in Figure 7. It may be seen from this figure that the cylindrical tank support is encased in a layer of foam insulation and groups of multi-foil insulation are stapled to this foam at various points along its length. The number of foils attached at each point and the location of

each attachment point are determined by heat transfer calculations on the multi-foil insulation and tank support skirt so that the average foil temperature matches the foam temperature at each attachment point.

Other penetrations into the tank through the insulation layer are shown in Figures 3, 4 and 5. The general approach to the design of these penetrations is the same as for the support. The penetrating tube or wire is encased in a sleeve of rigid foam insulation and the multi-foil insulation is attached at points along this sleeve where the average foil temperature matches the foam temperature. The foam, multi-foil assembly is then encased in a metal housing to prevent a collapse and damage to the multi-foil insulation during ground hold and ascent. The total heat leak through these penetrations is composed of a number of components; conduction down the penetrating member, radiation down tubes, gas conduction down tubes, and conduction down the foam sleeve. The designs shown have calculated total heat leaks as indicated in Table III.

As discussed more fully in Appendix E, we anticipate that the power reactor together with its radiators will have to be deployed about 20 feet aft of the hydrogen tank in order to reduce heat inleakage to the tank due gamma and thermal radiation from the reactor system to tolerable limits. This need introduces an unwanted complication into the design of the feed system support.

5. Meteoroid Protection

The meteoroid protection system for this vehicle is based on the bumper concept. A thin membrane is used as the bumper and the multi-foil

insulation serves as the witness plate.

The bumper used in the present design is the .005-inch thick Mylar sheath which is deployed outward from the surface of the insulation during parking orbit. This Mylar cover completely encloses the tank during transfer, and doubles as a vacuum jacket for the insulation during the pre-launch and ascent phases of the mission. It is in the form of a bag, having the general shape of the hydrogen tank but being somewhat larger. This bag is divided into two parts by the tank support penetration. The forward portion is clamped rigidly to the forward penetration and to the main structure of the vehicle, and the after portion is bonded to the main structure of the vehicle and clamped to the aft penetration. There are a number of holes evenly distributed around the circumference of the sheath adjacent to the clamp at the after ends. At assembly the portion of the sheath which contains these holes is tucked under and the sheath is clamped with a tubular clamping ring, as shown in Figures 4, 5 and 7. Thus the sheath is continuous and vacuum-tight while clamped with the tubular clamp ring, but communicates with the environment when the clamp ring is released. The entire insulation-sheath composite is wrapped with a wide mesh net system as shown in Figure 8. This net holds the entire system against the tank wall during transportation of the vehicle and during the pre-launch and ascent phases. It is held together by two cords which have fusable links in them, and may be released by releasing the links.

The selection of the bumper-witness-plate system used here is discussed in more detail in Appendix D, and the projected mode of operation of this system at various stages in the mission is discussed in Section II-G to follow.

E. EXPULSION SYSTEM

1. Requirements

Expulsion is the process by which propellant is withdrawn from the storage tank. It is primarily important in delivering fluid to the propellant metering and control system for eventual usage in the arc-jet engine, but may also be of importance if fluid need be vented overboard for pressure control.

During the parking orbit, with the arc-jet engine inoperative, no fluid is expelled to the feed system. Furthermore, it appears feasible to do no venting but simply permit the tank pressure to rise as a result of heat inleakage. Our analyses indicate that if conduction were the only mechanism for heat transfer, as would be the case in a zero-g environment, the pressure in the tank would rise to something less than 100 psia during the 48-hour parking orbit. Actually, true zero-g conditions are not attained in the parking orbit. Acceleration fields with $\frac{g}{g_0}$ of at least 10^{-7} to 10^{-6} are anticipated. Even with this low field, the Rayleigh Number, based on the diameter of the tank as a characteristic dimension, is of the order of 10^{8}, indicating that natural convection will be significant. Natural convection in the fluid would expedite heat transfer from the

tank walls to the bulk liquid and would reduce the pressure rise in the tank below the figure noted.

During the powered flight, withdrawal of the propellant as a vapor reduces the requirements for thermal protection of the hydrogen storage. By withdrawing vapor a greater heat leakage into the vessel can be tolerated without pressure rise. If, on the other hand, pure liquid were withdrawn from the tank,either a more effective thermal protection system would have to be employed or it would be necessary to vent additional fluid overboard to maintain a constant pressure. Hence, phase separation is desirable so that, throughout most of the powered flight, vapor can be withdrawn from the tank by the propellant feed system.

2. Passive System

Since vapor expulsion is only required during powered flight when a significant acceleration field exists, it is possible to use what might be termed as a "passive" system in which phase separation is accomplished by the "g" field. The 0.5-pound thrust acting on the 8500-pound vehicle will produce an acceleration field for which $\frac{g}{g_0} = 5.89 \times 10^{-5}$. The thrust and resulting acceleration field are expected to be quite steady, and external forces which might produce liquid sloshing are not foreseen. Under these conditions two types of forces, those due to the acceleration field and those due to surface tension, must be considered in predicting the disposition of the liquid and gas phases. The ratio of acceleration field forces to surface tension forces is given by the Bond Number, defined

by

$$\text{Bond Number, Bo} = \frac{\rho D^2 g}{\sigma}$$

ρ = density of liquid

D = characteristic dimension of vessel

g = acceleration field

σ = coefficient of surface tension

Large Bond Numbers (substantially greater than one) indicate that acceleration forces predominate while small Bond Numbers (substantially less than one) indicate that surface tension forces are dominant. In the present case, using the tank diameter as the characteristic dimension, the Bond Number is 151; the acceleration field forces are clearly dominant. The liquid will settle in one end of the tank and the interface between the liquid and vapor phases will be an essentially flat surface. The conditions are shown in Figure 9. Expulsion of vapor may be simply accomplished by a withdrawal tube at the end of the tank, as shown in the figure.

The fluid disposition shown in Figure 9 is an equilibrium condition which would obtain within a few minutes after the initiation of thrust. During the start-up, and for a few minutes thereafter, it is possible that some liquid would enter the withdrawal tube. To maintain proper operation of the metering and control system during this period, the temperature-stabilizing heat exchanger should be designed to accept liquid and still maintain the gas exit temperature within the desired limits. This feature can readily be designed into the exchanger as is shown in Section F following. Thus, withdrawal of liquid for short periods of time, either

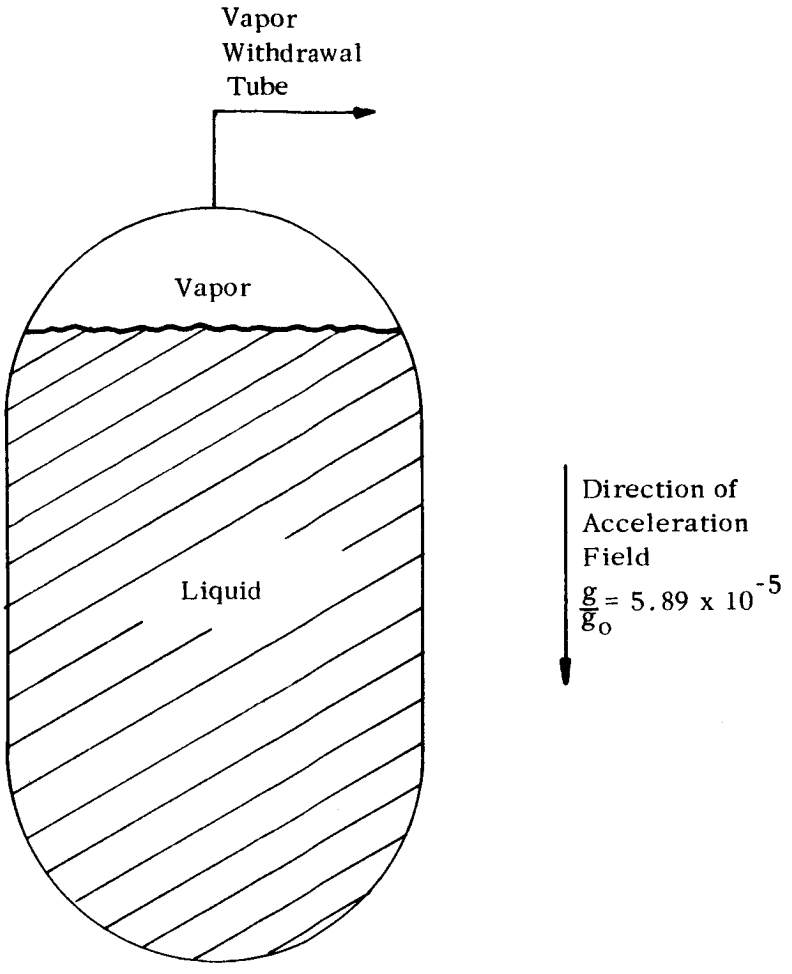

FIGURE 9 HYDROGEN DISPOSITION DURING ARC-JET POWERED FLIGHT

during start-up or powered flight (for reasons not now foreseen) would not impair the functioning of the propellant feed system.

Upon initiation of thrust, any pressure build-up that occurred during the parking orbit would be largely dissipated as a result of the natural convection mixing brought on by the intensified acceleration field. Since a tank pressure of at least 40 psia is required for proper functioning of the propellant feed system, temperature of the liquid at ground-launch should be close to the value corresponding to a saturation pressure of 40 psia (about $43.5^{\circ}R$). Heat absorbed by the fuel during the parking orbit would cause the pressure level of the mixed fluid to be somewhat above 40 psia after arc-jet engine thrust initiation.

Once the equilibrium fluid disposition is achieved and vapor is being withdrawn at the constant rate of 5×10^{-4} lbs/sec, a total heat input to the liquid in the tank of about 100 watts must be supplied in order to maintain the tank pressure constant. The average heat inleakage through the insulation, supports and piping is set at about 50 watts; an additional 50 watts must be supplied artificially for purposes of control. Such heat input can readily be provided by a heater placed in the liquid. The device might be called a pressure-stabilizing heater (PSH).

Toward the end of the mission, the tank is filled with saturated gas, a large portion of which must be withdrawn for use by the engine. When all liquid is exhausted and propellant is still being withdrawn, the tank pressure can be maintained by sensible heating of the remaining gas. This heating would also be accomplished by the PSH; it places the most

stringent demand on the PSH and dictates its design.

The heat input required to maintain the tank pressure constant after all liquid is gone and gas is being withdrawn is given by

$$q = w R T\left(\frac{\gamma}{\gamma - 1}\right)$$

where

q = heat input

w = discharge mass flow rate

R = gas constant

T = instantaneous absolute gas temperature

γ = ratio of specific heats

To maintain constant tank pressure the product of density and temperature must be substantially constant. As gas is withdrawn and the density decreases, the gas temperature must rise. The required heat input also rises, according to the above equation. In addition, for a given heater temperature the ΔT for heat transfer between the heater and the remaining gas diminishes as the gas temperature rises. Hence, the worst condition for which the PSH should be designed occurs at the termination of propellant discharge. The higher the final propellant temperature, the smaller the mass of gas remaining in the storage tank, but the larger the heater surface area required. Analysis indicates that it is desirable to heat the gas up to about $530^{\circ}R$, at which temperature only about 12 pounds of propellant remain in the storage tank. Calculations of the natural convection heat transfer coefficients that may be expected in the

acceleration field caused by the arc-jet engine shows that a value of about 0.74 Btu/hr-sq.ft^{o}F may be expected. If a heater temperature of 960^{o}R (500^{o}F) is utilized, a heater area of about 6.3 sq.ft. would suffice. The heater would be placed in the bottom of the fuel tank to maximize the natural convection circulation in the fluid. A cylinder with a diameter of about 12 inches and a heated length of 25 inches would provide sufficient area with a substantial safety factor. The cylinder would be constructed of aluminum plate, with the heater wires imbedded. The general arrangement is shown in Figure 5.

3. Active System

Based on our present knowledge, a passive expulsion system as described above would meet the requirements of the mission. However, all aspects of the mission have not as yet been fully defined. Circumstances may be envisioned in which the operation of a passive system would be compromised. For example, a passive system may not be practical for a mission incorporating prolonged thrust direction changes that would cause the liquid to assume equilibrium positions such that the vapor withdrawal tube received liquid for long periods of time (excessive tank pressure buildup could occur). Therefore, we have given some consideration to active systems which do not rely on the acceleration field caused by the arc-jet engine thrust to separate the fluid phases.

Perhaps the simplest kind of an active system for insuring vapor withdrawal would be one which induces fluid motion; the fluid disposition results from and is controlled by the inertia forces associated with the

motion. For example, phase separation can be achieved by swirling the fluid about the longitudinal axis of the tank at relatively low velocities. The ratio of fluid inertia forces to surface tension forces is indicated by the Weber Number, defined as below:

$$\text{Weber Number, We} = \frac{\rho V^2 D}{\sigma}$$

where

ρ = density of liquid

V = velocity of liquid

D = characteristic dimension

σ = coefficient of surface tension

The ratio of fluid inertial forces to acceleration field forces is expressed by the Froude Number:

$$\text{Froude Number, Fr} = \frac{V}{\sqrt{gD}}$$

(Same symbols as for Bond and Weber Numbers)

If swirling motion with a fluid velocity of the order of one foot per second were induced, a Weber Number of 8,400 and a Froude Number of 7.5 would pertain. Thus, the fluid inertial forces would be dominant and the disposition of fluid in the tank would be essentially determined by the swirl. The liquid would be centrifuged to the outer walls of the tank while the gas would form a cylindrical core along its axis. By placing the inlet of the withdrawal tube at the center of the tank, vapor withdrawal would be insured once the equilibrium fluid distribution was

achieved. To overcome the viscous effects which would tend to slow down the rotation, a circulator to operate either continuously or intermittently throughout the mission would be required. The effects of the fluid swirl on the vehicle system and the possibilities of offsetting any adverse effects by devices external to the storage tank are not clear to us at the present time. Certainly, the guidance and orientation systems of the vehicle would have to take into account the presence of the fluid swirl. It is possible that from the standpoint and guidance and orientation or for reasons we do not now appreciate, swirling the fluid in the fuel tank may not be an acceptable technique for achieving phase separation. Because of these uncertainties we have not pursued this technique any further.

Our previous work for NASA, in which no mission was defined and in which the level of acceleration fields was unknown, had led us to the conclusion that an active expulsion system consisting of a phase-separating heat exchanger constituted a good approach to the expulsion problem. The technique was described in our Final Report* on previous work. It involves withdrawing fluid (of unknown quality) from the tank, flashing it to a

---

*Fowle, A. A. et al, "Investigation of Propellant Feed Systems for Electrothermal Engines", Final Report, Phase I, Contract No. NAS8-1695, NASA Marshall Space Flight Center, Huntsville, Alabama, October 1961.

lower pressure, then vaporizing it by exchanging heat with the fluid remaining in the tank. A fairly compact heat exchanger using rotary motion to induce fluid flow across the heat transfer surfaces has been evolved. The description and operation of the device are included in Appendix G of this report. In cases where a passive system is not adequate or where separation by fluid swirl is not acceptable, a device of this type would be useful.

F. METERING AND CONTROL SYSTEM

1. Introduction

The metering and control components for the hydrogen feed system are identified and their functions explained in sections describing the overall characteristics of the feed system. Attention is directed particularly to Sections II-C, II-E, and II-G in Appendices A and H. In this section a summary of the control elements and their function is given; typical component specifications are listed; the availability of these items is assessed; and the design requirements and characteristics of unique items are set forth.

2. Component Identification

a. General

The control components can be grouped into four major functional categories. These categories are:

Pre-launch controls

Propellant storage and expulsion controls

Propellant flow controls

Monitoring Instrumentation

b. Pre-launch Controls

The pre-launch controls are employed during loading of the storage tank and readying the system for flight. These controls include the fill line on-off solenoid valve, the vent on-off solenoid valve, the pre-launch pressure relief valve, and the insulation vent and purge valves.

c. Propellant Storage and Expulsion Controls

The storage and expulsion controls govern the propellant storage and feed stream withdrawal process. The in-flight pressure relief valve, the let-down valve, the tank pressure control switch, and tank heater are grouped in the propellant storage and expulsion control category.

d. Propellant Flow Controls

The propellant flow controls modulate the flow of gas to the arc-jet engine, according to propulsion requirements. The propellant flow controls include the temperature-stabilizing heat exchanger, flow control pressure regulator, flow controller, the propellant on-off solenoid valve and the line pressure relief valve.

Hydrogen vapor (and/or liquid) supplied by the propellant expulsion system at approximately -423^{o}F passes through the temperature-stabilizing heat exchanger which warms the vapor to 80^{o}F (540^{o}R). The flow control pressure regulator maintains the gas pressure at 32.2 psia. The flow controller accepts gas at constant temperature and pressure and varies the mass flow according to the command signal. From the flow controller the gas is fed directly to the arc-jet engine.

A solenoid valve located between the temperature-stabilizing heat exchanger and the flow control pressure regulator blocks the flow of propellant when the arc-jet engine is not operating. The valve eliminates leakage of propellant through the flow controller during periods of commanded zero flow. The pressure relief valve in the line from the tank to the temperature-stabilizing heat exchanger (in system with phase-separating heat exchanger, only) prevents damage to the line if the pressure exceeds safe limits. During normal operation, the pressure will not reach the cracking point of the valve, so no propellant will be lost.

e. Monitoring Instrumentation

The monitoring instrumentation supplies information on system conditions and performance to the ground. The monitoring instruments are: the pre-launch liquid level transducer, the pre-launch pressure transducer, the in-flight pressure transducer, liquid level sensors, and the thermocouple vacuum gage tubes.

As its name implies the pre-launch liquid level transducer indicates the level of liquid hydrogen in the storage tank as it is being filled and while holding on the ground. The transducer is a differential pressure device which indicates the difference in pressure between the top and bottom of the tank. The liquid level sensors signal when the liquid hydrogen has reached the correct level during the filling process. The pre-launch transducer monitors pressure within the storage tank before launch. During flight, the in-flight pressure transducer through the telemetry system relays information on tank pressure to the ground. The

thermocouple vacuum gage tubes monitor the condition of the vacuum insulation around the liquid hydrogen storage tank.

3. Component Specifications

a. General

Typical specifications for the control elements of the hydrogen feed system follow. They are based on a feed system that requires a phase-separating heat exchanger. They have been established to provide a background for the procurement, design and development of components, as necessary. They are not to be construed as final.

b. Pre-launch Controls

The pre-launch controls will be subjected to environment temperatures ranging from -423°F to +150°F and conditions as outlined in Section II-B. The pre-launch control components will not be required to operate within specification under the acceleration, shock, and vibration environment, but they must not leak or show damage when subjected to these conditions.

1) Fill Line On-Off Solenoid Valve

Maximum Allowable Working Pressure: 125 psi differential

Maximum Pressure Drop: 5 psi for saturated hydrogen liquid at 45 psia (nominal temperature -423°F) flowing at a rate of 1500 lb/hr.

Configuration: Normally closed - power to open

Leakage: Less than 0.10 standard cc/sec with an upstream pressure of 125 psia and a downstream pressure 1×10^{-6} mm Hg absolute when closed and at a temperature of -423°F.

Power Supply: 115 volts 400 cps

Operating Life: 150 days

2) Vent On-Off Solenoid Valve

Maximum Allowable Working Pressure: 110 psi differential

Maximum Pressure Drop: 2 psi for saturated hydrogen vapor at 50 psia (nominal temperature -423°F), flowing at a rate of 1100 lb/hr.

Configuration: Normally closed - power to open

Leakage: Less than 0.10 standard cc/sec with an upstream pressure of 110 psia and a downstream pressure 1×10^{-6} mm Hg absolute when closed and at a temperature of -423°F.

Power Supply: 115 volts 400 cps

Operating Life: 150 days

3) Pre-launch Pressure Relief Valve

Open Pressure: 25 psig

Reseat Pressure: 20 psig

Fluid: Hydrogen vapor saturated at the upstream pressure

Nominal Operating Temperature: -423°F

Capacity: a) 500 lb/hr at 25 psig upstream pressure discharging to 1 atmosphere downstream pressure.
b) 1100 lb/hr at 35 psig upstream pressure discharging to 1 atmosphere downstream pressure.

Operating Life: 10 days

4) Insulation Vent and Purge Valves

Standard bellows sealed vacuum valves for 1/4-inch line.

Must meet environmental requirements.

c. Storage and Expulsion Controls

The control components will be subjected to an environment whose temperature varies from -423°F to +150°F and to conditions outlined in Section II-B. The storage and expulsion control components will not be required to operate satisfactorily during acceleration and vibration, but the components must not become damaged during these periods.

1) In-Flight Pressure Relief Valve

Open Pressure: 105 psia

Reseat Pressure: Not less than 100 psia

Fluid: Hydrogen vapor saturated at the upstream pressure

Nominal Operating Temperature: -423°F

Capacity: 5.5 lb/hr at 109 psia upstream pressure discharging to 1×10^{-6} mm Hg absolute downstream pressure.

Leakage: Less than 0.1 standard cc/sec when closed with an upstream pressure of 98.0 psia or less and a downstream pressure of 1×10^{-6} mm Hg absolute.

Operating Life: 150 days

2) Let-Down Valve

Inlet Pressure: 84 psia to 109 psia

Outlet Pressure: 43.4 ± 4.3 psia

Maximum Flow Rate: 5×10^{-4} lb/sec

Fluid: Hydrogen liquid, vapor or combination

Fluid temperature: $-423^{\circ}F$

Operating Life: 150 days

3) Tank Pressure Control Switch

Switch Closes: $84 + 0.5 - 0.0$ psia

Switch Opens: $87 + 0 - 0.5$ psia increasing

Medium Operating: Hydrogen vapor at $-65^{\circ}F$

Non-operating: Liquid and/or gaseous hydrogen at $-423^{\circ}F$

Contact Rating: 5 amps at 115V 400 cps non-inductive. The use of external relays will be considered.

Operating Life: 250,000 operations

d. Propellant Flow Controls

The propellant flow control components must withstand temperatures from $-423^{\circ}F$ to $+150^{\circ}F$ and the conditions outlined in Section II-B. The components will not be required to operate during periods of acceleration and vibration, but they must not be damaged by this environment.

1) Flow Controller (Reference Section II F-5 and Appendix H)

Maximum flow rate = 5×10^{-4} lbs/sec

Control accuracy = $\pm$ 10% full scale

Exit pressure = 1 atm.

Inlet pressure = 32.2 ± 1.6 psia

Inlet temperature = $540 \pm 5^{\circ}R$

Control current for maximum flow = 10 ma.

2) Flow Control Pressure Regulator

The performance specifications for the flow control pressure regulator are determined by the flow controller requirements.

Inlet Pressure: 38.6 to 47.2 psia

Discharge Pressure: 32.2 ± 1.6 psia

Maximum Flow Rate: 5×10^{-4} lb/sec

Fluid: Hydrogen gas

Fluid Temperature: $80^{\circ}F$

Operating Life: 150 days

3) Temperature-Stabilizing Heat Exchanger (Reference Section II F-6)

Inlet pressure: 40 - 90 psia

Discharge pressure: 40 - 90 psia

Maximum flow rate: 5×10^{-4} lb/sec

Inlet temperature: $43.6^{\circ}R$ - $51^{\circ}R$

Inlet quality: 0 - 100%

Outlet temperature: $540^{\circ}R \pm 5^{\circ}R$

4) Propellant On-Off Solenoid Valve

Normal Inlet Pressure: 38.7 to 47.3 psia

Maximum Allowable Working Pressure:	110 psi differential
Maximum Flow:	5×10^{-4} lb/sec
Fluid:	Hydrogen gas at $80^{\circ}F$
Maximum Pressure Drop:	0.10 psi

Minimum Operating Temperature: -423°F with liquid or gaseous hydrogen

Configuration: Normally closed power to open

Leakage Rate: 1) less than 0.10 standard cc/sec with upstream pressure of 110 psia and a downstream pressure of 1×10^{-6} mm Hg absolute when closed at 80°F.
2) less than 0.10 standard cc/sec with upstream pressure of 110 psia and downstream pressure of 1×10^{-6} mm Hg when closed at -423°F.

Power Supply: 115V 400 cps

Operating Life: 150 days

5) Line Pressure Relief Valve

Open Pressure: 105 psia

Reseat Pressure: Not less than 100 psia

Fluid: Hydrogen vapor saturated at the upstream pressure

Nominal Operating Temperature: -423°F

Capacity: 5.5 lb/hr at 109 psia upstream pressure discharging to 1×10^{-6} mm Hg absolute downstream pressure.

Leakage: Less than 0.1 standard cc/sec when closed with an upstream pressure of 98.0 psia or less and a downstream pressure of 1×10^{-6} mm Hg absolute.

Operating Life: 150 days

e. Monitoring Instrumentation

The performance specifications for the monitoring instruments are what we believe to be adequate for the purpose for which they are intended. However, it is realized that factors other than those considered in this

report will enter into the selection and specification of instrumentation.

The monitoring instrumentation will not be required to operate during periods of acceleration, shock and vibration. The instruments must, however, sustain the shock and vibration and acceleration environment without destruction.

1) Pre-launch Liquid Level Transducer

Pressure Range:	0-0.5 psi differential
Transducer Element:	Potentiometer
Resistance:	20,000 ohms
Linearity:	1% full scale
Temperature:	-65°F to +150°F

2) Pre-launch Pressure Transducer and In-Flight Pressure Transducer

Pressure Range:	0-125 psia
Transducer Element:	Potentiometer
Resistance:	20,000 ohms
Linearity:	1% full scale
Temperature:	-65°F to +150°F

3) Thermocouple Vacuum Gage Tube

Range: 0-50 torr

Vacuum gage tubes will not be required to operate during or after being subjected to shock and vibration. They must maintain a vacuum-tight seal at all times.

4) Liquid Level Sensors

Sonoswitch (or equivalent)

Manufactured by Powertron Ultrasonics Corp., Plainview, New York.

4. Component Availability

a. General

The components needed to meet the requirements of the control system are divided into three categories, graded in accordance with their relative availability. The first category contains components whose specifications are not critical, and manufacturer's catalogue data may be used. The second category contains components having performance requirements that are critical but whose development is not expected to extend the practice of selected manufacturers very far. The third group includes components that are unique to this control system, i.e., the flow controller and temperature-stabilizing heat exchanger. A separate discussion of these last items is given in paragraphs 5 and 6 following.

b. Standard Components

The components whose performance requirements are not critical and which may be selected from a manufacturer's standard line are:

Pre-launch liquid level transducer

Pre-launch pressure transducer

In-flight pressure transducer

Thermocouple vacuum gage tubes

Insulation vent and purge valves

c. Special Components

The components with critical performance requirements are:

Pre-launch pressure relief valve

Vent on-off solenoid valve

In-flight pressure relief valve

Tank pressure control switch

Let-down valve

Fill-line on-off solenoid valve

Line pressure relief valve

Propellant on-off solenoid valve

Flow control pressure regulator

To learn if these components are available or can be produced without a major extension of the state of the art, a survey was made of 38 manufacturers who might produce these components. The manufacturers were divided into two groups. The first group contains manufacturers of valves, pressure relief valves, and pressure regulators. In the second group are manufacturers of pressure switches. An inquiry letter with component specifications attached was sent to each manufacturer. The manufacturer was asked if his product met any of the attached specifications or if his product could be modified to meet these specifications. In addition, he was asked to state if he was interested in developing the components. The names and addresses of manufacturers in each group are given in Tables IV and V. Typical inquiry letters for each group are given on the pages immediately following.

As would be expected, the replies to the inquiry varied widely. The answers ranged from definite quotes for development or modification of products to no-interest replies because the specified components are outside the manufacturers normal product line with potential quantities too small to be of interest. Table VI lists the manufacturers who either stated they produce components which can be modified to meet the specifications or who indicated an interest in developing the components. Also listed in Table VI are the components in which the manufacturer is interested. No estimate has been made of the capabilities of the manufacturers listed in Table VI.

TABLE IV

MANUFACTURERS CONTACTED FOR PRESSURE REGULATORS, PRESSURE RELIEF VALVES, AND SOLENOID VALVES

Aerodyne Controls Corp.
90 Gazza Blvd.
Farmingdale, New York

Airesearch Division
Garrett Corp.
Phoenix, Arizona

Automatic Switch Co.
Florham Park
New Jersey

B. H. Hadley, Inc.
P. O. Box 31
Pomona, California

The Bendix Corporation
Friez Instrument Division
1400 Taylor Avenue
Baltimore, Maryland

The Bendix Corporation
Pioneer Central Division
Hickory Grove Road
Davenport, Iowa

Circle Seal Products Co., Inc.
2181 E. Foothill Blvd.
Pasadena, California

E. B. Wiggins Oil Tool Co., Inc.
E. Olympic Blvd. and Lorena Street
Los Angeles 23, California

Flodyne Controls, Inc.
1701 Elizabeth Avenue East
Linden, New Jersey

Flow Systems, Inc.
842 Production Place
Newport Beach, California

Grove Valve and Regulator Co.
6529 Hollis Street
Oakland 8, California

Hydromatics Inc.
7 Lawrence Street
Bloomfield, New Jersey

Minneapolis-Honeywell Regulator Co.
Aeronautical Division
2600 Ridgeway Road
Minneapolis 40, Minnesota

Pesco Products Division
Borg Warner Corp.
24700 North Miles Road
Bedford, Ohio

Pneu Hydro Valve Company
52 Horse Hill Road
Cedar Knolls, New Jersey

Reaction Motors Division
Thiokol Chemical Corp.
Denville, New Jersey

Stewart Warner Corp.
Southwind Division
1514 Drover Street
Indianapolis, Indiana

Valcor Engineering Corp.
365 Carnagie Avenue
Kenilworth, New Jersey

Vickers, Inc., Division
Sperry Rand Corp.
882 Willis Avenue
Albertson, New York

Whittaker Controls
9601 Canoga Avenue
Chatsworth, California

TABLE V

MANUFACTURERS CONTACTED FOR PRESSURE SWITCHES

Aero Mechanism Inc.
7750 Burnet Avenue
Van Nuys, California

Aerodyne Controls Corp.
90 Gazza Blvd.
Farmingdale, New York

Aerotec Industries, Inc.
Aircraft Equipment Division
Dept. W
Greenwich, Connecticut

Airwork Corp.
307 Sherman Avenue
Millville, New Jersey

American Gas and Chemical, Inc.
P. O. Box 101
Gracie Station
New York 28, New York

Aro Corporation of California
17110 Gale Avenue
City of Industry, California

The B. G. Corporation
321 Broad Avenue
Ridgefield, New Jersey

Baldwin-Lima-Hamilton Corp.
42 Fourth Avenue
Waltham, Mass.

Barton Instrument Corp.
580 Monterey Pass Road
Monterey Park, California

The Bendix Corp.
Friez Instrument Division
1400 Taylor Avenue
Baltimore, 4, Maryland

The Bendix Corp.
Montrose Division
Montrose, Pennsylvania

The Bendix Corporation
Pioneer Central Division
Hickory Grove Road
Davenport, Iowa

The Bristol Co.
P. O. Box 1290-A.W.
Waterbury 20, Connecticut

Crescent Engineering and Research Co.
5440 N. Peck Road
El Monte, California

Custom Component Switches, Inc.
21111 Plummer Street
Chatsworth, California

Fairchild Controls Corp.
225 Park Avenue
Hicksville, New York

Giannini Controls Corp.
1600 S. Mountain Avenue
Duarte, California

Grove Valve and Regulator Co.
6529 Hollis Street
Oakland 8, California

Metal Bellows Corp
604 Mica Lane
Wellesley Hills, Mass.

Minneapolis-Honeywell Regulator Co.
Aeronautical Division
2600 Ridgeway Road
Minneapolis 40, Minnesota

Reaction Motors Division
Thiokol Chemical Corp.
Denville, New Jersey

Robertshaw-Fulton Controls Co.
Fulton Sylphon Division
Box 400
Knoxville 1, Tennessee

TABLE V (continued)

Statham Instruments, Inc.
12401 W. Olympic Blvd.
Los Angeles 64, California

Stewart Warner Corp.
Southwind Division
1514 Drover Street
Indianapolis, Indiana

United Controls Corp.
P. O. Box 3104
Seattle, Washington

Vickers, Inc., Division
Sperry Rand Corp.
882 Willis Avenue
Albertson, New York

Whittaker Controls
9601 Canoga Avenue
Chatsworth, California

Wiancko Engineering
P. O. Box 5020
Pasadena, California

TYPICAL INQUIRY LETTER FOR PRESSURE REGULATORS, PRESSURE RELIEF VALVES, AND SOLENOID VALVES

Arthur D. Little, Inc., is currently engaged in the specification and design of a system which requires several pressure regulators, relief valves, and solenoid valves for the control of gaseous and liquid hydrogen. These components are for use as in-flight hardware in a space vehicle application and will be subject to the following environmental conditions:

Temperature	$-423^{\circ}F$ to $+150^{\circ}F$	
Pressure	1 atm to vacuum	
Acceleration (steady state)	6.5 g's	
Vibration	5-10 cps	3 g's
	10-400 cps	4 g's
	400-3000 cps	7.5 g's

The performance specifications for individual components are given on the attached sheets.

Please send me data sheets or other literature and price information for any of your products which will meet the requirements specified. If your product can be modified to meet the specifications, please state an approximate price for the modified component and include a brief statement of the modifications necessary.

The specifications for the components required are such that a development effort may be necessary. If you are interested in developing these components, I would appreciate your indicating to me your estimate of the development effort required.

Very truly yours,

TYPICAL INQUIRY LETTER FOR PRESSURE SWITCHES

Arthur D. Little, Inc., is currently engaged in the specification and design of a system which requires a pressure switch. This switch will be employed to sense the pressure of liquid and/or gaseous hydrogen. The switch is for in-flight use in a space vehicle application and will be subject to the following environmental conditions:

Temperature	$-423^{\circ}F$ to $+150^{\circ}F$	
Pressure	1 atm to vacuum	
Acceleration (steady state)	6.5 g's	
Vibration	5-10 cps	3 g's
	10-400 cps	4 g's
	400-3000 cps	7.5 g's

The performance specifications for the switch are given on the attached sheet.

Please send me data sheets or other literature for any of your switches which will meet the requirements specified. If your product can be modified to meet the specifications, please state an approximate price for the modified component and include a brief statement of the modifications necessary.

The specifications for the switch required are such that a development may be required. If you are interested in developing these switches, I would appreciate your indicating to me your estimate of the development effort required.

Very truly yours,

TABLE VI

MANUFACTURERS INDICATING INTEREST IN SUPPLYING COMPONENTS FOR HYDROGEN SYSTEM

	Pre-Launch Pressure Relief Valve	In-Flight and Line Pressure Relief Valves	Vent On/Off Solenoid Valve	Propellant On/Off Solenoid Valve	Let Down Valve	Flow Control Pressure Regulator	Tank Pressure Control Switch
Aerodyne Controls Corp.	x	x	x	x	x	x	x
Aero Mechanism, Inc.							x
B. H. Hadley, Inc.	x	x			x	x	
Bendix Corp. Montrose Division							x
Circle Seal Pro. Co.	x	x	x	x			
Custom Component Switches, Inc.							x
Pesco Products Div. Borg Warner Corp.	x	x	x	x	x	x	
Reaction Motors Div. Thiokol Chemical Corp.	x	x	x	x	x	x	
Valcor Eng. Corp.			x	x			
Whittaker Controls	x	x			x	x	
Wiancko Engineering							x

5. Flow Controller

The flow of propellant gas to the arc jet engine is modulated according to propulsion requirements by the flow controller. Figure 10 is a schematic diagram which illustrates the principles of operation of the flow controller. Gas at constant temperature and pressure enters the controller through the inlet, passes through the metering orifice and leaves the controller through the control orifice to be delivered to the engine.

As the gas passes through the metering orifice, the pressure decreases. The difference in gas pressure between the upstream face and the downstream face of the piston produces a force which moves a plug into the control orifice. As the plug moves into the orifice, the orifice area decreases and gas flow is reduced. A decrease in gas flow causes a decrease in the pressure differential across the faces of the piston. When a control force is applied, the plug is withdrawn from the control orifice. The increased gas flow creates a pressure differential across the piston which counteracts the control force. The orifice plug is moved until the pressure difference acting on the piston balances the control force applied.

The control force is provided by an electromagnet which develops a force that is proportional to the square of the control current applied. This square relationship between control force and control current when combined with the square root relationship between flow rate and control force results in a device with a gas flow rate which varies linearly with control current.

The action of the flow controller is based upon balance of two opposing forces. Any other forces, such as spring forces or friction forces which are present in the controller will upset this balance and introduce an error

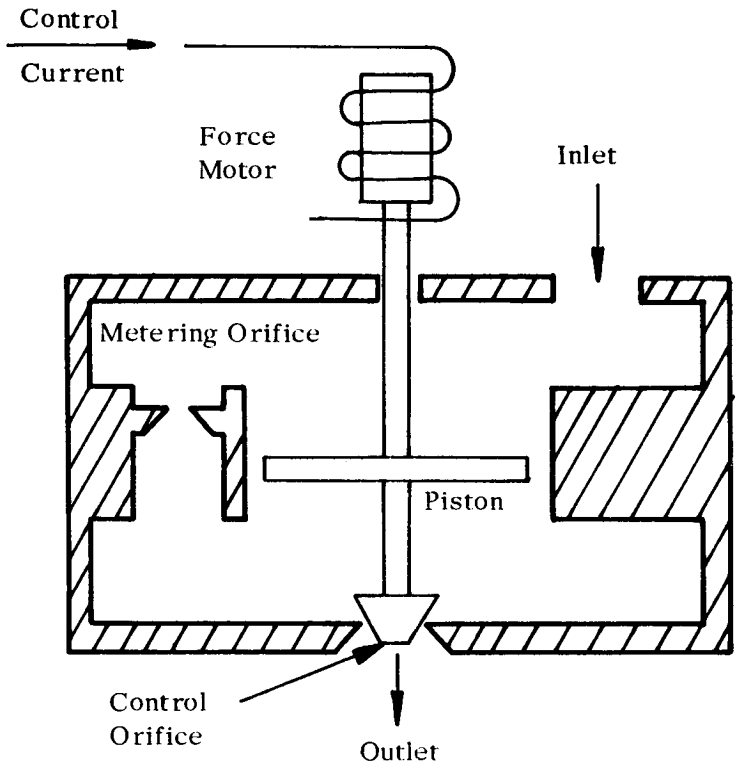

FIGURE 10 SCHEMATIC DIAGRAM OF FLOW CONTROLLER

in the control. It is important that care be employed in the mechanical design of the flow controller to reduce these forces to a minimum. In addition, of course, the controller must be designed to withstand the vibration and accelerations during the launch phases of the flight. It will not, however, be called upon to operate within specification at that time.

The major design characteristics for the flow controller are summarized in Table VII. A more complete discussion of the flow controller, operation, and design will be found in Appendix H.

6. Temperature Stabilizing Exchanger (TSX)

The purpose of the TSX is to bring the hydrogen feed stream to the proper temperature level regardless of variations in inlet conditions. An outlet temperature of 540°R is selected to correspond approximately to the expected equilibrium temperature of the feed stream piping between the TSX and arc-jet so that heat transfer subsequent to the TSX is minimized. However, the selection of 540°R is at this time fairly arbitrary and could be changed to accommodate special requirements of the arc-jet or parent vehicle. To be consistent with the passive expulsion system described in Section II-E, the TSX should maintain the proper discharge temperature with any inlet condition varying from saturated gas to saturated liquid. The heat addition required to warm the feed stream to 540°R is not vastly different for saturated vapor and saturated liquid inlet conditions, due to the high specific heat of the gas. The enthalpy increase in going from saturated vapor at 43°R to gas at 540°R is 1730 Btu/lb, while that going from saturated liquid to gas at 540°R is 1920 Btu/lb, only some 11 percent more. If the TSX is designed

to accept saturated liquid, its performance on saturated gas would then be essentially the same. For the propellant flow rate of 5×10^{-4} lb/sec, the total heat input with liquid feed is 3450 Btu/hr. Of course, it is conceivable that a portion of this heat could be supplied by direct exchange with parts of the parent vehicle, but this option has been dismissed in favor of making the feed system operation independent.

As previously pointed out, it is convenient to use a constant wall temperature heated tube as a metal-to-gas heat exchanger to facilitate maintaining constant discharge temperature. The tube would be wrapped with heater

TABLE VII

DESIGN PARAMETERS OF FLOW CONTROLLER FOR HYDROGEN GAS

Quantity	Value
Flow Rate, Maximum	5×10^{-4} lbs/sec full scale
Accuracy of Control	$\pm$ 10 percent of full scale
Inlet Pressure, P_o	32.2 ± 1.6 psia
Inlet Temperature, T_o	$540 \pm 5^{\circ}R$
Outlet Pressure, P_e	Approximately 1 atm
Maximum Control Orifice Area, A_o	3.95×10^{-3} in^2
Metering Orifice Area, A_o	1.68×10^{-2} in^2
Piston Area, A_b	4 in^2
Maximum Input Control Current	10 ma
Winding Resistance at $20^{\circ}C$	2270 ohms

wire and the winding density varied so as to distribute the heat flux in accordance with the local stream temperature and maintain an essentially constant wall temperature. Design calculations show that a heater tube with 0.31-inch I.D. x 180 inches long provides enough surface area to warm the feed stream to within $1^{\circ}R$ of the tube wall temperature, with a pressure drop of approximately 0.16 psi. The temperature of the tube at the discharge end would be monitored by a thermal sensing element and used to control the power input to the heater winding. A tube with a 1/2-inch O.D. would weigh just under 3 pounds and would provide enough thermal inertia that a simple on-off control can be used without excessive cycling. Since the design maintains the gas temperature within one degree of the tube temperature, the tube temperature can fluctuate by $\pm 4^{\circ}R$ and still maintain the absolute temperature of the discharge gas within $\pm$ 1% of the desired value. This temperature interval is consistent with the use of an on-off control system and would result in about two on-off cycles per minute. The total weight of tube, heater and controls should not exceed 10 pounds.

7. Power Requirements

The average electric power drain during hydrogen arc-jet operation is approximately 1060 watts. Of this total, 50 watts is consumed by the internal tank heater and 1010 watts by the TSX, (subject to the qualifications stated in paragraph 6, preceding). The peak power requirements during arc-jet operation are approximately 1600 watts. The increase over the average is due to the demand of the off-on heater control. Peak power requirements for all other in-flight feed system control elements total 1.75 watts. This latter figure also corresponds to the maximum standby power requirement.

G. PROJECTED SYSTEM OPERATION

This section describes the operational characteristics of the hydrogen arc-jet feed system. It outlines the sequence of events experienced by the system during the projected mission and discusses the projected mode of operation of its components. The control elements and automatic features included in the system were selected to program the sequence of operations along the predetermined schedule. In some cases, control signals must originate external to the arc-jet feed system.

1. Fabrication

During fabrication of the tank shell, the thin sheets which comprise the shell will have to be supported by jigs and fixtures at all times. After the closing weld has been made on the tank, it must either be physically supported or pressurized to about 5 psig in order to prevent the shell from buckling. After the shell has been closed, it must be pressure-tested and vacuum leak-tested. Since the tank will be operated at a pressure at which the stresses in the tank wall are very close to the maximum allowed by a fracture toughness analysis, pressure cycling of the tank must be avoided, and pressure testing must be performed a minimum number of times.

A logical pressure-testing sequence might be as follows: Pressure test at a stress level close to the maximum allowable stress level to determine the pressure-retaining capabilities of the shell; helium leak test at ambient temperature using a low helium pressure inside the tank; and then helium leak test at tank operating temperature, using low helium pressures inside the tank. Next, perform the remaining fabrication operations; apply insulation, attach piping, etc. Following the complete fabrication of the insulated tank, a boil-off test in a vacuum chamber is recommended to check the insulation system, since the effectiveness of this system is a strong function of the care that was taken in its installation. At the completion of the boil-off test, the tank and feed system are ready to be incorporated in the entire vehicle.

2. Transportation

Since transportation may impose more severe loadings on the system than will be encountered in operation, extreme care must be exercised in the shipment of the vehicle to the launch facility. Probably the best approach is to package the entire vehicle in a container which will isolate it from acceleration and shock loadings. It may be transported with its axis in the horizontal plane while supported from the support ring on the tank. Again, there must be adequate safeguards to insure that the five-pound internal pressure is always maintained.

3. Pre-Launch

After the arc-jet vehicle has been installed on top of the booster but several days prior to launch, it is desirable to conduct a final leak test on the hydrogen tank vessel. This test is in the nature of a go-no-go test and is designed to reveal any leaks in the tank shell of a size which would jeopardize the mission. This test will be conducted by purging the space between the Mylar sheath and the tank wall with carbon dioxide. The carbon dioxide at approximately atmospheric pressure is introduced into the insulation space through the insulation purge line and flows around the aft head, through purge holes in the tank support ring, around the shell and forward head of the tank, and out the insulation vent valve. After all other gases have been eliminated from the insulation space, the insulation purge and vent valves are closed and the tank will be partially filled with liquid hydrogen until the entire tank wall is at liquid hydrogen temperature. This will cause all gases except hydrogen and helium to condense by the cryopumping action of the tank wall and will create a vacuum in the insulation space. If there

is a hydrogen leak in the tank wall, the hydrogen which leaks into the space will not be cryopumped, and the pressure in this space will rise at a rate proportional to the size of the hydrogen leak. By monitoring the pressure rise in this space as a function of time, the magnitude of any leaks may be determined. If there are no leaks in the tank shell or if there are leaks smaller than those which would jeopardize the mission, the hydrogen will be drained from the tank, and the tank will be allowed to warm up. If there are leaks greater than the maximum allowable, the entire tank will have to be removed and replaced with one which passes the above test.

Prior to the start of the final filling operation, the insulation space must be purged with carbon dioxide, as in the pre-launch checkout. The tank is then filled with hydrogen in an operation which will take about 4-1/2 hours using a hydrogen flow rate of 1500 lbs/hr. This rate was used in sizing relief valves, fill lines, etc. During the initial phases of filling, while the tank is cooling down to liquid hydrogen temperature, the fill rate will have to be considerably lower than this in the range of 300 lbs/hr. The cooldown of the tank will take about a half hour, after which time hydrogen may be added to the tank at the full rate of 1500 lbs/hr. Since there will be a boil-off rate of approximately 500 lbs. of hydrogen an hour, while the tank is at ground level, the net hydrogen accumulation in the tank during the fill operation is 1000 lbs/hr. Since the tank holds approximately 4000 lbs. of liquid hydrogen, the filling operation will take about four hours. During the tank filling operation, tank pressure and hydrogen liquid level may be monitored with the instrumentation provided. After the liquid level in the tank reaches the required level, topping will be controlled by the

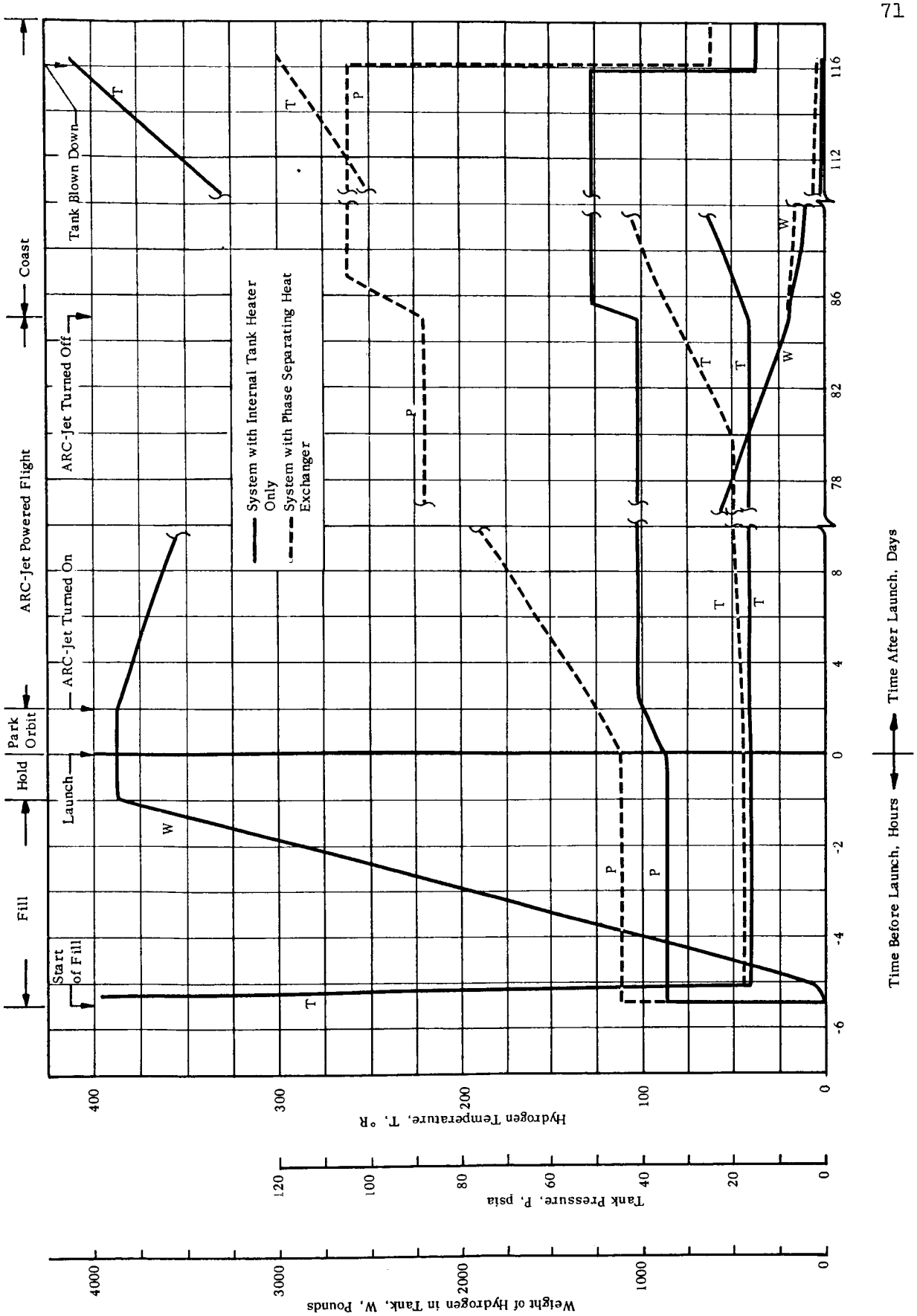

FIGURE 11 WEIGHT, PRESSURE, AND TEMPERATURE PROFILE OF HYDROGEN STORAGE

6. Transfer Trajectory

At the start of the transfer trajectory the temperature stabilizing control is turned on and a command signal is fed to the flow controller. After the temperature-stabilizing control has reached operating temperature, the propellant on-off solenoid valve is opened, and the system becomes operative. At this point, the internal tank here is also actuated and is controlled by the tank pressure control switch. During the early phases of transfer orbit, the tank heater will be on continuously until the tank pressure has been increased to the normal operating pressure. From this point on, the pressure and temperature of the propellant in the tank will remain constant, and the quantity of propellant decreases linearly with time. Several days before the end of the propulsion period the last bit of liquid in the tank is evaporated. After this time the tank heater continues to operate to keep the tank pressure up, and the tank temperature increases gradually. At the end of the 85-day propulsion period, the temperature-stabilizing control is turned off, the tank heater is turned off, and the propellant on-off solenoid valve is closed. At this point there will be about 205 pounds of gaseous propellant in the tank.

7. Coast

During the coast phase, heat leakage into the tank serves to increase the tank pressure and temperature. After several days the pressure has increased to the point where the in-flight pressure relief valve opens. From this point on, this relief valve serves to hold the tank pressure at the maximum allowable working pressure by venting propellant as its temperature rises. Therefore, the amount of available propellant reserve decreases with increasing time, as may be noted in Figure 11 (The topic of propellant

liquid level sensors in the top of the tank. These sensors will control an on-off valve in the hydrogen fill line to maintain the required liquid level during the entire hold operation.

The pre-launch pressure relief valve is set to control the tank pressure during the entire fill and hold sequence. This pressure will be in the range of 35 psia for the system with the internal heater only, and 45 psia for the alternate system. Due to the agitation of the fluid, the hydrogen liquid will be saturated at this pressure. The pressure and temperature of the propellant and the amount of propellant in the tank as a function of time during the entire mission are shown in Figure 11 for both systems. The sequence of events during the fill operation and during subsequent phases of the mission may be noted from this figure.

Immediately prior to launch, the vent on-off solenoid valve is closed, removing the pre-launch pressure relief valve from the system, the fill line on-off solenoid valve is closed, and all quick-disconnect fittings are uncoupled.

4. Ascent

During the early phases of the ascent, the tank will be subject to the high ground level heat-leak rates. This heat inleakage will cause boiling of some of the hydrogen which will increase the pressure in the bottled-up tank. This pressure increase will effectively subcool the liquid and suppress further boiling and pressure rise for the short length of time the vehicle is at low altitudes. During ascent the tank is subjected to some aerodynamic heating. The amount of this heating is small and the tank pressure and temperature will remain essentially unchanged due to it.

As the vehicle ascends through the atmosphere the ambient pressure will soon drop to the point where it is equal to the pressure between the Mylar sheath in the insulation space and the tank wall. At this point, the tubular clamping rings at the after end of both sheaths will be released and the space between the sheath and the tank will communicate with the environment through the holes in the sheath. This is done to prevent the pressure inside the sheath from rising above the ambient pressure thus causing the sheath to bulge and possibly rip or become damaged.

5. Parking Orbit

After the high acceleration forces of launch are over, the net system holding the sheath against the tank is released. This is done by melting the fusable links in the cords holding the net system together. At the same time, integral tubular passages in the sheath are inflated with a slight positive gas pressure, causing the sheath to expand to its full diameter, completely enclosing the hydrogen tank and standing off from it a distance of three or four inches.

After injection of the vehicle into parking orbit, the heat leak through the insulation penetrations, etc., will be around the design value of 50 watts. During the 48-hour parking orbit period, this heat leak will result in a slight increase in tank pressure, as shown in Figure 11. It will be noted from this figure that, at the end of parking orbit, the tank pressure is still not up to operating pressure. Toward the end of the parking orbit, when power is available from the reactor and the telemetering system has been turned on, the tank pressure may be monitored from the ground from signals generated by the in-flight pressure transducer.

reserve is discussed in more detail in Appendix A). The system may be re-actuated at any time during the coast period by turning on the tank heater control, the temperature-stabilizing control, by opening the propellant on-off solenoid valve, and feeding a command signal to the flow controller.

III. AMMONIA FEED SYSTEM

A. INTRODUCTION

A thermal arc-jet system using ammonia as a propellant is considered as a competitive alternate to a hydrogen fuel system. Although a higher specific impulse is achieved with hydrogen, the low density of liquid hydrogen necessitates large storage volumes and the low storate temperature presents a stringent requirement for an extremely effective thermal protection system. Advanced thermal insulation systems are presently under development, but the predicted performance of advanced concepts remains to be proved. A feed system using ammonia with its high liquid density, latent heat and conventional operating temperature range presents fewer development problems and, consequently, is seriously considered for first generation arc-jet operations.

B. BASIS FOR DESIGN

The mission parameters for the ammonia system, as specified by NASA, are presented in Table VIII.

TABLE VIII

MISSION PARAMETERS FOR AMMONIA FEED SYSTEM

Power	30 kw
Impulse	750 sec
Propellant Wt. Flow	8.82×10^{-4} lb/sec
Pressure to Arc Chamber	1 to 2 atmos.
Weight Flow and Pressure Tolerance	$\pm$ 10%
Propulsion Time	60 days
Stay Time	90 days
Propellant Reserve	3 weight %

The mission consists of a launch to a 500 nautical mile parking orbit where the vehicle remains for about forty-eight hours. Then the arc-jet system is started up and utilized to propel the vehicle from the parking orbit to a 22,400 nautical mile, twenty-four hour, synchronous final orbit.

The vehicle weight is 8500 pounds, the maximum steady acceleration on the system is a 6.5 g loading encountered during the launch phase. The maximum lateral loading is expected to be 1.5 g. Prior to launch, up to a six-hour hold time on the ground may be required. One other requirement is that the propellant tankage must fit within a ten-foot diameter cylindrical envelope.

Since a complete and final mission profile has not been established and since some configurational details of the space vehicle are still uncertain (for example, the orientation of the radiators with respect to the propulsion and payload package has not yet been established) our

system design is based on reasonable assumptions in areas where definite specifications are not available.

C. SYSTEM DESCRIPTION

The ammonia system is shown schematically in Figure 12. It consists of a storage tank, an expulsion and metering system, and auxiliary instrumentation and controls. The flow circuit, and the instruments and controls are functionally identical to those in the hydrogen system so they will not be discussed further here. There is no insulation on the tank. It should be noted that the direction of launch and the direction of thrust during arc-jet powered flight are in different directions, accounting for some of the components being located in different positions than in the hydrogen system.

The over-all assembly of the system is shown in Figure 13. The tank itself is a toroid supported on a conical member and is shown in detail in Figure 14. It has eight reinforcing ribs welded to it, 45 degrees apart, and two aluminum ribs riveted between each pair of reinforcing ribs. The Mylar meteorite bumper is bonded around the outside of the ribs, completely enclosing the tank. The bottom end of the support cone connects to the main structure of the vehicle in a de-mountable joint which may be used as the point of separation of the arc-jet vehicle from the previous stage.

The elements of the metering and control system are mounted on the tank support cone. The electrical components of this system are contained in a hermetically-sealed and pressurized junction box. The tank heater and the inlet tube for the expulsion system are located in the tank so

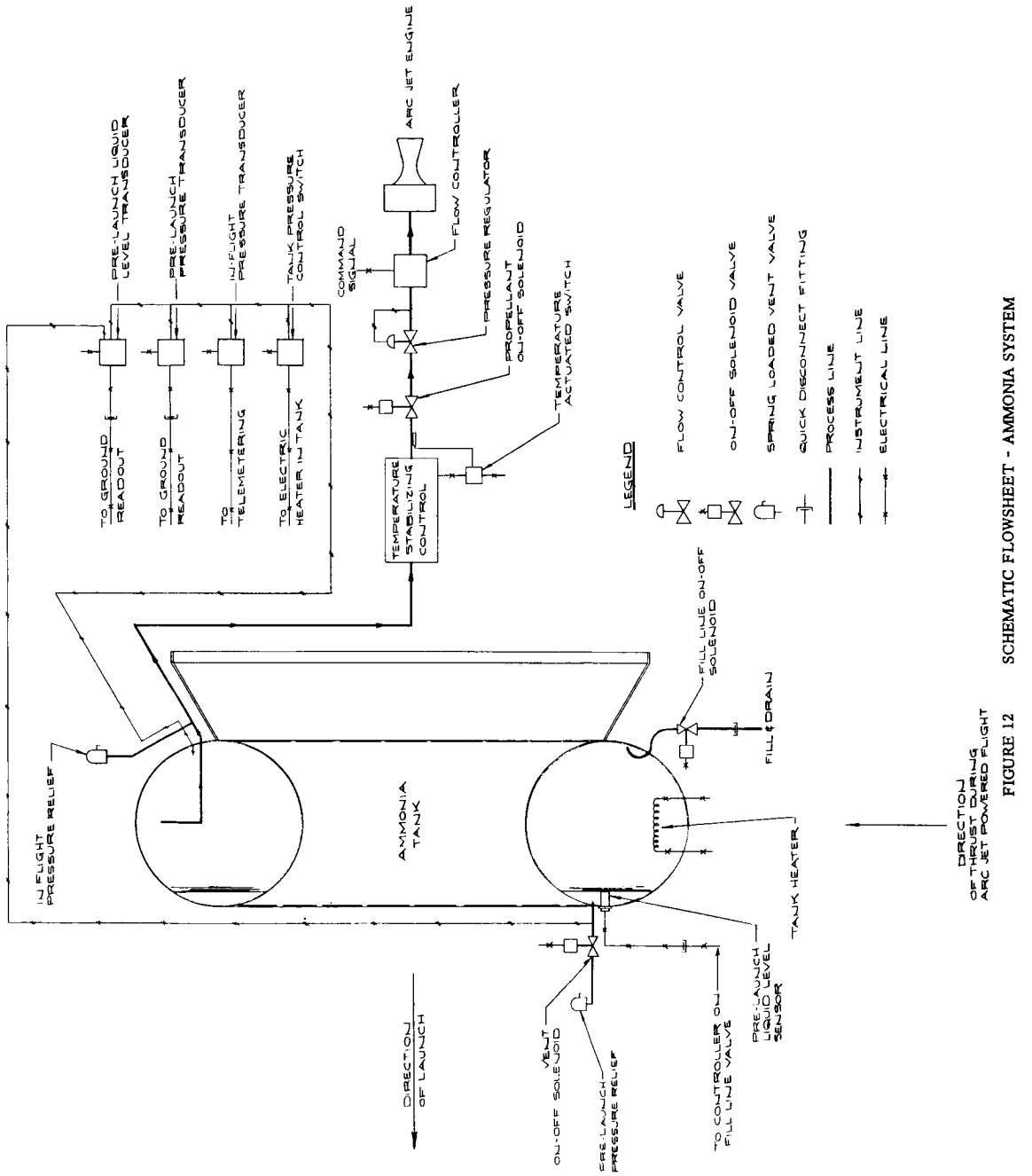

FIGURE 12 SCHEMATIC FLOWSHEET - AMMONIA SYSTEM

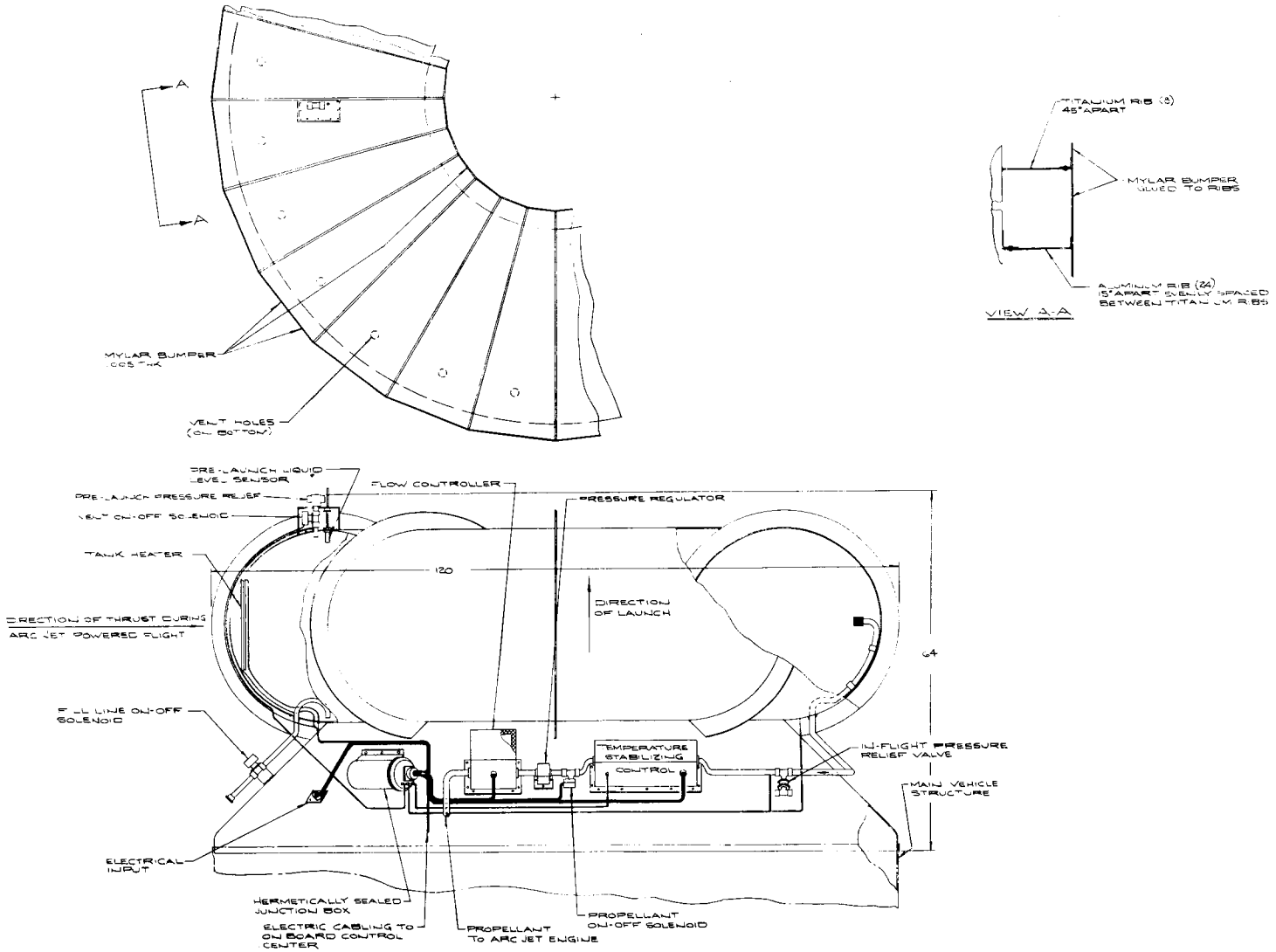

FIGURE 13 OVER-ALL ASSEMBLY - AMMONIA SYSTEM

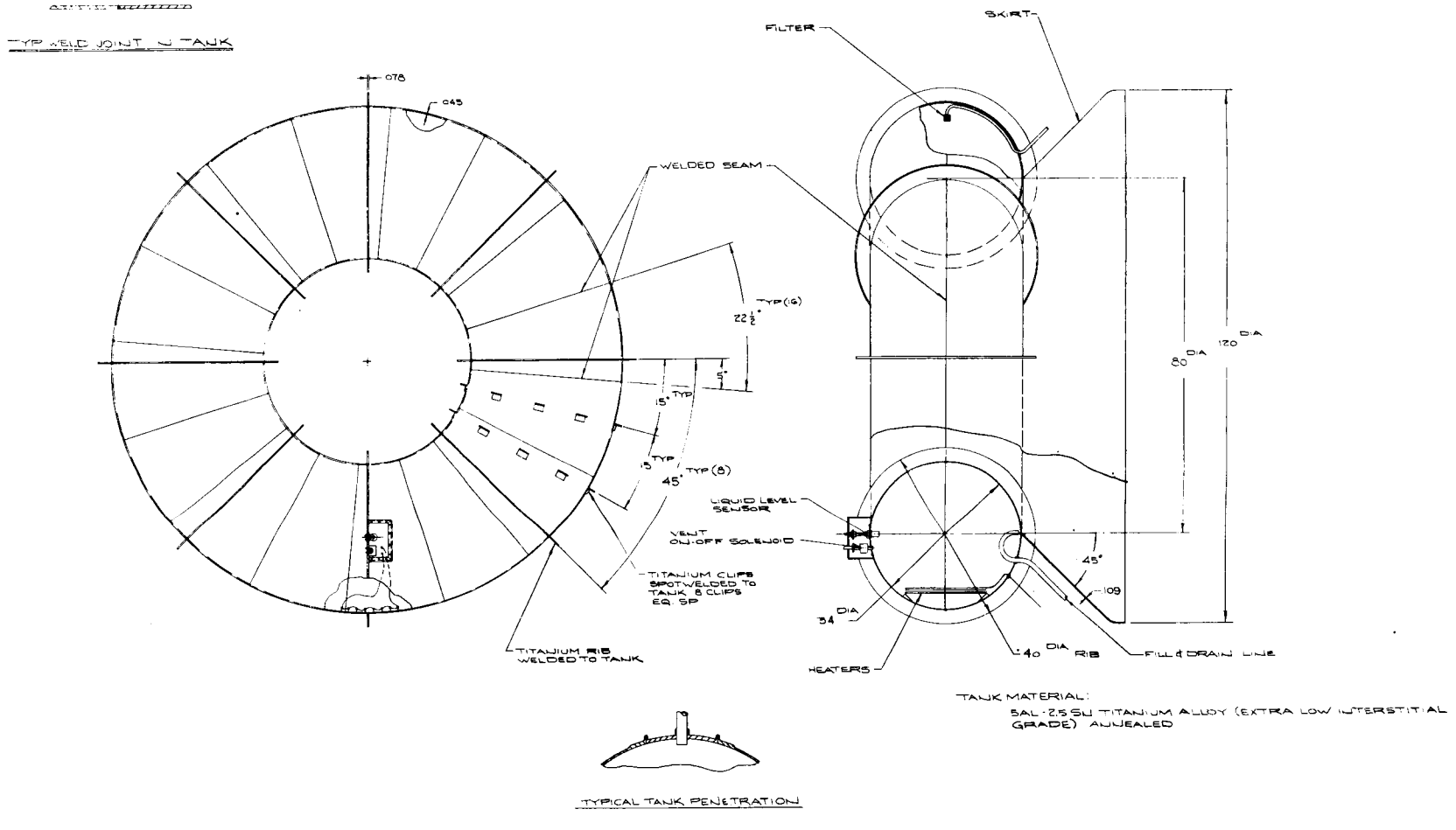

FIGURE 14 SHELL ASSEMBLY - AMMONIA TANK

that during arc-jet powered flight they are in the liquid and vapor phases respectively. Other items are located as shown on the flowsheet. Other components of the arc-jet vehicle, e.g., payload, may be placed in the void volumes within the over-all tank envelope. The over-all system weight is 433 lbs, as is shown in the weight breakdown in Table IX.

D. THE STORAGE VESSEL

1. Capacity and Pressure Requirements

The vessel capacity is based on the design flow rate of 8.82×10^{-4} lbs/sec of ammonia over a 60-day propulsion period. A 3-percent propellant reserve is added, as is a leakage allowance of 10 pounds of ammonia and a 20-pound allowance for residual unrecoverable gas in the vessel at the end of the mission. Therefore, the design weight of propellant is 4740 pounds.

The stored fluid, under saturation conditions, will occupy the maximum volume at the maximum system pressure. Therefore, an upper limit must be set on storage pressure before a design volume can be selected. For reasons outlined in Section III-F we have set a nominal storage vessel operating pressure at 80 psi and, after allowances are made for the operating range of a pressure relief valve, a maximum allowable working pressure of 100 psia for the tank.

At 80 psia, the 4740 pounds of liquid occupy a volume of 121 ft^3 and at the maximum pressure of 100 psia, they occupy 122.5 ft^3. We have selected a design volume of 130 ft^3 which allows for a 5 percent ullage at the operating pressure, plus an additional 3 ft^3 for the structure and heat transfer surfaces which may be placed within the tank.

TABLE IX

AMMONIA SYSTEM WEIGHT BREAKDOWN

Item	Weight
Ammonia Tank and Reinforcing Ribs	227 lbs.
Support Cone	157
Miscellaneous Structure	13
Piping and Valving	8
Instrumentation and Controls	13
Meteorite Bumper	15
Total Tank and Expulsion System	433 lbs.
Ammonia in Tank at Lift-off	4740
Total System at Lift-off	5173 lbs.

2. Thermal Balance

During the voyage from parking orbit to synchronous orbit, the vehicle will encounter conditions of variable heat exchange with its surroundings. Initially, radiation inputs to the vessel from the space environment will include earthshine, albedo, and sunshine which will vary as the vehicle spirals outward from the earth as a result of periodic shadowing. During the last half of the mission, the thermal balance between the vehicle and the universe is no longer appreciably altered by the earth's shadowing effect.

Heat transfer between other portions of the craft and the tankage merit consideration. Heat exchange with the SNAP-8 and payload radiators can be minimized by orienting them to have a minimum view factor with the tankage, and by the use of shadow shields. Heating due to gamma radiation from the SNAP-8 should also be controlled by means of deployment of the power plant and shielding.

The surface of the ammonia vessel is designed so that there is no appreciable net heat exchange with its environment at a surface temperature of $45^{\circ}F$. For an adiabatic surface temperature of $45^{\circ}F$ coatings having emittances and absorptances values in a practical range are called for. A specific storage vessel and vehicle integration can be provided with surface coatings such that the wall temperature is maintained approximately constant at $45^{\circ}F$. Use of black surfaces for the exterior surface of the tank and the interior surface of the meteoroid bumper and a black and white checkerboard painted surface on the outward facing surface of the bumper is appropriate for this purpose.

Fluctuations in the temperature (and hence pressure) of the stored ammonia which would take place as a result of variations in the heat exchange with the environment will be compensated by varying the power input to the tank pressure control heaters.

Further configurational details are necessary for an accurate thermal design but the problems presented by the need for thermal control of the tankage system are not of a critical nature.

3. Meteoroid Protection

The assessment of the requirements for protection of the ammonia tank from meteoroid damage find their substance in the evaluations of Appendix D.

The vulnerable exposure factor for the ammonia tank is about 1.3×10^{3} meter^{2}-days. As in the case of the hydrogen vessel we conclude that the ammonia vessel having a minimum wall thickness set by structural requirements needs protection against meteoroids. The meteor bumper concept offers protection at minimum weight penalty and is adopted.

Based on the nomogram (Figure D1 of Appendix D) a probability of no failure in the range of 50 to 98 percent is provided by protecting against meteoroids less than 2×10^{-4} grams. By protecting against meteoroids less than 2×10^{-3} grams, the probability of no failure is increased to the 93 to 99.8 percent range.

Following the argument of Appendix D we reason that a 5 mil mylar bumper or equivalent spaced 3 or 4 inches from a 0.020 or 0.010-inch thick second skin will provide the measure of protection required. We have added .020-inch to the pressure shell of the propellant storage tank to serve the dual purpose of providing meteoroid protection and of stiffening the primary

structure. If we adopt a less conservative view (allowable due to the uncertainties of present knowledge) and stipulate that some combination of a 5-mil bumper and a 10-mil second skin can provide the needed protection against meteoroids, a weight saving of some 60 pounds results for the toroidal tank.

4. Structural Design

The vessel for the ammonia propellant system must be constructed of a metal which has a high strength per unit weight in the region of -30°F temperatures. Many materials were investigated. Selection was narrowed down to three metals:

a) Annealed 5 Al-2.5 Sn titanium alloy with extra low interstitial content,

b) AISI 301 stainless steel, and

c) 2014-T6 aluminum.

The titanium alloy was chosen primarily because of its higher stress to weight ratio, as shown in the table below; however, it may be argued that protection against the meteoroid hazard may actually be the design criterion for minimum tank weight, in which case the proper selection is not clear.

TABLE X

SOME PROPERTIES OF HIGH STRENGTH MATERIALS FOR THE AMMONIA VESSEL

Metal	ρ - Density (lb/in^3)	σ - Tensile Strength at -30°F (lb/in^2)	σ/ρ
Titanium (5Al-2.5 Sn)	0.162	122,000	760,000
Aluminum (2014 T-6)	0.096	63,500	662,000
Stainless Steel (AISI 301)	0.29	168,000	580,000

Two tank concepts were considered: the toroidal and the spherical. These designs were compared on the basis of the following preliminary specifications:

Capacity	4740 lbs LNH_3
Tank working pressure	100 psia
Size	130 cu. ft. volume (which includes 6 cu. ft. for 5% ullage).

The toroidal tank was selected over the spherical for two reasons. First, the torus has a lower center of gravity (desirable during launch) and, second, the toroidal configuration lends itself to the design of a compact, launchable arc-jet and payload system.

The weights of the two tanks were not a deciding factor in our selection. These weights are tabulated below:

TABLE XI

WEIGHT COMPARISONS FOR A TOROIDAL AND SPHERICAL AMMONIA TANK

Torus	Weight
Shell - .045" shell thickness which includes .020" for meteoroid protection	194 lbs.
Rings - 8 required 3" x .078" thick	33 (total for 8)
Support - cone frustum .109" thick	157
Total Weight:-	384 lbs.

Sphere	Weight
Shell - .036" shell thickness which includes .020" for meteoroid protection	106 lbs.
Support - cone frustum .109" thick	226
Total Weight:-	332 lbs.

We expect the weight penalty of 50 pounds associated with the toroidal tank to be substantially reduced if not eliminated in a comparison of the weights of an integrated design of the tank-vehicle system.

The maximum stresses in the toroidal tank due to the internal pressure, occur at the minimum radius of the figure of revolution. These stresses determined the shell thickness. The minimum shell thickness is calculated using a maximum allowable working stress equal to 91 percent of the yield strength of the tank material. To keep the vessel supported during launch at 6.5 g requires eight equally-spaced rings (see Figure 14). The stress limits in the tank wall due to internal pressure and the size and weight of the stiffening rings are lessened when .020" is added to the shell thickness for meteoroid protection.

The support system for both tanks is a frustum of a cone. The required thickness was determined by the theoretical expression for the critical load at which buckling occurs in a thin wall cone,

$$t = \sqrt{\frac{P \times 3\,(1 - \nu^2)}{2\pi\, E \cos^2 \alpha}}$$

where E is Young's modulus, ν is Poisson's ratio for the support materials, P is the load to be supported by the cone in pounds and α is the

semi-vertex angle of the cone - in this case 45 degrees. The theoretical thickness obtained was then doubled since tests indicate that the actual thickness required to prevent budkling is approximately twice the theoretical value. In addition, to compensate for vibration and other unknowns, a factor of safety of 1.5 was used.

The support cone of the sphere weighs more than that for the torus because the cone slant height has to be longer to reach the ten-foot vehicle diameter.

E. EXPULSION SYSTEM

1. Requirements

Since the ammonia can be stored in thermal equilibrium with the storage tank, at only nominal pressure levels, the problem of excessive pressure rise resulting from heat inleakage from the surroundings does not exist. Thus, during the parking orbit vapor venting to maintain constant tank pressure would not be required. Since pressure build-up due to heat leak from the surroundings is not a problem, either vapor or liquid may be withdrawn from the storage tank. If vapor is withdrawn, heat will have to be added to the fluid remaining in the storage tank to maintain its pressure and temperature (and the thermal equilibrium with the tank). If liquid is withdrawn, the heat required for vaporizing it would be supplied external to the tank, in the temperature-stabilizing heat exchanger. It will be convenient to withdraw the same phase throughout most of the mission and to know in advance which phase will be withdrawn.

2. Passive System

As with hydrogen, it is possible to rely on the acceleration field produced by the thrust of the arc-jet engine to separate the phases and provide means for establishing the disposition of the liquid in the storage tank. The thrust of 0.66 pound acting on the vehicle mass of 8500 pounds results in an acceleration field with $\frac{g}{g_o} = 7.77 \times 10^{-5}$. Using as the characteristic dimension the 34-inch diameter of the torus, the Bond Number in this acceleration field is about 15, indicating that acceleration field forces would be dominant. The fluid disposition would be expected to be as shown in Figure 15. The curvature of the interface between liquid and vapor due to surface tension effects (i.e., the fluid wetting the walls) would be somewhat more pronounced than with hydrogen due to the lower Bond Number. However, the interface would still be an essentially flat surface. The configuration shown in Figure 15 is the equilibrium disposition of the fluid which should be reached within a few minutes after initiation of thrust by the engine. During that time, as the fluid moves toward its equilibrium position, some liquid might be withdrawn. Therefore, the temperature-stabilizing heat exchanger should be designed to accept liquid for short periods of time.

3. Active System

As previously noted, the ammonia storage vessel is designed so that it is in near thermal equilibrium with its environment. Therefore, the effect of withdrawal of liquid or vapor from the tank on its thermal

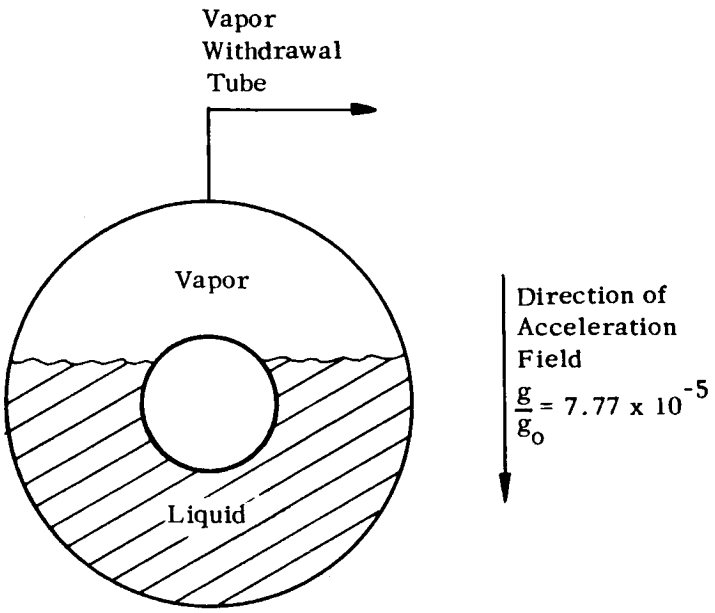

Bond Number = 15

FIGURE 15 AMMONIA DISPOSITION DURING ARC-JET POWERED FLIGHT

protection system is not an issue and a satisfactory feed system can be designed to handle both phases.

The only apparent value of a positive phase-separating device would be that it would reduce the temperature control requirements for the temperature-stabilizing heat exchanger during periods when, for any reason, phase-separation by passive means is not accomplished. As these control requirements do not present much of a problem, we see little value in the use of a positive phase-separating device for the ammonia system.

F. METERING AND CONTROL SYSTEM

1. System Description

The components of the ammonia feed control system are shown in the schematic flowsheet, Figure 12. The purpose and function of each component shown is identical to the corresponding component of the hydrogen feed system, and in the interests of brevity there will be no further discussion of these components here.

2. Component Specifications

The difference between the ammonia and hydrogen feed control systems lies in the performance specifications for the control components. As in the case of the control system for the hydrogen feed system all components with the exception of the in-flight pressure transducer will not be required to operate during periods of shock, vibration, and acceleration. The components will, however, be required to withstand without damage the specified shock, vibration and acceleration attendant to ground handling and launch operations. The in-flight pressure transducer must function satisfactorily

during all conditions.

Table XII provides the basis for the specification of the operating pressure ranges for the valves and storage tank. The pressure profile of the feed stream allows for choked flow operation of the flow controller, line pressure drops, typical valve operational requirements, and storage of ammonia as a saturated liquid at 45°F. The temperature drop across the let-down valve (about 30°F) is sufficient to allow the use of a phase-separating heat exchanger, but as previously stated, we see little value in its use.

Table XII reflects a relatively conservative design approach in that it allows the thermal balance of the storage to be maintained at relatively high temperatures. This reduces problems of thermal control: provisions for the ground hold period, shielding from the power plant radiators, etc.

1) Fill Line On-Off Solenoid Valve

Maximum Allowable Working Pressure: 100 psi differential

Maximum Pressure Drop: 2 psi for saturated ammonia vapor at 50 psia (nominal temperature -30°F) flowing at a rate of 5000 lb/hr.

Configuration: Normally closed - power to open

Leakage: Less than 0.10 standard cc/sec with an upstream pressure of 110 psia and a downstream pressure of 1×10^{-6} mm Hg absolute when closed and at a temperature of -30°F.

Power Supply: 115 volts 400 cps

Operating Life: 150 days

TABLE XII

PRESSURE AT VARIOUS POINTS IN CONTROL SYSTEM FOR AMMONIA

Tank Burst Pressure	110 psia
Tank Maximum Allowable Working Pressure	100
In-Flight Pressure Relief Valve Opens	96
In-Flight Pressure Relief Valve Re-seats	91
In-Flight Pressure Relief Valve Starts to Leak	89
Maximum Control Point for Tank Pressure Controller	84
Nominal Control Point for Tank Pressure Controller	80
Minimum Control Point for Tank Pressure Controller	76
Maximum Control Point for Let-Down Valve	47.7
Nominal Control Point for Let-Down Valve	43.4
Minimum Control Point for Let-Down Valve	39.1
Maximum Control Point for Flow Control Pressure Regulator	33.6
Nominal Control Point for Flow Control Pressure Regulator	32.0
Minimum Control Point for Flow Control Pressure Regulator	30.4

2) Vent Solenoid Valve

Maximum Allowable Working Pressure - 100 psi differential

Maximum Pressure Drop - 2 psi for saturated ammonia vapor at 50 psia (nominal temperature -30°F) flowing at a rate of 3000 SCFH

Configuration - Less than 0.10 standard cc/sec with an upstream pressure of 110 psia and a downstream pressure of 1×10^{-6} mm Hg absolute when closed and at a temperature of -30°F.

Power Supply - 115 volts 400 cps

Operating Life - 150 days

3) Liquid Level Sensor

Sonoswitch - Mfg. by Powertron Ultrasonics Corp., Plainview, New York

4) In-Flight Pressure Relief Valve

Open Pressure: 96 psia

Reseat Pressure: Not less than 91 psia

Fluid: Ammonia vapor saturated at the upstream pressure

Nominal Operating Temperature: $-30^{\circ}F$

Capacity: 4 lb/sec at 96 psia upstream pressure and 1×10^{-6} mm Hg absolute downstream pressure.

Leakage: Less than 0.1 standard cc/sec when closed with an upstream pressure of 89 psia or less and a downstream pressure of 1×10^{-6} mm Hg absolute.

Operating Life: 150 days

5) Let-Down Valve

Inlet Pressure: 76 psia to 84 psia

Outlet Pressure: 43.4 ± 4.3 psia

Maximum Flow Rate: 8.82×10^{-4} lb/sec

Fluid: Ammonia liquid, vapor or any combination

Fluid Temperature: $-30^{\circ}F$

Operating Life: 150 days

6) Line Pressure Relief Valve

Open Pressure: 96 psia

Re-seat Pressure: Not less than 91 psia

Fluid: Ammonia vapor saturated at the upstream pressure

Nominal Operating Temperature: $-30^{\circ}F$

Capacity: 4 lb/sec at 96 psia upstream pressure and 1×10^{-6} mm Hg absolute downstream pressure.

Leakage: Less than 0.1 standard cc/sec when closed with an upstream pressure of 89 psia or less and a downstream pressure of 1×10^{-6} mm Hg absolute.

Operating Life: 150 days

7) Propellant On-Off Solenoid Valve

Normal Inlet Pressure: 39.1 - 47.7 psia

Maximum Allowable Working Pressure: 100 psi differential

Maximum Flow: 8.82×10^{-4} lb/sec

Fluid: Ammonia gas at $80^{\circ}F$

Maximum Pressure Drop: 0.10 psi

Minimum Operating Temperature: $-30^{\circ}F$ with liquid or gaseous ammonia

Configuration: Normally closed - power to open

Leakage Rate: Less than 0.1 standard cc/sec with an upstream pressure of 100 psia and a downstream pressure of 1×10^{-6} mm Hg absolute when closed at $-30^{\circ}F$ and at $80^{\circ}F$.

Power Supply: 115 volts 400 cps

Environment: As specified

Operating Life: 150 days

8) Flow Controller (See Section III F-4 following)

Maximum flow: 8.82×10^{-4} lb/sec

Control accuracy: $\pm$ 10% full scale

Outlet pressure: approximately 1 atm.

Inlet gas pressure: 32.2 ± 1.6 psia

Inlet gas temperature: $540^{\circ} \pm 5^{\circ}R$

Control current for maximum flow: 10 ma.

9) Flow Control Pressure Regulator

Inlet Pressure: 39.1 to 47.7 psia

Discharge Pressure: 32.2 ± 1.6 psia

Maximum Flow Rate: 8.82×10^{-4} lb/sec

Fluid: Ammonia gas

Fluid Temperature: $80^{\circ}F$

Operating Life: 150 days

10) Temperature-Stabilizing Heat Exchanger (See Section III F-5 following)

Inlet Pressure: 45 psia

Inlet Temperature: $477^{\circ}R$

Quality: 0 - 100%

Exit Temperature: $540 \pm 4^{\circ}R$

Exit Pressure: 44.9 psia

Maximum Flow: 8.82×10^{-4} lb/sec

Maximum Heat Input: 550 watts

11) Tank Pressure Control Switch

Switch Closes: 77 ± 1 psia decreasing

Switch Opens: 83 ± 1 psia increasing

Medium: Liquid and/or gaseous ammonia at -30°F

Contact Rating: 5 amps at 115 volts 400 cps non-inductive. The use of external relays will be considered.

Operating Life: 250,000 cycles

12) Pre-launch Liquid Level Transducer

Pressure Range: 0 - 0.75 psi differential

Transducer Element: Potentiometer

Resistance: 20,000 ohms

Linearity: 1% full scale

Temperature: -30°F to +150°F

13) Pre-launch Pressure Transducer, In-Flight Pressure Transducer

Pressure Range: 0 - 115 psia

Transducer Element: Potentiometer

Resistance: 20,000 ohms

Linearity: 1% full scale

Temperature: -30°F to +150°F

3. Component Availability

a. General

As with the hydrogen system, the ammonia control system components are divided into three categories, graded in accordance with their

relative availability. These categories are standard components, special components, and the unique components which are considered in paragraphs 4 and 5 below.

b. Standard Components

Components which may be selected from manufacturer's catalogue data are:

Pre-launch Liquid Level Transducer

Pre-launch Pressure Transducer

In-flight Pressure Transducer

c. Special Components

Components with critical performance requirements are:

The Fill Line On-Off Solenoid Valve

The Vent On-Off Solenoid Valve

In-flight Pressure Relief Valve

Line Pressure Relief Valve

Let-down Valve

Propellant On-Off Solenoid Valve

Flow Control Pressure Regulator

Tank Control Pressure Switch

The manufacturers surveyed as to their interest in providing controls for the ammonia system are listed in Tables XIII and XIV. Table XV lists those manufacturers who expressed interest in providing components for the ammonia system. Once again, no evaluation of manufacturer capability was made.

TABLE XIII

MANUFACTURERS CONTACTED FOR PRESSURE REGULATORS, PRESSURE RELIEF VALVES, AND SOLENOID VALVES

Aerodyne Controls Corp.
90 Gazza Blvd.
Farmingdale, New York

Aerotec Industries, Inc.
Aircraft Equipment Division
Dept. W
Greenwich, Connecticut

Airwork Corporation
307 Sherman Avenue
Millville, New Jersey

The Bendix Corporation
Friez Instrument Division
1400 Taylor Avenue
Baltimore 4, Maryland

The Bendix Corporation
Pioneer Central Division
Hickory Grove Road
Davenport, Iowa

Circle Seal Products Co., Inc.
2181 E. Foothill Blvd.
Pasadena, California

Flodyne Controls, Inc.
1701 Elizabeth Avenue East
Linden, New Jersey

Grove Valve and Regulator Co.
6529 Hollis Street
Oakland 8, California

Minneapolis-Honeywell Regulator Co.
Aeronautical Division
2600 Ridgway Road
Minneapolis 40, Minnesota

Pesco Products Div.
Borg Warner Corporation
24700 North Miles Road
Bedford, Ohio

Pneu-Hydro Valve Company
52 Horse Hill Road
Cedar Knolls, New Jersey

Reaction Motors, Division
Thiokol Chemical Corporation
Denville, New Jersey

Stewart Warner Corporation
Southwind Division
1514 Drover Street
Indianapolis, Indiana

Vickers Company
882 Willis Avenue
Albertson, L.I., New York

Whittaker Controls, Inc.
9601 Canoga Avenue
Chatsworth, California

TABLE XIV

MANUFACTURERS CONTACTED FOR PRESSURE SWITCHES

Aerodyne Controls Corp.
90 Gazza Blvd.
Farmingdale, New York

Aero Mechanism, Inc.
7750 Burnet Avenue
Van Nuys, California

Aerotec Industries, Inc.
Aircraft Equipment Division
Dept. W
Greenwich, Conn.

Airwork Corporation
307 Sherman Avenue
Millville, New Jersey

Aro Corporation of Calif.
17110 Gale Avenue
City of Industry, California

The Bendix Corporation
Friez Instrument Division
1400 Taylor Avenue
Baltimore 4, Maryland

The Bendix Corporation
Pioneer Central Division
Hickory Grove Road
Davenport, Iowa

Fairchild Controls Corp.
225 Park Avenue
Hicksville, New York

Flow Systems, Inc.
842 Production Place
Newport Beach, California

Giannini Controls Corporation
235 Bear Hill Road
Waltham, Massachusetts

B. H. Hadley, Inc.
P. O. Box 31
Pomona, California

Minneapolis-Honeywell Regulator Co.
Aeronautical Division
2600 Ridgway Road
Minneapolis 40, Minnesota

Reaction Motors, Division
Thiokol Chemical Corporation
Denville, New Jersey

Stewart Warner Corporation
Southwind Division
1514 Drover Street
Indianapolis, Indiana

Vickers Company
882 Willis Avenue
Albertson, L.I., New York

TABLE XV

MANUFACTURERS INDICATING INTEREST IN SUPPLYING COMPONENTS FOR AMMONIA SYSTEM

	IN FLIGHT LINE PRESSURE RELIEF VALVE	VENT ON/OFF SOLENOID VALVE	PROPELLANT ON/OFF SOLENOID VALVE	LET DOWN VALVE	FLOW CONTROL PRESSURE REGULATOR	TANK PRESSURE CONTROL SWITCH
Aerodyne Controls Corp.	x	x	x	x	x	x
Aero Mechanism, Inc.						x
B. H. Hadley, Inc.	x			x	x	
Bendix Corporation Montrose Division						x
Circle Seal Pro. Co.	x	x	x			
Custom Component Switches, Inc.						x
Pesco Products Div. Borg Warner Corp.	x	x	x	x	x	
Reaction Motors Div. Thiokol Chem. Corp.	x	x	x	x	x	x
Valcor Eng. Corp.		x	x			
Whittaker Controls	x			x	x	
Wiancko Engineering						x

d. Unique Control Components

The components in the ammonia feed control system with unique capability requirements are the temperature stabilizer and the flow controller.

4. Flow Controller

The operation of the flow controller using ammonia gas as a propellant is the same as that for the flow controller using hydrogen and the procedures followed in its design are the same. The results of the design procedure are summarized in Table XVI. For detailed information, refer to the section on the hydrogen gas flow controller, Appendix H.

5. Temperature-Stabilizing Heat Exchanger (TSX)

As with hydrogen, this exchanger accepts fluid expelled from the storage tank and brings it to the temperature level acceptable to the metering and control system (estimated at 540^{o}R). To facilitate the use of a passive expulsion system the exchanger should be designed to accept either liquid or vapor and still maintain the desired exit temperature. The enthalpy increases for bringing saturated vapor and saturated liquid at 45 psi to gas at 540^{o}R are 36.6 Btu/lb and 592.1 Btu/lb respectively requiring heat inputs of 116 and 1875 Btu/hr respectively. The heat input to the fluid must increase by a factor of over 16 when the inlet condition changes from vapor to liquid. To cope with this requirement, an arrangement such as shown in Figure 16 is desirable. The TSX is made in two sections, a vaporizer and a superheater. Due to the very high heat fluxes achievable in the wetted tube, the vaporizer section can be much shorter than

TABLE XVI

MAJOR DESIGN PARAMETERS OF FLOW CONTROLLER FOR AMMONIA GAS

Quantity	Value
Flow Rate, Maximum	8.82×10^{-4} lbs/sec, full scale
Accuracy of Control	$\pm$ 10% of full scale
Inlet Pressure, P_o	32.2 ± 1.6 psia
Inlet Temperature, T_o	540 ± 5 deg. R
Outlet Pressure, P_e	Approximately 1 atm.
Maximum Control Orifice Area, A_c	2.33×10^{-3} in^2
Metering Orifice Area, A_o	1.00×10^{-2} in^2
Piston Area A_b	4 in^2
Maximum Input Control Current	10 ma
Winding Resistance at 20°C	2270 ohms

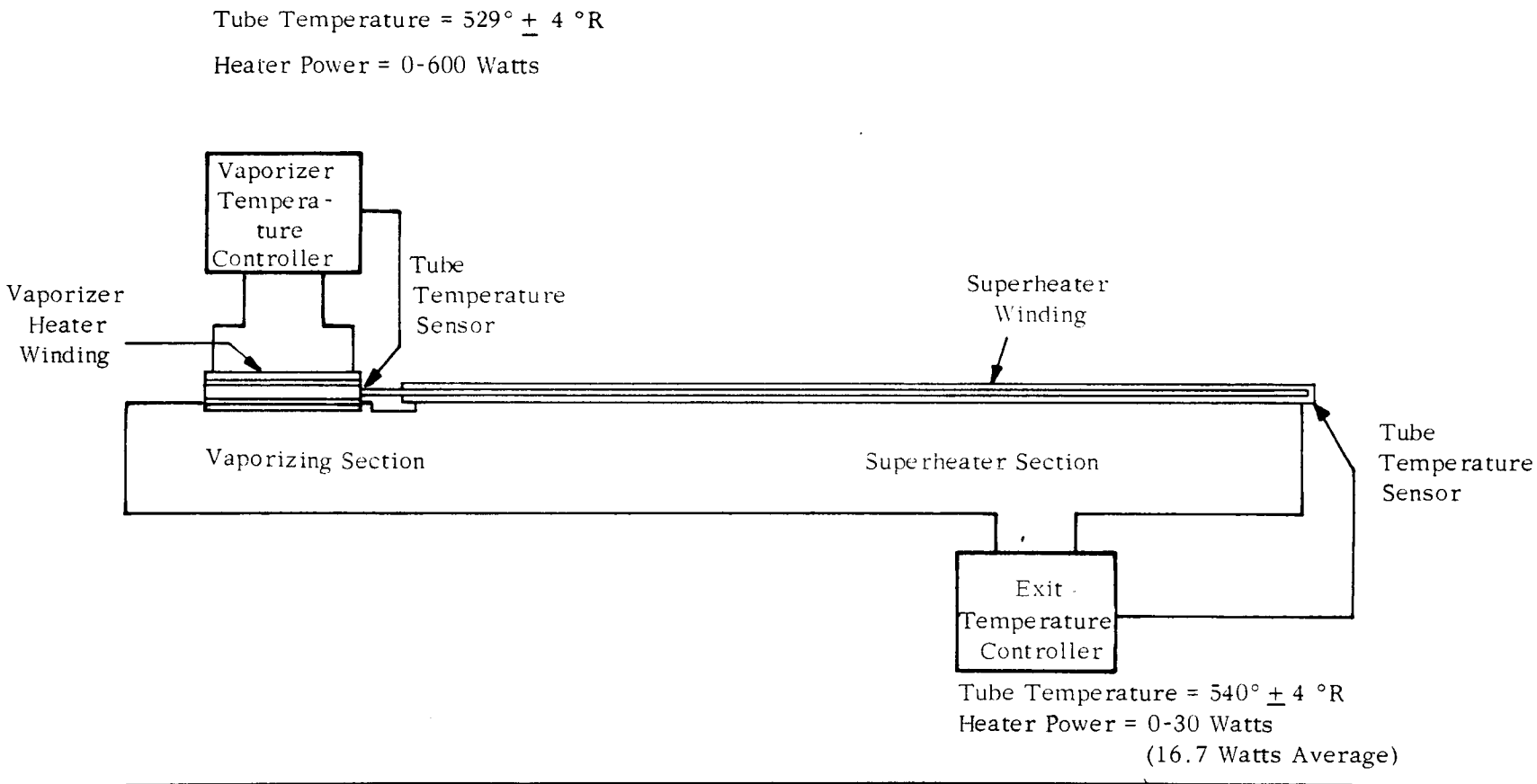

FIGURE 16 SCHEMATIC DIAGRAM OF AMMONIA TSX HEATER CIRCUITS

the superheater, despite the fact that with liquid at the inlet most of the heat input goes into vaporization. Two separate heater windings are placed on the tube, a superheater winding and a vaporizer winding. The superheater winding extends the entire length of the exchanger, that is, it is also wound on the vaporizer section. The power input to this winding is cycled on and off to maintain the temperature of the tube at the exit at 540 $\pm$ 4°R. The vaporizer heater is operated by an on-off controller which senses the temperature at the exit of the vaporizer section. The vaporizer controller would be adjusted to turn the vaporizer heater on at 525°R and to turn it off at 533°R (529°R $\pm$ 4°R). The exchanger is designed so that under normal conditions, with vapor feed at the inlet, the temperature at the exit of the vaporizer section would be about 529°R. The vaporizer heater would not be energized and the entire heat exchanger would function as a superheater. If, for some reason, the feed contained liquid, the temperature at the vaporizer exit would drop below 525°R and the vaporizer heater would be energized so as to control the temperature at that point to 529 $\pm$ 4°R. This arrangement has the advantage that the vaporizer controller, which handles the large power input associated with vaporizing any liquid feed, would only operate for short periods of time during start-up or when the vehicle is perturbed so that liquid is expelled. The superheater controller and heater would operate during the whole mission, but at a power level of only 0 to 50 watts.

Design calculations indicate that an aluminum tube with .250-inch ID by 160 inches long by 1/2-inch OD would provide enough surface area

to superheat the gas to within one degree of 540°R. The superheater winding would be disposed on the outside of the tube so as to maintain a constant tube wall temperature when the feed was all vapor. The first 20 inches of the tube would form the vaporizer section. The wall thickness there would be increased so as to increase the vaporizer's thermal inertia and permit the use of an on-off heater control. The vaporizer heater winding would be placed on the outside of the superheater winding. The total pressure drop in this heat exchanger, even with liquid at the inlet, is less than 0.1 psi. The total weight of the tube, heater and controls should not exceed 10 pounds.

6. Power Requirements

The average electric power requirements for the ammonia feed system during arc-jet operation is approximately 600 watts. Peak power requirements are approximately 1000 watts. The standby power requirement is 1.75 watts.

APPENDIX A

SIZING OF THE HYDROGEN STORAGE VESSEL

A. INTRODUCTION

This appendix describes some of the functional features of the liquid-hydrogen tank for the arc-jet feed system. The tank size and shape are presented, the operating pressure is determined, and the tank launch weight as a function of liquid reserve is discussed. Two systems are considered, one using an internal tank heater only and the other, the alternate system, using a rotary phase-separating heat exchanger.

B. SUMMARY

The hydrogen tank design under consideration for both systems is summarized in Table A-I.

TABLE A-I

SUMMARY OF TANK DESIGN

Configuration	-	cylindrical with hemispherical heads
Diameter	-	9' - 6"
Over-all length	-	16' - 2"
Volume	-	916 ft^3
Capacity	-	3885 lbs. of H_2
Ullage Volume	-	5 percent
Maximum Allowable Working Pressure	-	51.0 psi differential (system with heater only) 109 psi differential (alternate system)
Nominal Operating Pressure	-	41.2 psia (system with heater only) 88.5 psia (alternate system)
Tank Pressure at Launch	-	35 psia (system with heater only) 45 psia (alternate system)

C. DISCUSSION

1. General

For a hydrogen flow rate of 5×10^{-4} lb/sec. and a propulsion time of eighty-five days, the amount of propellant required for propulsion is 3670 pounds if the specific impulse of the engine remains constant for flows within the $\pm$ 10 percent tolerance band around the nominal flow rate. For a usable reserve of 5 percent left in the tank at the end of the propulsion time, the amount of propellant must be increased by 5 percent or 193 pounds. There will be about 12 pounds of hydrogen gas in the tank when the tank is drained as much as is practical. This propellant must be considered as non-usable reserve and must be added to the propellant in the tank at launch. A leakage loss through valves, etc., of 10 pounds has been allowed, which also must be added to the launch weight. These propellant requirements are summarized in Table A-II.

TABLE A-II

PROPELLANT REQUIREMENTS

Used for Propulsion	3670 lbs.
Usable Reserve (5 percent)	193
Left in the Tank	12
Allowable for Leakage Loss	10
Total:-	3885 lbs.

Taking an ullage volume of 5 percent at launch (this is equivalent to a two-foot vapor space in the top of the tank), and a tank pressure of 45 psia; 3873 pounds of liquid, and 12 pounds of vapor will be in the tank at launch, and the required volume is 919 ft^3.

2. Tank Configuration

In making comparisons of various configurations, the following specifications were used: tank volume, 919 ft^3; tank material, annealed 5 Al-2.5 Sn titanium alloy; allowable design stress, 248,000 psi; maximum allowable working pressure, 109 psi differential.

The selection of the tank material and the allowable stress level is discussed in Appendix B, and the specification of the tank working pressure is discussed below. The working pressures are different for the two systems under consideration, so the higher pressure was arbitrarily selected as a basis for the comparisons made. However, the conclusions reached would be the same if the lower pressure had been used instead.

Two tank shapes were considered, spherical and cylindrical with hemispherical heads. The spherical configuration gives the lightest possible weight tank due to the more efficient utilization of material in the shell. This is true regardless of the number of spheres used if only shell weight is considered. Of course, the weight of supports, interconnecting piping, etc., will increase with the number of spheres. A single spherical tank with a volume of 919 ft^3 is 12 feet 1 inch in diameter, and two spheres with the same total volume are 9 feet 7 inches in diameter. Since the maximum tank diameter has been specified at ten feet, the two-sphere configuration is the only one which can be considered further. These two spheres have an "ideal tank" weight of 167 pounds

---

*An "ideal tank" is defined here as a tank that is composed of a head and shell whose thicknesses are determined by membrane stresses only.

if made of annealed 5 Al - 2.5 Sn titanium using an allowable design stress of 248,000 psi and designed for a maximum allowable working pressure of 109 psia. The minimum over-all length of the tankage using this configuration is 19 feet 2 inches. The length and weight of a cylindrical tank with hemispherical heads will depend upon the diameter of the tank. This dependence is shown in Figure A-1 which is a plot of tank length and "ideal tank" weight versus tank diameter. The weights shown in this figure were determined using the same volume pressure, etc., as for the two-spherical tank configuration. As may be seen, both weight and length decrease with increasing diameter, the minimum being the limiting case of a tank with zero shell length, i.e., a sphere. Thus, it is advantageous to use the largest diameter tank possible. A 9-foot 6-inch diameter has been selected because this size tank will still leave adequate room in the 10-foot 0-inch diameter envelope for insulation, supports, structure, etc.

A comparison of over-all tankage length, "ideal tank" weight, and diameter for the two-sphere configuration and the cylindrical tank configuration is shown in Table A-III.

TABLE A-III

TANK SIZE AND WEIGHT FOR TWO CONFIGURATIONS

	Diameter	Over-all Length	"Ideal Tank" Weight
2 Spherical Tanks	9' - 7"	19' - 2"	167 lbs.
1 Cylindrical tank with Hemispherical Heads	9' - 6"	16' - 2"	196 lbs.

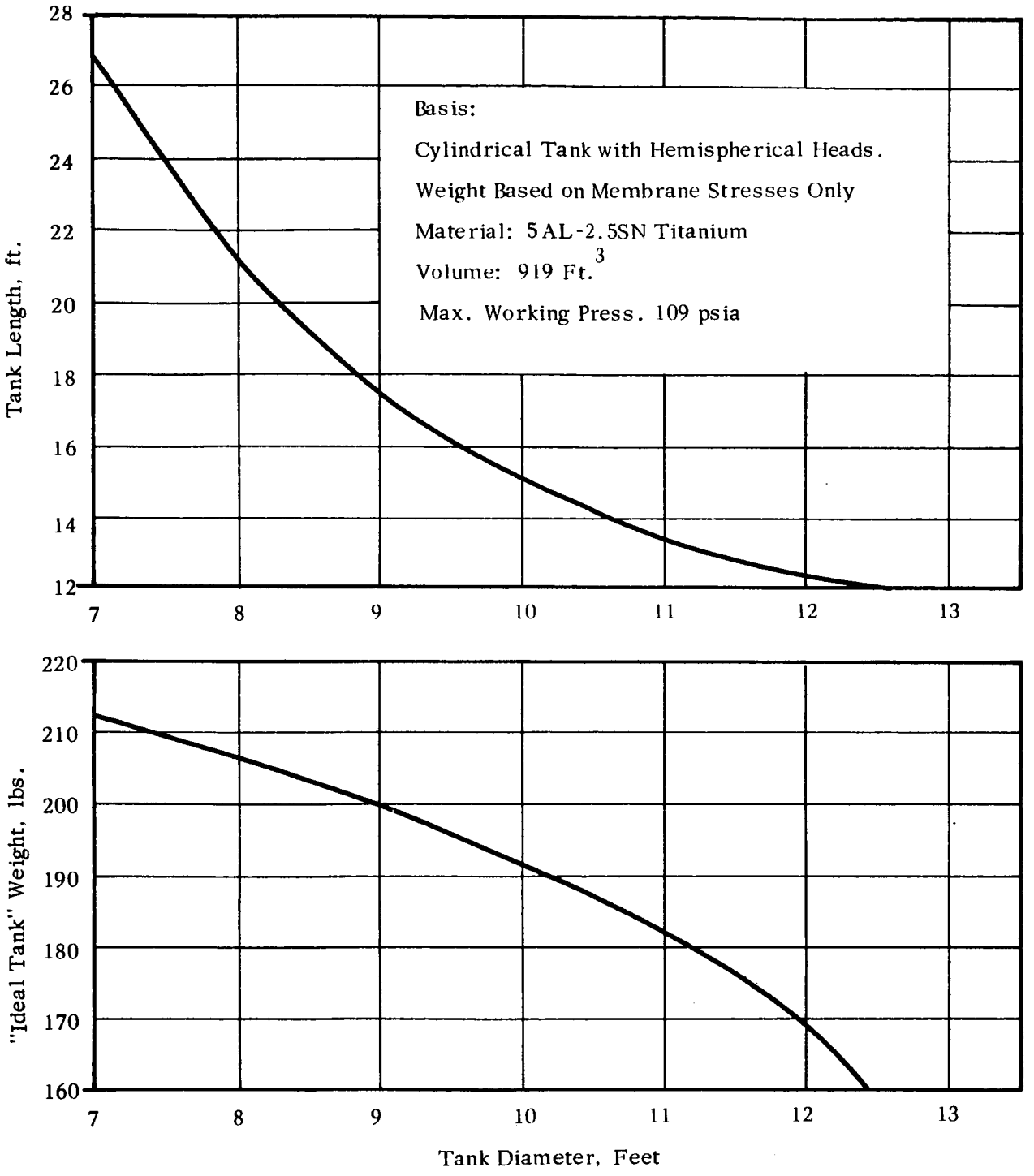

FIGURE A1 TANK LENGTH AND "IDEAL TANK" WEIGHT AS A FUNCTION OF DIAMETER

The cylindrical configuration is smaller in enclosing volume than the two-sphere configuration, but is 29 pounds heavier, based on shell weight alone. The added structure and duplicate piping, etc., required by the spherical configuration would undoubtedly weigh more than 29 pounds. Thus, in the actual case, cylindrical tankage would weigh less than spherical tankage in addition to giving a smaller, less complicated system. Therefore, it is deemed the proper configuration for the present application.

3. Operating Pressure

The tank operating pressure should be selected to give the lowest weight for the total system. This is equivalent to saying that the tank weight should be as low as possible since the weight of the other elements in the system are essentially independent of the tank operating pressure. In light of this, the tank pressure has been set at the minimum level at which it will supply an adequate pressure differential across the expulsion and metering system for it to function properly. This tank pressure, is set by the characteristics of the expulsion and control system and is determined by starting at the engine and working backwards through the control system, taking into account anticipated fluctuations of controlled variables about their nominal set points. Hydraulic loads caused by accelerating the hydrogen during boost are not considered here since the tank will not be under full pressure at launch; hence it will not undergo maximum membrane stresses until the pressure is increased to operating pressure in parking orbit.

A simplified flowsheet of the system using the internal heater is shown in Figure A-2. In this system saturated vapor is taken into the withdrawal tube, heated to approximately 70°F in the temperature-stabilizing controller, throttled to the desired pressure in the pressure regulator, metered for the desired mass flow in the flow controller, and introduced into the engine. The tank pressure controller maintains the tank pressure at the desired level by turning the tank heater on and off, and the in-flight pressure relief valve protects the tank from overpressurization.

The alternate system using the rotary phase-separating heat exchanger is shown in Figure A-3. In this system the propellant of any quality is withdrawn from the tank and throttled through the let-down valve. The low pressure propellant re-enters the tank and passes through a heat exchanger, in which any liquid in the stream is heated and vaporized by the propellant remaining in the tank. The pressures in the tank and heat exchanger are regulated so that the equilibrium temperature of the fluid in the tank is higher than that of the fluid in the heat exchanger by a specified amount. In this case a temperature difference of at least 2.8°K will be maintained across the heat exchanger. The propellant from the heat exchanger leaves the tank and goes to the temperature-stabilizing control where it is heated to approximately 70°F. From here it goes to the pressure regulator, where the pressure is reduced to 32.2 $\pm$ 1.6 psia, the required inlet pressure for the flow controller. The flow control pressure regulator will not be required if the let-down valve is able to control the inlet pressure to the flow controller within the above limits.

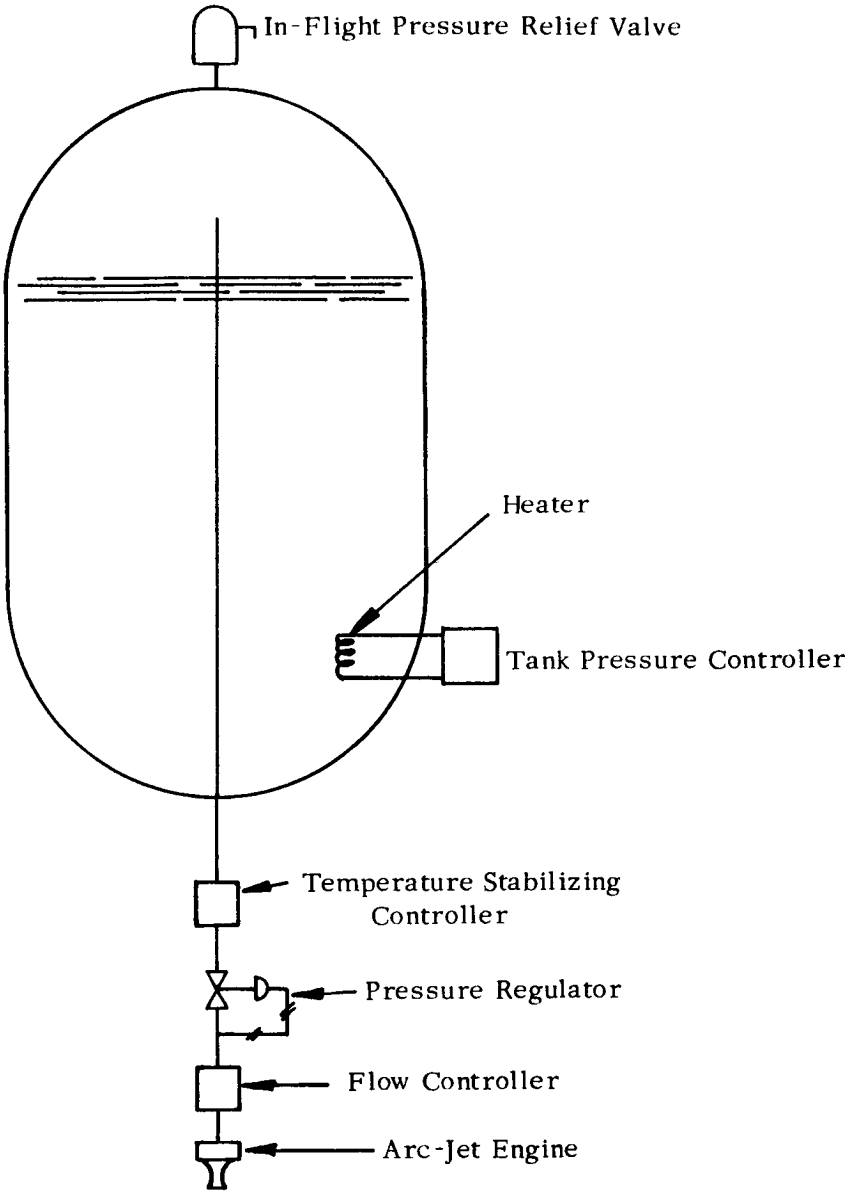

FIGURE A2 SIMPLIFIED FLOWSHEET OF SYSTEM USING AN INTERNAL TANK HEATER ONLY

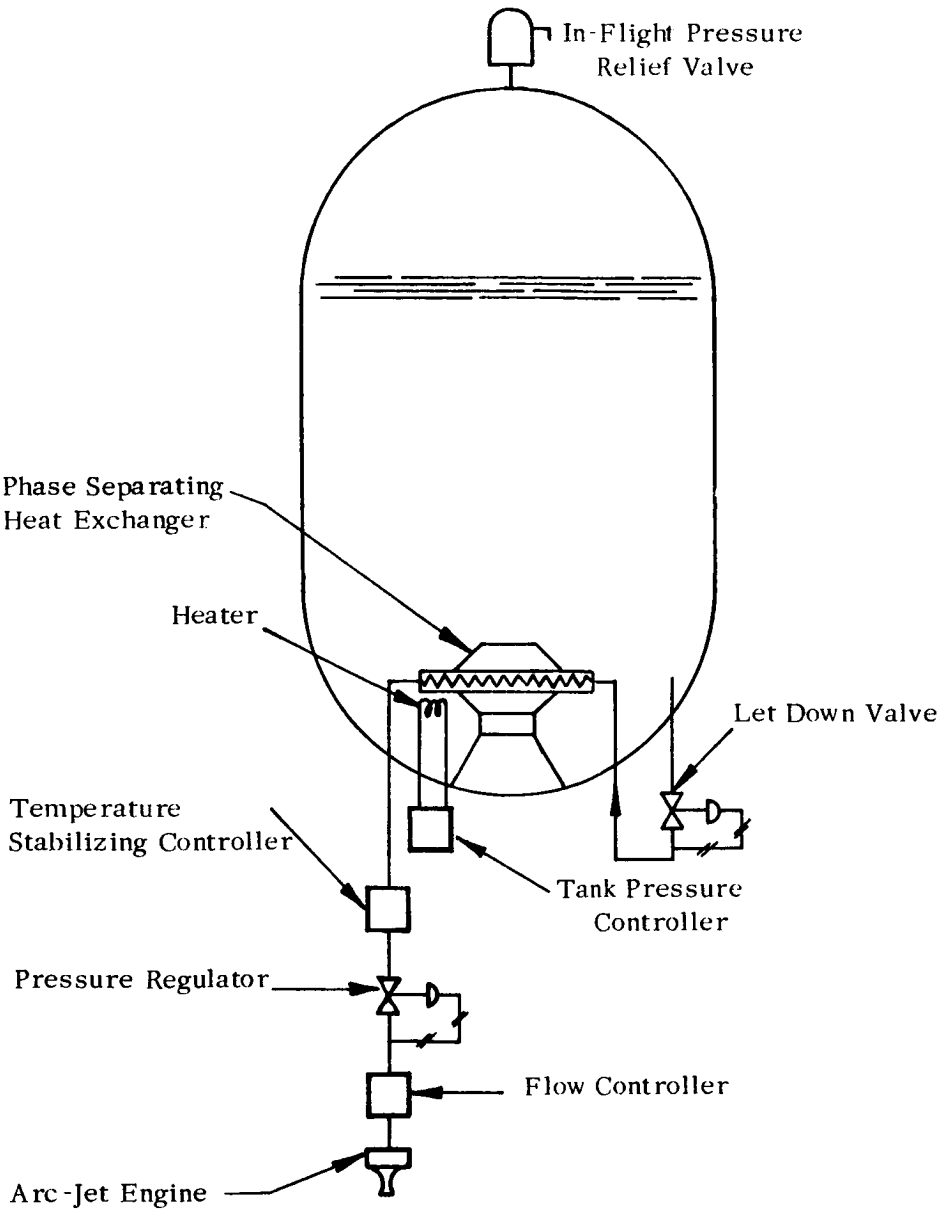

FIGURE A3 SIMPLIFIED FLOWSHEET OF SYSTEM USING A ROTARY PHASE-SEPARATING HEAT EXCHANGER

Other items in the system are the tank pressure controller and the in-flight relief valve as before.

An estimate of the required tank pressure for both systems is shown in Table A-IV, which indicates that a tank with a nominal operating pressure of 41.2 psia and a maximum allowable working pressure (MAWP) of 51.0 psia differential is required for the system with the internal heater only, and a tank with a nominal operating pressure of 88.5 psia and a MAWP of 109 psia differential is required for the system with the rotary phase-separating heat exchanger.

Referring to Table A-IV and using the alternate system as an example, the tank MAWP is determined as follows, starting at the flow controller and working backwards through the system. The pressure required at the inlet to the flow controller is 32 $\pm$ 1.6 psia, so the maximum pressure at this point is 33.6 psia. Adding 5 psi to this for pressure drop across the flow-control pressure regulator and 0.5 psi for friction pressure drop through the expulsion system, gives 39.1 psia as the minimum pressure in the heat exchanger. This pressure is controlled by the let-down valve, thus 39.1 psia is the minimum controlled pressure permitted by this valve. Assuming this valve can control its downstream pressure to $\pm$ 10 percent of its set point, the maximum controlled pressure is 47.7 psia. The equilibrium temperature for a vapor pressure of 47.7 psia is 25.0^{o}K. This is the highest temperature at which liquid can exist in the heat exchanger. Design considerations on the phase-separating heat exchanger require a temperature difference of at least 2.8^{o}K between the fluid in the tank

TABLE A-IV

ESTIMATED PRESSURE AT VARIOUS POINTS IN CONTROL SYSTEM

	System with Internal Heater Only	System with Rotary Phase-Separating Heat Exchanger
Tank Burst Pressure	56.7 psia	121 psia
Tank Maximum Allowable Working Pressure	51.0	109
In-Flight Pressure Relief Valve Opens	49.0	105
In-Flight Pressure Relief Valve Re seats	47.0	100
In-Flight Pressure Relief Valve starts to leak	45.5	98
Maximum Control Point for Tank Pressure Controller	43.3	93
Nominal Control Point for Tank Pressure Controller	41.2	88.5
Minimum Control Point for Tank Pressure Controller	39.1	84.0
Maximum Control Point for Let-Down Valve	--	47.7
Nominal Control Point for Let-Down Valve	--	43.4
Minimum Control Point for Let-Down Valve	--	39.1
Maximum Control Point for Pressure Regulator	33.6	33.6
Nominal Control Point for Pressure Regulator	32.0	32.0
Minimum Control Point for Pressure Regulator	30.4	30.4
Maximum Inlet Pressure to Flow Controller	33.6	33.6
Minimum Inlet Pressure to Flow Controller	30.4	30.4

and the propellant in the heat exchanger passages. This means that the propellant in the tank must be at a pressure such that the equilibrium temperature is 25.0 + 2.8 = 27.8°K. This pressure is 84.0 psia and is the lowest pressure permissible in the tank. If 84.0 psia is taken as the lowest excursion for the tank pressure, and the tank pressure controller is able to control to within ± 5 percent of its set point, the upper limit of controlled tank pressure is 93.0 psia. The nominal operating pressure, or the set point of the tank pressure controller, is half way between these two values, or 88.5 psia. The tank MAWP must be somewhat above this due to the operating characteristics of the in-flight pressure relief valve, which is the ultimate pressure protection device on the tank. This type of valve typically starts to leak at a pressure about 10 percent below the pressure at which the valve is wide open. Setting this start-to-leak pressure 5 percent higher than the maximum pressure allowed by the pressure controller, or at 97.9 psia, means that the safety relief should be wide open at 109 psia. The in-flight relief valve will be sized to prevent the tank pressure from rising above 109 psia when the tank is closed off and subjected to the highest heat leak which it is reasonable to protect against, thus the tank MAWP has been set at 109 psia. The tank will be designed so that the membrane stress at the MAWP is equal to the allowable stress of the material, i.e., 91 percent of the yield strength of the tank material. Therefore, the tank burst pressure will be 121 psia.

The MAWP for the system using the internal heater only is determined in a similar fashion. In order to determine the effect of tank operating pressure on tank weight, the "ideal tank" weight was calculated as a function of tank operating pressure. The basis used was the same as in the tank configuration section above, i.e., a tank volume of 919 ft^3, a diameter of 9 feet 6 inches, and a MAWP of 1.23 times the nominal operating pressure, as in Table A-IV. The shell material was annealed 5 Al - 2.5 Sn Titanium alloy with an allowable stress of 248,000 psia. Only membrane stresses were considered, and the tank weight was based on thicknesses determined by these stresses, with a lower limit of 0.010-inch, the minimum practical gage. Figure A-4, which plots "ideal tank" weight as a function of nominal tank operating pressure and tank MAWP shows the results of these calculations. From this figure it may be seen that the "ideal tank" weight is constant for all nominal operating pressures below about 35 psia, since in this range of pressures both the head and the shell must be made of minimum gage material. As the nominal operating pressure increases to 70 psia, the weight of the required tank increases as the shell thickness is increased. As pressure increases above 70 psia, tank weight increases even more rapidly as both the head and shell thicknesses are increased. For a MAWP of 51.0 psia, the "ideal tank" weight is 119 pounds, and for a MAWP of 109 psia the "ideal tank" weight is 196 pounds.

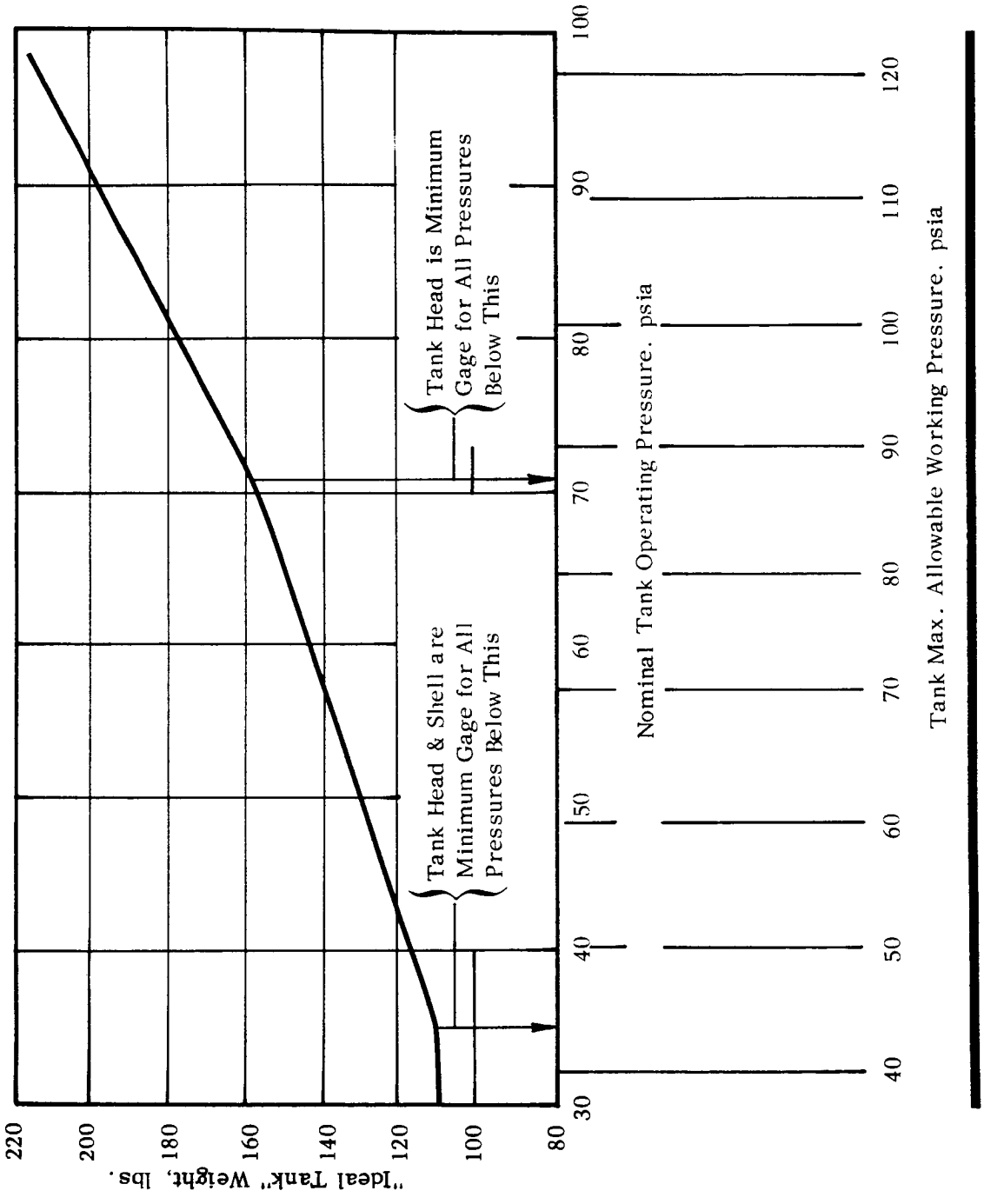

FIGURE A4 "IDEAL TANK" WEIGHT AS A FUNCTION OF TANK PRESSURE

D. PROPELLANT RESERVE

The present system is designed to have a 5 percent usable gas reserve in the tank at the end of the initial propulsion period. In it the last bit of liquid in the tank is vaporized prior to the end of the propulsion period. After this time, the propellant temperature is increased by the tank heater to keep the tank pressure at the operating point. By the end of the propulsion period, the tank temperature will have increased to $167^{\circ}R$ for the system with the internal heater and to $78^{\circ}R$ for the alternate system. The tank will contain 205 pounds of hydrogen vapor reserve at this point.

Figure A-5 shows how this 5 percent reserve decreases during the coast period as vapor is vented to limit tank pressure. During the initial stages of the coast period the amount of propellant remains constant as heat leak increases the temperature of the propellant slightly, and increases the pressure from the nominal operating point to the pressure at which the vent valve opens. After this time, propellant must be vented to limit the tank pressure, and the total amount of propellant decreases as shown in the figure. Twelve pounds of the propellant in the tank is not usable because it cannot be removed from the tank at a pressure high enough to use in the arc-jet engine. The tank temperature will eventually reach a point at which it is in thermal equilibrium with its surroundings, and will remain constant. After this point has been reached it will no longer be necessary to vent the tank. Other amounts of reserve will decay in the same general pattern as described above.

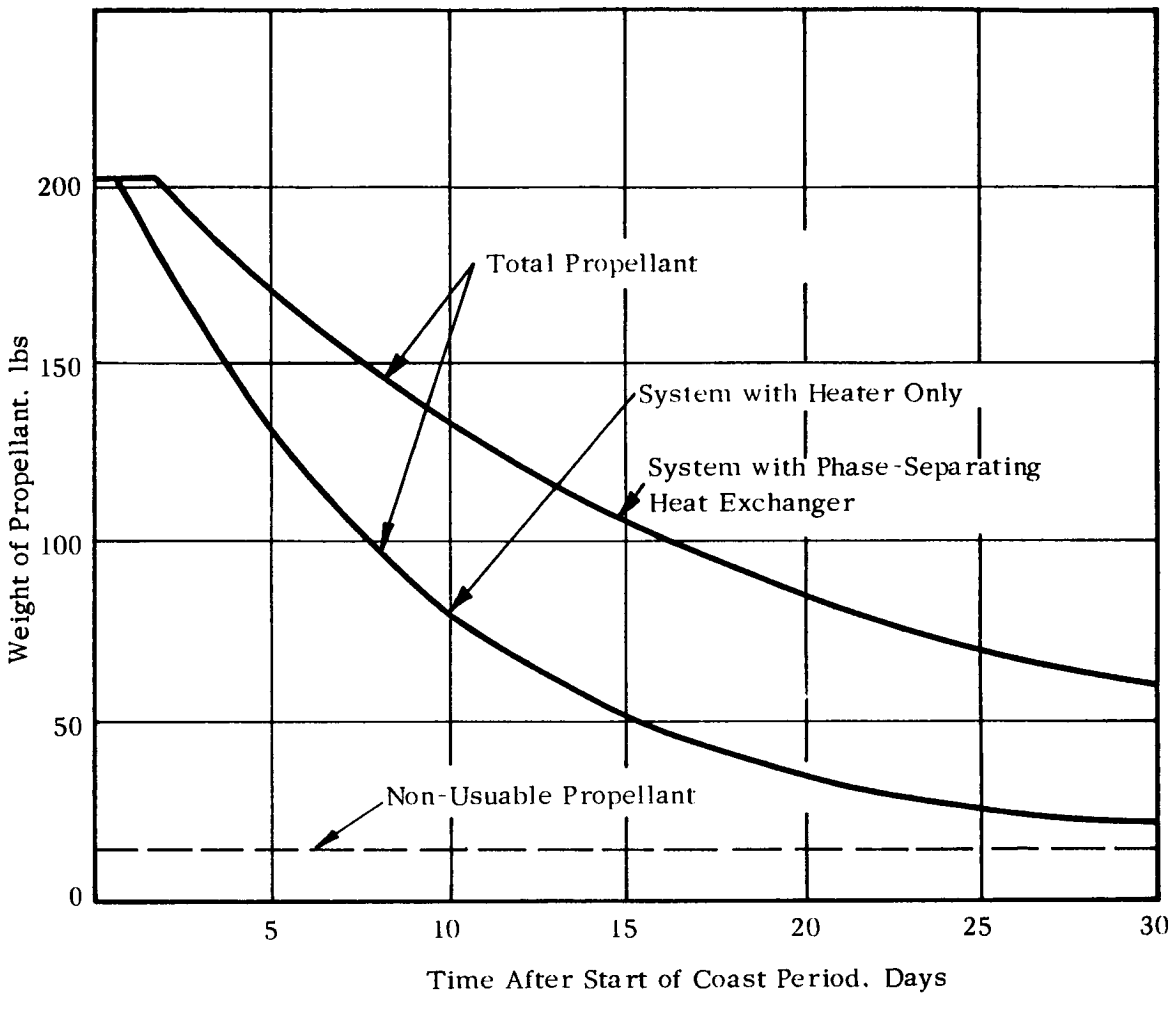

FIGURE A5 WEIGHT OF PROPELLANT VS TIME AFTER START OF COAST PERIOD FOR 5 PERCENT RESERVE

The preceding discussion is based on having 5 percent usable reserve in the tank at the beginning of the coast period. The system built on this basis will have a launch weight which is about 210 pounds heavier than a "zero reserve" system, i.e., a system which has no usable propellant in the tank at the end of the initial propulsion period. This increase in launch weight is predominantly (about 90 percent) propellant weight.

If different amounts of reserve propellant are required or if the same amount is required at some time after the start of the coast period, the launch weight penalty will be different. These penalties are quite severe if reserve propellant is required at an appreciable time after the start of the coast period because of the relatively rapid venting of propellant necessitated by heat leak. Figure A-6 indicates the additional launch weight over a "zero reserve" system incurred by requiring a given usable reserve in the tank at any time up to thirty days after the start of coast. For points on the smooth part of these curves, there will be only vapor in the tank at the beginning of the coast period, while for points on the straight portions past the discontinuity, there must be some liquid in the tank at the beginning of the coast period. It is evident that there are severe weight penalties associated with requiring a reserve, especially if it is required some time after the initial propulsion period. For example, requiring a five percent reserve at the end of thirty days coasting increases the launch weight 900 pounds, or about 20 percent of the entire feed system weight.

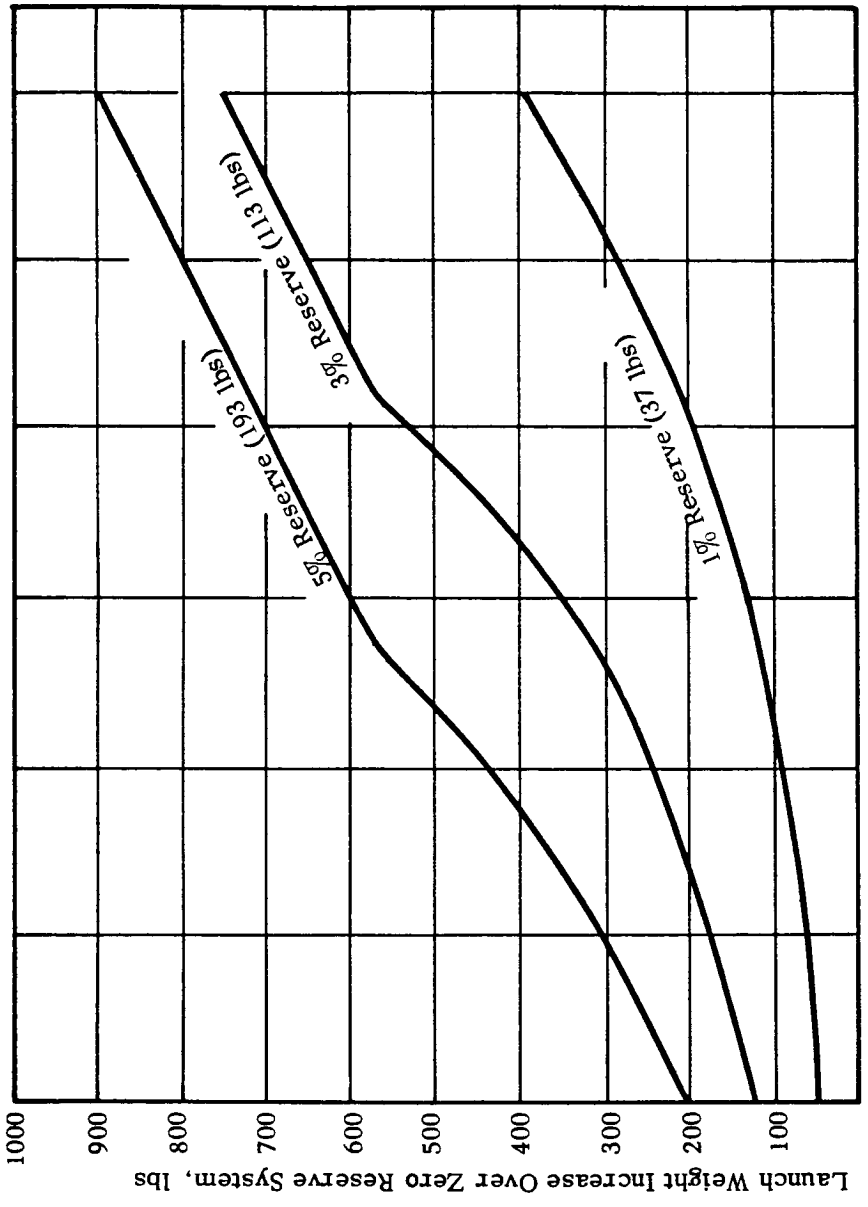

FIGURE A6 LAUNCH WEIGHT INCREASE FOR VARIOUS PROPELLANT RESERVES VS. TIME AFTER START OF COAST PERIOD

There are several other methods of operation which might reduce the weight penalty associated with a particular reserve requirement, (for example by allowing the tank pressure to drop toward the end of the initial propulsion period), but the weight penalties associated with these schemes do not appear to be substantially different from those indicated above. Additionally, most of them will not permit propellant to be withdrawn from the tank over substantial portions of the coast period.

APPENDIX B

MATERIAL SELECTION FOR THE HYDROGEN STORAGE VESSEL

A. INTRODUCTION

The inner vessel of the hydrogen propellant tank for the arc-jet vehicle must be constructed of a material which has a high strength per unit weight and suitable toughness and ductility at -423°R. A number of materials which possess these properties in varying degrees were investigated in order to select one which gave the lightestweight tank consistent with reliability.

Reinforced plastics and alloys of aluminum, stainless steel, and titanium, were considered using the following representative tank specifications as a basis for comparison:

Capacity:	4000 lb. LH_2
Shape:	Cylindrical with hemispherical heads
Size:	9 ft. 6 in. dia. x 17 ft. OA length
Design Pressure:	55 psi differential

An additional condition was that the tank would not have to withstand buckling loads or be self supporting but would rely upon internal pressure to keep it from collapsing. The non-self supporting tank was selected as a result of a weight study summarized in a latter discussion.

B. SUMMARY AND CONCLUSIONS

Annealed 5 Al. - 2.5 Sn titanium alloy with extra low interstitial content has been selected as the material for the liquid hydrogen tank.

This is an all alpha alloy with a tensile strength of 125,000 psi and yield strength of 120,000 psi at room temperature and a tensile strength of 276,000 psi and yield strength of 273,000 psi at liquid hydrogen temperature. This material is selected because it will give the lightest weight tank. Additionally, no more severe problems in design or fabrication are foreseen for this material than would exist for any other material of the thin gages required for the present application. The tank design is based on using internal pressure to give the tank rigidity, i.e., the tank if unpressurized will not be self supporting under all loading conditions. It also utilizes the high tensile and yield strengths of titanium at -423°F to the fullest extent. This implies the use of a fracture analysis as well as a yield strength analysis in the design of the tank since the probability of brittle fracture increases as the operating stresses in the tank wall increase. In all probability the actual design allowable stresses for the final vehicle will have to be determined by actual testing of miniature tanks at -423°F.

C. DISCUSSION

1. Material Properties

The following is a brief discussion of the materials considered.

a. Stainless Steel

Of the stainless steels, only those in the austenitic 300 series have sufficient low temperature toughness for use at cryogenic temperatures. Of this series, alloys 301, 302, 304, 304 ELC, and 310 were investigated.

This group of alloys has the following general characteristics:

a) Alloying content increases with increasing alloy number

b) Tensile strength in the annealed condition decreases with increasing alloy number

c) Toughness increases with increasing alloy number for a given amount of cold work

In addition, the following statements may be made with respect to a particular alloy in the group.

a) Strength increases with decreasing temperature

b) Strength increases with increasing cold work

c) Sharp notch tensile strength increases with decreasing temperature. However, sharp-notch tensile strengths do not increase as rapidly as ultimate tensile strengths, therefore the ratio of sharp-notch tensile strength to ultimate tensile strength (sharp-notch tensile strength ratio) decreases with decreasing temperature.

d) Ductility and toughness decrease with increasing cold work.

e) There is an optimum degree of cold work which yields high strength and adequate toughness at low temperatures.

For AISI 301 alloy, this optimum degree of cold work is 60 percent. The strength of this 60 percent cold worked alloy is greater than the strengths of the other alloys investigated at their optimum degree of cold work, thus it was selected for comparison with the best alloys of the other materials under consideration. Figure B-1 shows strength as a function of temperature for this alloy.

Strength of the base metal alone cannot be used as the sole criterion for material selection since other factors of a practical nature must be taken into account. One of these is annealing of the metal at welded joints. The fact that annealing occurs necessitates reinforcement of welded joints or the use of thicker gages than required by the strength

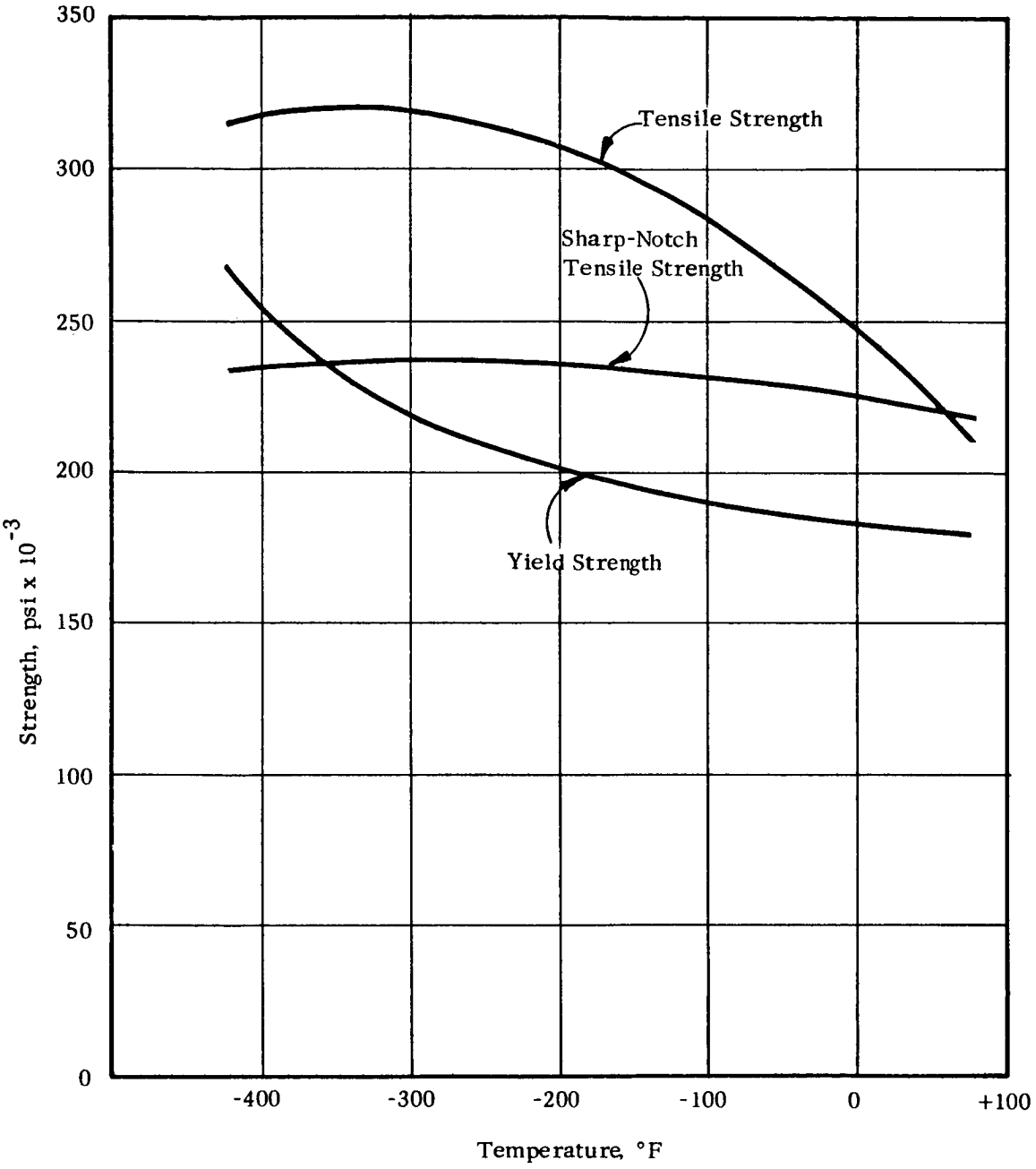

FIGURE B1 STRENGTH VS. TEMPERATURE FOR AISI 301 STAINLESS STEEL (60% Cold Reduced)

of the parent metal alone. The material may be chemically milled so a weld joint similar to the one shown in Figure B-2 has been used in these evaluations. Some properties are direction-dependent, notably toughness which is considerably less in the transverse direction of rolling than in the longitudinal direction. This direction-dependence will influence the direction in which sheet is placed in the final vessel, and may dictate the thickness of some sections. This material can be welded vacuum tight in thin gages (down to .005 inch thick) and can also be brazed and soldered. It has a low thermal conductivity, hence it can be used for penetrations. Further, it is a well-known material which can be readily worked in either the shop or field.

b. Aluminum

Aluminum alloys of the 2000 series (copper-aluminum alloys) and 5000 series (magnesium-aluminum alloys) were evaluated for this application. Alloys of the 6000 series (magnesium-silicon-aluminum alloys) were not evaluated in detail because strengths are below those of either of the above series, and alloys in the 7000 series (zinc-aluminum alloys) were not evaluated in detail, even though they have high strengths, because they have poor impact properties at -423^{o}F.

The strongest alloy of the 5000 series is the strain hardening alloy 5456 and the highest strength temper is H321 - a cold worked and stabilized temper. This alloy has a tensile strength of 57,000 psi and yield strength of 39,000 psi at room temperature. The strongest alloy of the 2000 series is the heat treatable alloy, 2014, and the

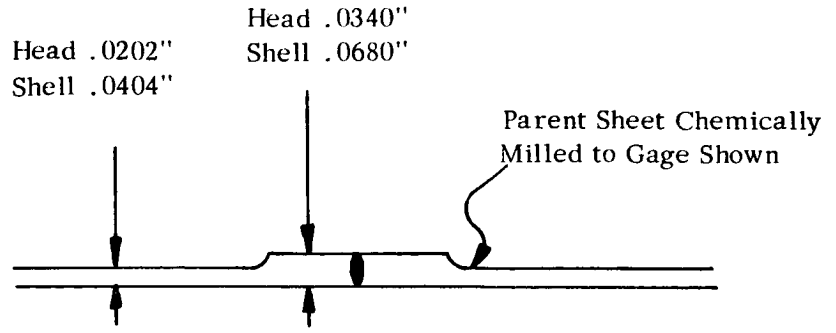

2014-T6 ALUMINUM

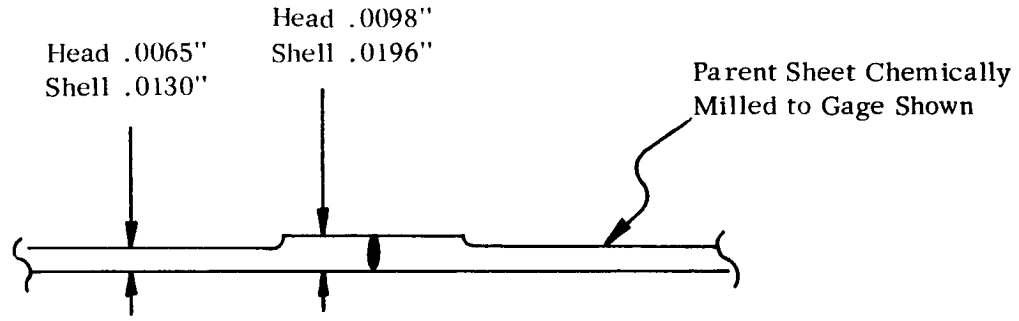

AISI 301 STAINLESS STEEL 60% COLD WORKED

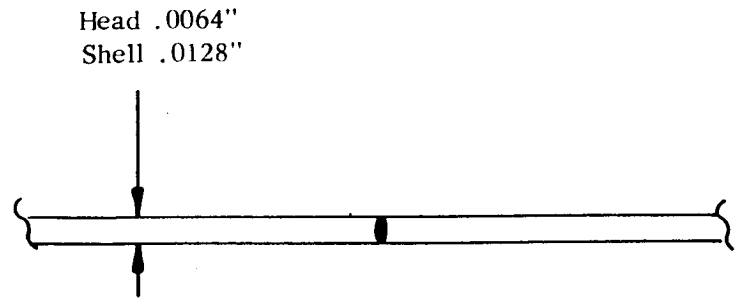

ANNEALED 5 AL-2:5 SN TITANIUM

FIGURE B2 TYPICAL WELDED JOINTS IN TANKS DESIGNED ON CRYOGENIC MATERIAL PROPERTIES

Note: Thicknesses from Table BI

strongest temper is T6 - a solution treated and aged temper. This alloy has a tensile strength of 70,000 psi and a yield strength of 65,000 psi at room temperature. Since 2014-T6 has superior strength properties, it alone was used in the comparison with other materials. Strength of this alloy is plotted as a function of temperature in Figure B-3. Alloy 2024-T6 has the following characteristics:

a) Strength increases with decreasing temperature

b) Sharp-notch tensile strength remains essentially constant with temperature, therefore the sharp-notch tensile strength ratio decreases with decreasing temperature.

c) The alloy has lower strengths at welds due to annealing. It may be worked by chemical milling, however, so that welded and heat effected areas may be left thick and the main section of the sheet milled down to minimum gage as shown in Figure B-2. Integral reinforcing ribs, bosses, etc. may also be formed in this manner.

d) It is easily worked.

e) It can be welded, although there is some question as to whether vacuum-tight joints can be made in thin gage material.

f) It has a high thermal conductivity, therefore, it cannot be used for penetrations into the tank and a dissimilar metal joint to a material with a low thermal conductivity must be made at the cold wall of the inner tank.

c. Titanium

There are two alloys of titanium which are generally candidates for use at cryogenic temperatures - 6 AL-4V, and 5 AL-2.5 SN. Of these, the latter is considered to have better toughness at low temperatures and so was used for comparison with the other materials. This alloy has a

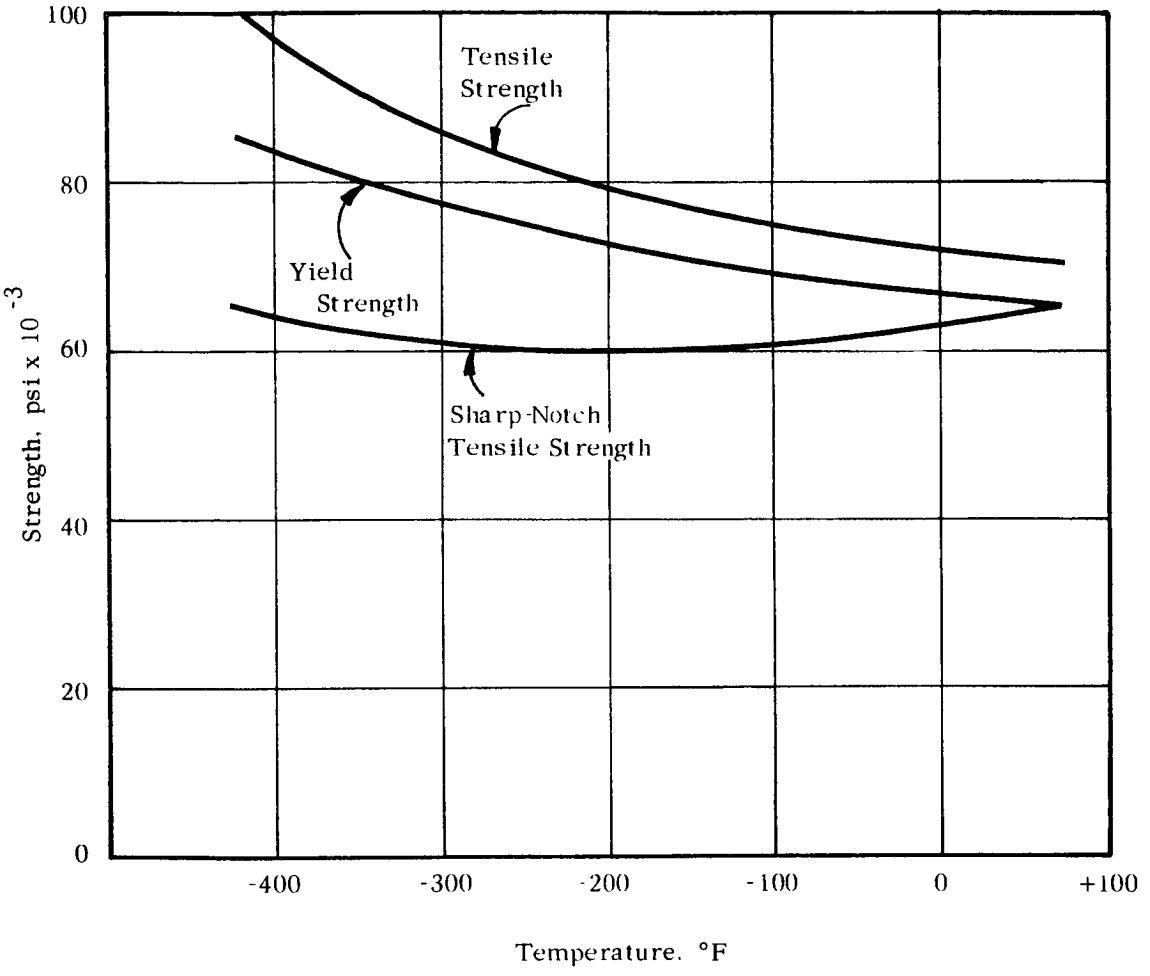

FIGURE B3 STRENGTH VS TEMPERATURE FOR 2014-T6 ALUMINUM

tensile strength of 125,000 psi and a yield strength of 120,000 psi at room temperature and all strength properties are isotropic. Figure B-4 is a plot of strength as a function of temperature for this alloy in the annealed condition. The alloy has the following characteristics:

a) Strength increases rapidly with decreasing temperature.

b) Sharp-notch tensile strength decreases with temperature and the sharp-notch tensile strength ratio drops off rapidly with decreasing temperature. The notch sensitivity is a function of the interstitial content of the alloy, increasing with increasing interstitial content. Therefore, only the low interstitial alloy has been considered here.

c) Vacuum-tight welds can be made in thin gages, but the material cannot be joined readily to other materials other than mechanically at the present time.

d) The material can be chemically milled, so thicker sections can be left for reinforcement, bosses, etc.

e) The material is toughest when used in the annealed condition, although it may be used with modest (i.e., 15 percent) amounts of cold work in formed sections. The effect of cold work on toughness is not completely defined at this time.

f) Severe forming operations are performed hot (800-1300^{o}F) so heated dies are required.

g) Weld efficiencies of 100 percent have been reported, therefore it is probable that no reinforcement of the weld joint will be required. A typical weld joint design is shown in Figure B-2.

d. Reinforced Plastics

Filament wound pressure vessels have been used for solid propellant cases and high-pressure gas storage on space vehicles, so this type of construction was considered for the present application. The fabrication technique consists essentially of winding a reinforcing material

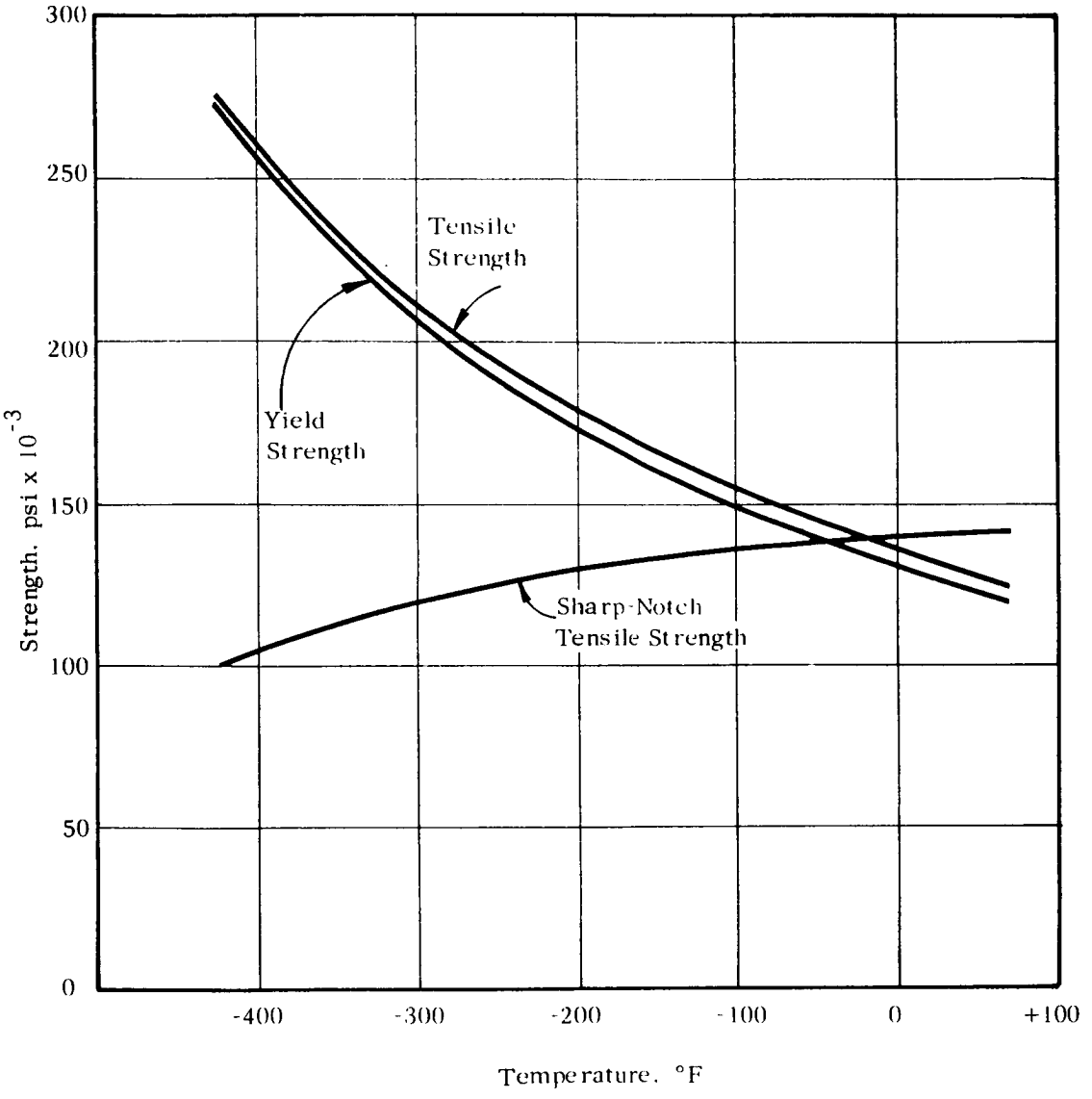

FIGURE B4 STRENGTH VS TEMPERATURE FOR 5 AL-2.5 SN TITANIUM (Annealed)

(usually glass fibers) and a resinous material around a mandrel the shape of the part to be formed. Thin sections of this material are porous so,in order that the thin wall required for the present application be vacuum-tight, a vacuum-tight liner of some sort would be required. This liner is a pressure vessel which, if made out of the minimum practical gage metallic material, would have a thickness and weight not considerably less than the all-metal tanks under consideration. Additionally, there is the problem of differential thermal contraction between the liner and the tank wall. This differential contraction sets up stresses at the liner-plastic interface which tend to weaken the tank. Several large, filament wound tanks have been made, on a developmental basis, but there is not sufficient evidence at this time to justify considering them further for a thin-walled vacuum-tight vessel to be used at liquid-hydrogen temperature. It appears that wound filament construction seems more suited at this time to relatively small vessels which must withstand high pressures at temperatures somewhere near ambient; therefore, this construction was not considered further.

e. Comparisons

The primary consideration in this study was to select a material which would result in the lightest weight tank. An evaluation was made by comparing the weights of "ideal tanks" made of each of the materials under consideration. An "ideal tank" is defined here as a tank that is composed of a head and shell whose thicknesses are determined by membrane stresses only, neglecting nozzles and reinforcement required at support points,

welds, discontinuities, etc. Since the weight of metal required for reinforcement, etc., will be a fairly constant proportion of the "ideal tank" weight for all three materials under consideration, the actual tank weights will be in the same relative order as the "ideal tank" weights. The "design stress", minimum head thickness, minimum shell thickness, and "ideal tank" weight are tabulated in Table B-I for designs based on material properties at room temperature and properties at -423°F. The "design stress" used in these evaluations was taken as 91 percent of the yield strength at the indicated temperature. Thus this comparison assumes that the material is yield strength limited and the prime mode of failure is tensile instability, i.e., local plastic yielding and associated thinning of the tank wall which ultimately results in rupture. The tank may also fail by brittle fracture without local yielding. This failure mode is discussed in Section 3, below.

Table B-I indicates the weight advantages which may be gained in using titanium as the tank material. For designs based on either room temperature properties or properties at liquid hydrogen temperatures, the aluminum and stainless steel tanks are nearly the same weight while the titanium tank is considerably lighter. It was this potential weight saving that dictated the choice of titanium as the tank material. This table also indicates the weight savings to be gained by using cryogenic properties as the basis for design. The present tank is required to withstand only modest pressures while at room temperature (2 psig required for rigidity), and while being filled pressure can be kept low until the

TABLE B-I

COMPARISON OF "IDEAL TANK" WEIGHTS FOR REPRESENTATIVE TANK

DESIGN BASED ON ROOM TEMPERATURE MATERIAL PROPERTIES

Material	"Design Stress"	Minimum Thickness Head	Minimum Thickness Shell	Weight of "Ideal Tank"
2014-T6 Aluminum	59,200 psi	.0265 in	.053 in	278 lb
AISI 301 Stainless Steel 60% Cold Worked	165,000 psi	.0095 in	.019 in	289 lb
5 Al-2.5 Sn Titanium Annealed	109,000 psi	.0144 in	.0288 in	242 lb

DESIGN BASED ON MATERIAL PROPERTIES AT -423^{o}F

Material	"Design Stress"	Minimum Thickness Head	Minimum Thickness Shell	Weight of "Ideal Tank"
2014-T6 Aluminum	77,800 psi	.0202 in	.0404 in	213 lb
AISI 301 Stainless Steel 60% Cold Worked	244,000 psi	.0065 in	.0130 in	198 lb
5 Al-2.5 Sn Titanium Annealed	248,000 psi	.0064 in	.0128 in	108 lb

entire tank has cooled down. Therefore, it is recommended that cryogenic properties be utilized to the maximum extent possible in light of toughness considerations, discussed below. These considerations will probably mean that actual tank wall thicknesses and weights will be heavier than shown on the cryogenic properties portion of Table B-I, but they should be lighter than for tanks designed to room temperature properties.

2. Rigid Tank vs. Pressurized Tank

There are two general approaches to the design of missile tankage. One, the pressurized tank approach, is to design the tank as a thin membrane capable of withstanding internal pressure forces only. A tank designed for this condition must generally be pressurized during handling and launch to prevent the skin from buckling by keeping it in tension at all times. The other approach, the rigid wall tank approach, is to design the tank skin to support all anticipated loads without being pressurized in addition to being able to hold the required pressure. A tank designed for the first condition will generally be lighter than one designed by the second, but it will require more care during fabrication, storage, handling, and launch and will have a lower factor of safety during operation.

Calculations were made to determine how much the tank under consideration would weigh if designed for each of the above conditions to determine the weight penalty associated with the rigid wall tank. These calculations were made for each of the three materials under consideration using the tank configuration and loading shown in Figure B-5.

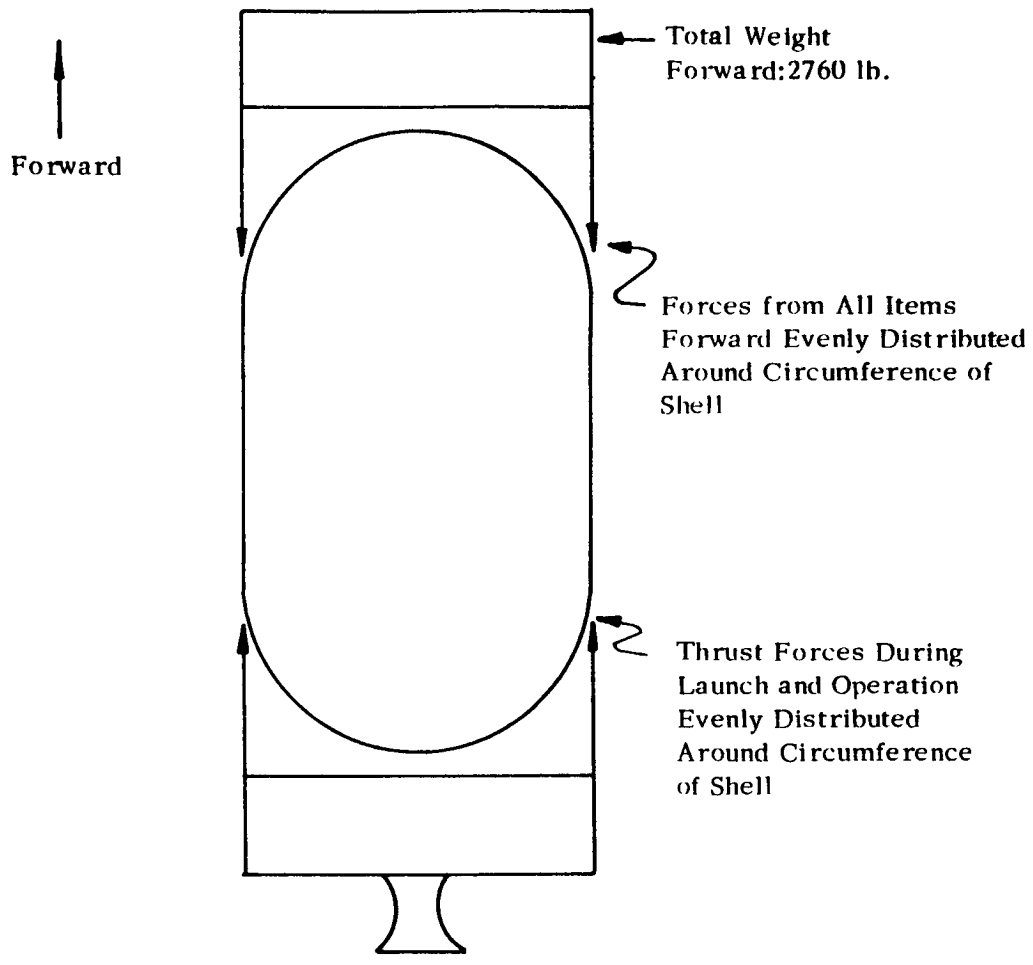

6.5 g's Maximum Axial
Acceleration During Launch

Weight Figures from Reference 2.

FIGURE B5 LOADINGS USED IN RIGID TANK VS PRESSURIZED TANK COMPARISON

Table B-II shows the results of these calculations. The tank wall thickness, tank weight for an "ideal tank" and safety factor K are tabulated for aluminum, stainless steel and titanium for four conditions of loading. The factor K, is the safety factor on buckling of the tank shell and is the ratio of the critical buckling stress to the actual stress in the wall. A minimum K factor of 15 was used in cases where the shell thickness was determined by buckling stresses rather than by pressure stresses. The comparison is based on designs using room temperature properties. In all cases a head that is thick enough to hold the pressure is self supporting.

The table shows that a tank capable of holding 55 psi internal pressure has a shell thick enough to support its own weight plus the payload under static conditions for all three materials under consideration (conditions A, B and C). The titanium tank is the lightest for these loading conditions. The aluminum tank is the most rigid and the stainless tank the least rigid for any condition of loading, as shown by the K values. If the tank must support the dynamic loads at launch without internal pressure, buckling strength determines the wall thickness and the tank shell for all three materials must be increased over that required by pressure alone. The aluminum tank requires the least increase in thickness and weight, the titanium tank the next, and stainless tank the most for the same factor of safety on buckling. The increase in tank weight is considerable for all three materials. This discussion assumes that payload forces are carried through the tank wall to the engine. It may

TABLE B-II

STRUCTURAL SUMMARY FOR TANK HAVING VARIOUS STRENGTH REQUIREMENTS

Strength Requirement	2014-T6 Aluminum				AISI 301 Stainless Steel 60% Cold Work				5 Al-2.5 Sn Titanium Annealed			
	t_s	t_h	W	K	t_s	t_h	W	K	t_s	t_h	W	K
A. Withstand 55 psi (1) internal pressure only	.053	.0265	278	-	.019	.0095	289	-	.0288	.0144	242	-
B. Withstand 55 psi Internal pressure and support its own weight under static conditions and no internal pressure	.053	.0265	278	381	.019	.0095	289	142	.0288	.0144	242	247
C. Withstand 55 psi Internal pressure and support its own weight plus payload under static conditions and no internal pressure	.053	.0265	278	41	.019	.0095	289	15	.0288	.0144	242	16
D. Withstand 55 psi internal pressure and support its own weight plus payload under 6.5 g's axial acceleration and no internal pressure	.092	.0265	404	15	.056	.0095	635	15	.074	.0144	475	15

t_s = shell thickness, in. t_h = head thickness, in. W = "Ideal tank" weight, lb. K = factor of safety on buckling

(1) This tank will also support its own weight plus the payload at 6.5 g's axial acceleration if pressurized to 2 psi.

be desirable from other considerations, e.g., heat leak requirements, to carry the payload forces completely around the tank in other structure, in which case the tank would have to support only its own weight.

The following conclusions may be drawn from the information in Table B-II.

1) There is a considerable weight penalty associated with requiring the tank to withstand dynamic launch loads without internal pressure, since the lightest rigid wall tank is 162 pounds heavier than the lightest pressurized tank.

2) If the tank is to rely on internal pressure for support during launch, the tank wall thickness is determined by pressure holding considerations, and the titanium tank is the lightest.

3) If the tank is to withstand dynamic launch loads without internal pressurization, the aluminum tank is the lightest, the titanium is heavier, and the stainless steel tank is the heaviest.

In the present case the pressurized tank approach was adopted to reduce the tank weight. The added care required during handling and the decreased factor of safety for the pressurized tank do not appear to offset the weight penalty attached to the rigid wall tank. This vehicle will have to be handled with extreme care in any event due to the nuclear reactor and other complex and delicate equipment on board. Additionally, it is not a weapon, so that the time element is not a dominant factor in handling operations. The added risk incurred by relying on pressure appears to be marginal since the pressure required for rigidity is low, in the order of 2 psi, and if the pressure drops off to below this value the flow system will not function. Additionally, this approach has been shown to be reliable by the Atlas ICBM, which relies on internal pressure for rigidity

during all stages of handling, shipping, and launch.

3. Fracture Toughness

Two primary modes by which a pressure vessel may fail are by tensile instability and by brittle fracture. Tensile instability occurs when some point on the vessel wall is stressed to its yield point, whereupon the wall yields and thins out. This thinning leads to further yielding and the process continues to rupture. Brittle fracture is a phenomenon associated with cracks and crack propagation and occurs when small cracks or defects grow under the influence of the applied stresses to the point where they are unstable, i.e., to the point where they propagate rapidly and cause failure of the vessel. Tensile instability occurs at a local stress equal to the yield point of the material, while brittle fracture may occur at stresses far below the yield point of the material and depend upon the material, the temperature, the applied stress field, and any irregularities in the body of the material or on its surface. The ratio of sharp-notch tensile strength to smooth coupon tensile strength, usually called the sharp-notch tensile ratio, is a qualitative indication of the susceptibility of a material to brittle fracture. As most missile tankage made to date have been fabricated of materials with a high sharp-notch tensile strength ratio (in the range of 0.9 - 1.0) at the operating temperature or have been operated at stress levels considerably below their yield strength, the probability of failure by brittle fracture is low. For these tanks, the prime mode of failure is by tensile instability so the yield strength, or some fraction of it, has been used as a design stress.

Thus, the sharp-notch tensile strength ratios have been used only as a screen to limit the consideration of useful materials to those having sharp-notch tensile ratios above a certain value which experience has shown to be safe, and yield strengths from the smooth tensile test have been used to set design stresses.

As operating temperatures of missile components are lowered from liquid oxygen temperature to liquid hydrogen temperature, tank materials which were heretofore ductile exhibit more brittle behavior. This is especially true of the high strength stainless steel and titanium alloys considered in this report. In fact it appears unlikely that a current production steel with a yield strength greater than 220,000 psi will be found which will not exhibit brittle behavior. Thus if the high strength of available materials at cryogenic temperatures is to be utilized fully, a more detailed quantitative approach must be taken toward brittle fracture, and techniques must be developed for designing tankage out of materials which exhibit brittle behavior.

These techniques, and the data necessary for their application, are receiving attention in the literature today and promise to receive even more in the near future. Basically a fracture toughness analysis considers the stresses in the area around the ends of a through-the-thickness crack in a material which is subjected to a tensile stress at right angles to the length of the crack. The magnitude of these stresses depend upon the properties of the material in question, the imposed tensile stress, and the length of the crack. At low values of applied stress the crack

is stable, i.e., remains as it is. As the stress increases some value will be reached at which the crack will start to increase in length. Initially, this process is self limiting, and the crack will not continue to grow unless the stress is increased. At some critical value of stress the process ceases to be self limiting and crack extension continues without further increase in stress until fracture occurs.

The intensity of the stress field surrounding the tip of the above described crack may be described by a parameter K, the stress intensity factor. This parameter may be calculated from a stress analysis of the crack, knowing certain properties of the material and crack. Further, the stress intensity factor at the point at which the crack becomes unstable is given the name fracture toughness and the symbol K_c. Fracture toughness is a material property and varies with material thickness, material temperature, and, in some sheet materials, direction of rolling. A notched or slotted tensile test coupon is generally used to determine fracture toughness. If the fracture toughness is known, the stress at which unstable propagation of a crack occurs may be determined from the following relationship:

$$\sigma_c = K_c \sqrt{\frac{1}{\pi a + \frac{K_c^2}{2\sigma_{ys}^2}}}$$

where;

σ_c = critical stress at which unstable crack propagation occurs, psi

K_c = fracture toughness of the material at the temperature and thickness in question, psi - in.

a = crack length, in.

σ_{ys} = yield strength of the material at the temperature to question, psi

Evidently, in order to determine the critical stress in a structure or conversely, whether a crack is stable under a known stress, something must be known about the length of crack which is expected. One approach used is to assume a crack length equal to twice the material thickness, and to design the vessel so the stress in the wall is below that at which this crack will become unstable. This approach arises from an assumption about the formation of through-the-thickness cracks. The assumption is that at a stress below the critical stress, certain point defects in the surface of the tank wall will propagate radially in one plane until they penetrate the thickness of the material. Thus while the crack front has moved one material thickness in opposite directions from the point of origin along the surface of the material, and the crack length on the surface of the material is twice the material thickness. Thus it is reasoned that a twice-the-thickness is the minimum that could be expected. The critical stress for a twice-the-thickness is denoted by the symbol $\sigma_{c\ 2t}$.

The above criterion has been applied to the present tank for the two materials under consideration for which fracture toughness data is

available. The value of $\sigma_{c\ 2t}$ has been calculated for the longitudinal and transverse material directions in the head and shell of the tank using the material thickness shown in Table B-I for a tank design based on material properties at -423°F. The ratio of the actual stress to $\sigma_{c\ 2t}$ is tabulated in Table B-III.

The fracture toughness for the stainless steel is less in the transverse direction than in the longitudinal direction, which accounts for the difference in the $\sigma / \sigma_{c\ 2t}$ ratio for equal stresses in these two directions in the head of the stainless tank. The fracture toughness of the titanium is the same in both directions. It should be mentioned that the above figures merely indicate trends, since the K_c values used in determining them were determined from thicker material than was used in these calculations. K_c is known to depend on material thickness, increasing with decreasing material thickness up to a point. The figures in Table B-III indicate the degree to which the actual stresses approach probable failure stresses for brittle fracture. Since the ratio of the actual stress to the failure stress for tensile instability has been set at .91, it is evident that the probability of failure of the vessel by brittle fracture is of the same order as the probability of failure by tensile instability. In any event it may be seen that AISI-301 stainless 60 percent cold worked and annealed 5 Al-2.5 Sn titanium are roughly equivalent as far as toughness is concerned in the present application.

The above analysis is necessarily limited since current fracture mechanics theory is incomplete and data on materials of interest is

TABLE B-III

RATIO OF ACTUAL STRESS IN THE TANK WALL TO THE STRESS AT WHICH A THROUGH-THE-THICKNESS CRACK OF TWICE THE MATERIAL THICKNESS IS UNSTABLE

Material	Head		Shell	
	Longitudinal Direction	Transverse Direction	Longitudinal Direction	Transverse Direction
AISI 301 Stainless steel 60% cold worked	.730	.878	.806	.535
5 Al-2.5 Sn Titanium Annealed	.794	.794	.940	.470

scarce. For instance, effects of more than one stress cycle or of a biaxial stress field are not known, and information is needed on the stress levels which produce propagation of a surface defect to a through-the-thickness crack. In the present application this latter event must be prevented even though the tank would not rupture, for the hydrogen leakage through a stable through-the-thickness crack of twice the tank wall thickness would be great enough to jeopardize the mission. Thus, the thickness and weight figures indicated in Table B-I should be considered as minimums in light of a tensile instability analysis. In actuality, the design stresses for the tank will have to be determined from further developments in theory and from further test work on test coupons or on miniature pressure vessels if weight is to be minimized. Theoretical and experimental work of this nature is presently being carried out in a number of places with special attention being given to 5 Al-2.5 Sn titanium alloy. The results of this work are encouraging and the specifications of techniques for utilizing the cryogenic strength of titanium should be available in the near future.

REFERENCES

B1. "Space Power Operation", Final Report for the period 3/1/61-8/31/61. Arc-Jet Application Study, Contract NAS 5-1034, General Electric Flight Propulsion Laboratory Dept.

B2. "Thermal Arc-Jet Engine Mission Study", Final Report Contract NAS 5-1033, Research and Advanced Development Division, Avco Corporation, Wilmington, Mass., December 1961.

B3. Goodman, J. W., "Final Report on Pressure Vessel Design Criteria", Space Technology Laboratories, Inc. TR-60-0000-19427.

B4. Bonney, E. A., Zucrow, M.J., and Besserer, C. W., Principles of Guided Missile Design Aerodynamics, Propulsion, Structures and Design Practice, D. Van Nostrand Co., Inc., 1956.

B5. Spieth, C. W., Establishing Tank Design Criteria for Liquid Hydrogen Rockets, Vol. I, Analytical and Parametric Studies, Beechcraft Engineering Report No. 8768, September 1960.

B6. Private Communication with W. F. Brown, Jr., National Aeronautics and Space Administration, Lewis Research Center, Cleveland, Ohio.

B7. Hanson, M. P., Stickley, G. W., and Richards, H. T., "Sharp-Notch Behavior of Some High-Strength Sheet Aluminum Alloys and Welded Joints at 75, -320, and -423^{o}F", ASTM Special Technical Publication No. 287, P. 3., June 1960.

B8. Alcoa Aluminum Handbook, Aluminum Company of America.

REFERENCES (2)

B9. Crane, C. H., and Smith, W. G., "Application of 2219 Aluminum Alloy to Missile Pressure Vessel Fabrication", Welding Research Supplement, January 1961, p. 33.

B10. Rice, L. P., Campbell, J. E., and Simmons, W. F., "Tensile Behavior of Parent Metal and Welded 5000-Series Aluminum Alloy Plate at Room and Cryogenic Temperatures", Advances in Cryogenic Engineering Vol. 7, p. 478, Plenum Press, New York, 1962.

B11. Kaufman, J. G., and Johnson, E. W., "New Data on Aluminum Alloys for Cryogenic Applications", Advances in Cryogenic Engineering, Vol. 6, p. 637, Plenum Press, New York, 1961.

B12. Espey, G. B., Jones, M. H., and Brown, Jr., W. F., "Factors Influencing Fracture Toughness of Sheet Alloys for Use in Lightweight Cryogenic Tankage", ASTM Special Technical Publication, No. 302, p. 140, June 1961.

B13. Podell, H. L. and Kotfilia, R. J., "Design and Fabrication of Titanium Rocket Chambers", American Rocket Society Report No. 1602, February 1961.

B14. Abkowitz, S., Burke, J. J., and Hiltz, Jr., R. H., Titanium in Industry, D. Van Nostrand Co., Inc., 1955.

B15. Private Communication with Titanium Metals Corporation of America, New York, N.Y.

REFERENCES (3)

B16. Hanson, M. P., "Smooth and Sharp-Notch Tensile Properties of Cold-Reduced AISI 301 and 304L Stainless-Steel Sheet at 75°, -320°, and -423°F", NASA TN D-592, February 1961.

B17. Watson, J. F. and Christian, J. L., "Low Temperature Properties of Cold-Rolled AISI Types 301, 302, 304 ELC, and 310 Stainless-Steel Sheet", ASTM Special Technical Publication No. 287, p. 170, June 1960.

B18. Watson, J. F. and Christian, J. L., "Mechanical Properties of High-Strength 301 Stainless-Steel Sheet at 70, -320, and -423°F in Base Metal and Welded Joint Configuration", ASTM Special Technical Publication No. 287, p. 136.

B19. Witzell, W. E., "Fracture Toughness of Stainless-Steel Sheet at Cryogenic Temperatures", American Rocket Society Paper No. 2418-62, April 1962.

B20. Gorcey, R., "Filament-Wound Pressure Vessels", Machine Design, June 22, 1961, p. 178.

B21. Werts, W. E., "Fabrication of Wire Wound Vessels for Motor Cases, Presented at National Aerospace Manufacturing Forum, Los Angeles, California, October 1961, Sponsored by SAE.

B22. Lemons, C. R., "Fabrication of Large Filament Wound Liquid Propellant Tanks", Presented at National Aerospace Manufacturing Forum, Los Angeles, California, October 1961, Sponsored by SAE.

REFERENCES (4)

B23. Watson, J. F. and Christian, J. L., "Low-Temperature Properties of K-Monel, Inconel-X, Rene 41, Haynes 25, and Hastelloy B Sheet Alloys", ASME Paper 61-WA-12.

B24. Durham, T. F., McClintock, R. M., and Reed, R. P., Cryogenic Materials Data Handbook, NBS - Contract No. AF 04(647)-59-3.

B25. Fracture and Strength of Solids, E. Orowan, Report on Progress in Physics, Vol. 12, p. 185, 1949.

B26. Yukawa, S., "Testing and Design Considerations in Brittle Fracture", ASTM Special Technical Publication No. 302, p. 193, June 1961.

B27. Fracture Testing of High-Strength Sheet Materials, A Report of a Special ASTM Committee ASTM Bulletin No. 243, p. 29, January 1960, and No. 244, p. 18, February 1960.

B28. The Slow Growth and Rapid Propagation of Cracks, Second Report of a Special ASTM Committee, Materials Research and Standards, Vol. 1, No. 5, p. 389, May 1961.

B29. Fracture Testing of High-Strength Sheet Materials, Third Report of a Special ASTM Committee, Materials Research and Standards, Vol. 1, No. 11, p. 877, November 1961.

B30. Screening Tests for High-Strength Alloys Using Sharply-Notched Cylindrical Specimens, Fourth Report of a Special ASTM Committee, Materials Research and Standards, Vol. 2, No. 3, p. 196, March 1962.

REFERENCES (5)

B31. Espey, G. B., Jones, M. H. and Brown, Jr., W. F., "Sharp-Edge-Notch Tensile Characteristics of Several High-Strength Titanium Sheet Alloys at Room and Cryogenic Temperatures", ASTM Special Technical Publication No. 287, p. 74, June 1960.

APPENDIX C

SUPPORT SYSTEM FOR THE HYDROGEN STORAGE VESSEL

A. INTRODUCTION

The mechanical support system for the inner hydrogen tank on the arc-jet feed system must support the tank and isolate it thermally from the rest of the structure on the vehicle. The system to be described was selected as the lightest weight one which would sustain all the imposed loads and have a heat leak equal to the target heat leak of 7 watts.

B. SUMMARY AND CONCLUSIONS

The investigation of a number of support methods and materials lead to the following conclusions concerning the present application:

1. The lightest weight support system will result if the tank is supported continuously around its circumference by a cylindrical ring of insulating material.
2. Fiber glass reinforced plastic is the most promising material for this support ring.

A design incorporating these features is shown schematically in Figure C-1. The fiber glass reinforced plastic support ring is .110-inch thick, has an unsupported length of 11.5 in., and weighs about 37 pounds.

C. DISCUSSION

1. Loads

The payload forces will not be taken through the tank wall or support structures, therefore the only loads on the tank and its support structure

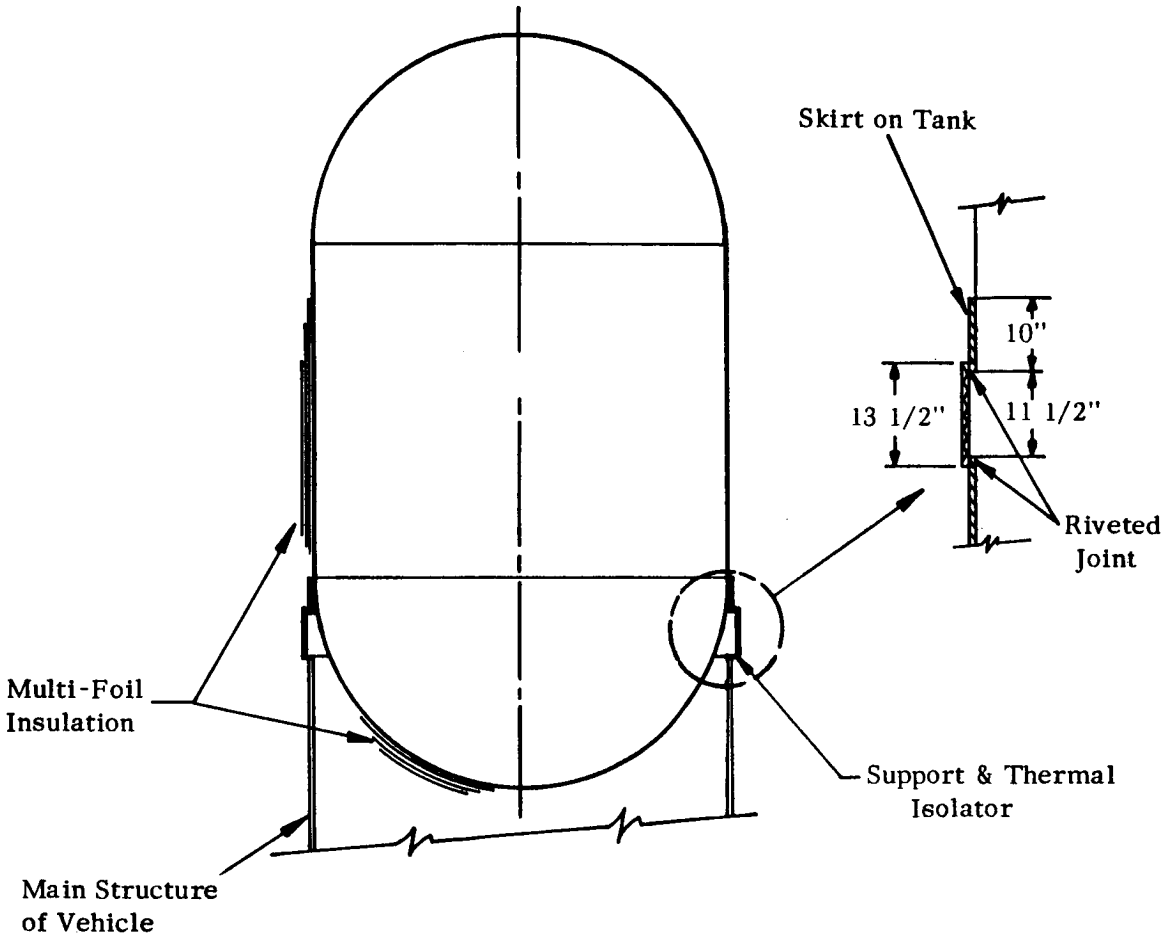

FIGURE C1 CONTINUOUS TANK SUPPORT SYSTEM

are those due to the tank and the liquid hydrogen. These loads are summarized in Figure C-2. The critical design condition occurs when the maximum acceleration in the longitudinal and transverse direction occur simultaneously. In addition to sustaining the above-mentioned loads, the support system must also be able to accommodate changes in tank dimensions with pressure and temperature. The tank diameter and length will increase with increasing pressure and will decrease with decreasing temperature as shown in Table C-I. The dimensional changes indicated in this table are those which would result if the tank were completely unrestrained.

TABLE C-I

DIMENSION CHANGES IN TANK WITH PRESSURE AND TEMPERATURE

	Increase in Dimension Between 0 psi & design pressure	Decrease in Dimension Between Room Temperature & -423°F
Shell Diameter	1.504 in.	.222 in.
Shell Length	.279	.175
Over-all Length	.897	.398

The increase in dimensions with pressure vividly demonstrates that the tank wall is a pressurized membrane, not unlike a balloon. The support system is designed so the stresses in both the tank wall and the support itself are below the maximum allowable, so that the heat leak is acceptable and the weight is as low as possible. The discussion which follows outlines some of the support systems investigated, discusses selection of the materials for the thermal isolating portion of the support, and compares

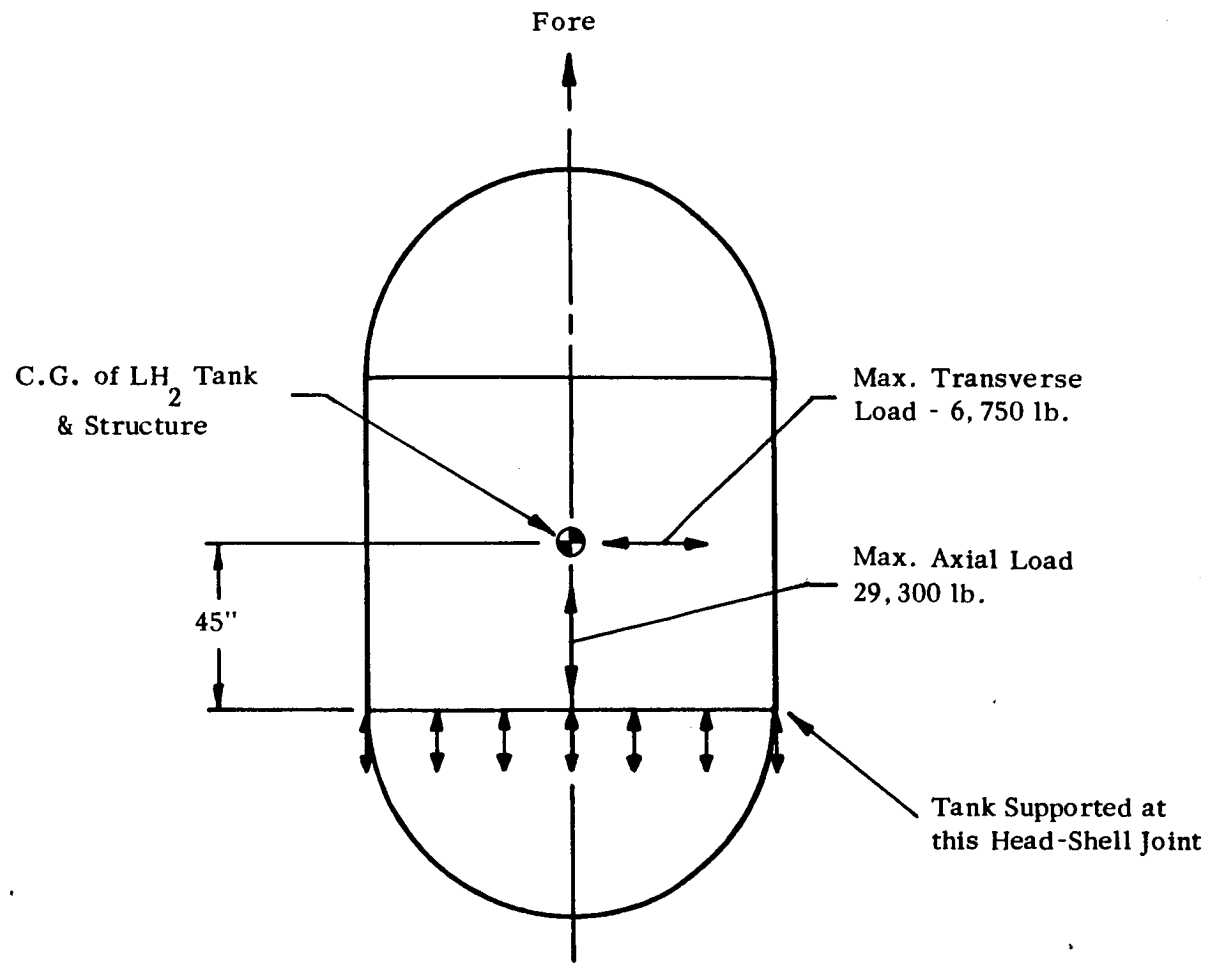

Total Wt. Taken as 4500 lb.

Max. Axial Accel. - 6.5 g's

Max. Transverse Accel. - 1.5 g's

FIGURE C2 LOADS ON TANK SUPPORT SYSTEM

several designs on the basis of weight.

2. Support Methods

The tank is supported at the aft head-to-shell joint simply because there appear to be no advantages in supporting it anywhere else. The tank will be pressurized to prevent the tank wall from being put into compression by bending due to transverse accelerations. The support system may be considered as composed of two primary elements, structural elements on the tank and main vehicle which are designed from mechanical considerations alone, and the thermal isolator which must provide a barrier to heat flow and transmit loads from the tank structure to the main vehicle structure. Starting with these considerations all support systems may be classified as one of two general types: 1) a continuous support system in which all the loads from the head-shell joint to the main structure of the vehicle are carried through a continuous shell made of a good thermal insulator; or 2) a point support system in which the loads are collected at a number of points around the circumference of the shell by structural members on the tank, transferred to the main structure of the vehicle through small thermal isolating supports at each point, and then redistributed around the circumference by structure on the main vehicle. As will be seen below, the thermal insulator in a continuous support system is heavier than the best insulator which can be used in a point support system. However, more structure is required for the point support system, which tends to counteract the weight advantage of the insulator itself. Thus the continuous support system is comprised of

relatively light structure and relatively heavy insulator, while the point support system is composed of relatively heavy structure and relatively light insulator.

The best continuous support system is shown in Figure C-1. In it the tank wall is extended in the form of a cylindrical skirt to a point about ten inches below the head-to-shell joint. This skirt transmits loads from the tank wall to a cylindrical shell made of a thermal insulator. The loads are then transmitted from the thermal insulating support shell to a continuous shell on the main structure of the vehicle. The tank skirt is long enough to permit the tank diameter to change as shown in Table C-I without transmitting any radial forces to the insulating support and is thick enough to withstand the imposed forces without buckling. The insulating support is proportioned so that the heat flux through it is tolerable (the projected design has a heat leak of 7 watts) and so it will sustain the imposed loads without buckling. The joints between the dissimilar materials are able to transmit the loads, and the joint at the cold end of the insulating ring is able to accommodate differential thermal contraction between the two materials.

A number of other continuous support systems were examined, but all of them required more structure and/or were more complex than the above system without showing any offsetting advantages. The one exception to this was a system in which the entire tank was slung in a net wrapped around the outside of the insulation. This system was discarded because it was not deemed advisable without any supporting experimental data to

rely upon the relatively flimsy multi-foil insulation to carry mechanical loads, especially those imposed by vibrations during boost.

Several point support systems are shown in Figure C-3. The system shown in Figure C-3A has the support point right in the tank wall in the form of a series of tabs protruding from the wall. The thermal insulators transmit the loads from these tabs to corresponding support points on the main structure of the vehicle, from which the stresses are distributed to a cylindrical shell. The tab on the tank is essentially a cantilever beam and will induce excessive bending moments in the tank wall unless additional structure of some sort is provided to distribute the point loads. Additionally, some provision must be made for changes in diameter of the tank with pressure and temperature. If the tank wall is permitted to move, a complicated support is required, and if the tank wall is prevented from moving by making the support sufficiently rigid, large radial forces are developed between the tank and the support as the pressure in the tank is increased. In either case, the calculations that can be made to determine the interrelations between radial forces, deflections, and stresses are uncertain because the potential deflections are very large compared to the thickness of the tank wall so the assumptions made in simple theory of shells do not apply. Thus, since this configuration requires heavy structure and uncertain design calculations, it was dropped from further consideration.

Figure C-3B shows the most promising point support system investigated. It uses a skirt-type extension of the tank shell to transmit

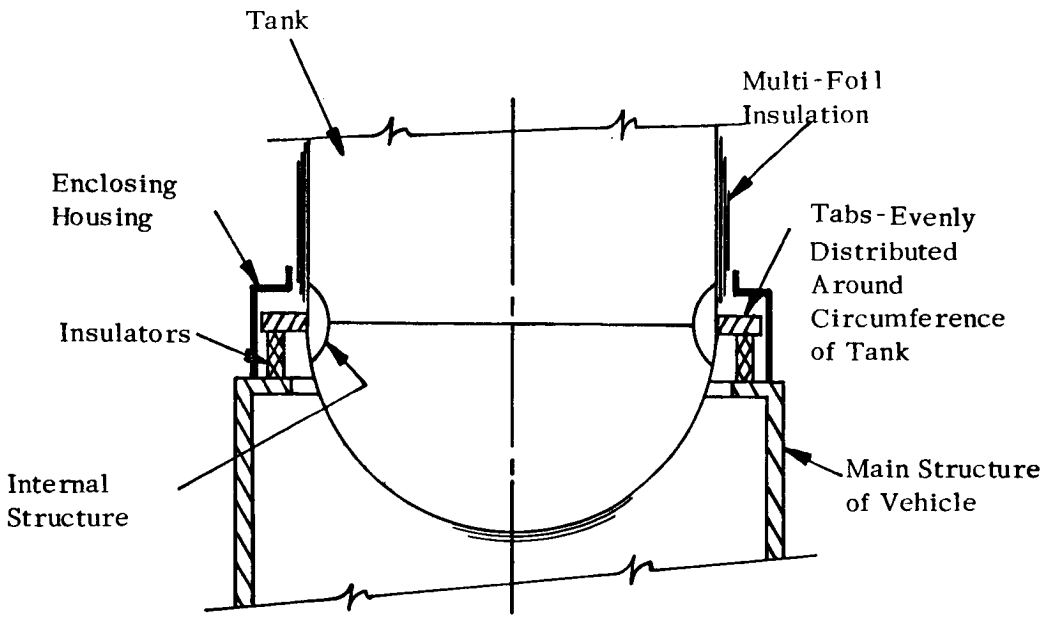

A. SUPPORT IN TANK WALL

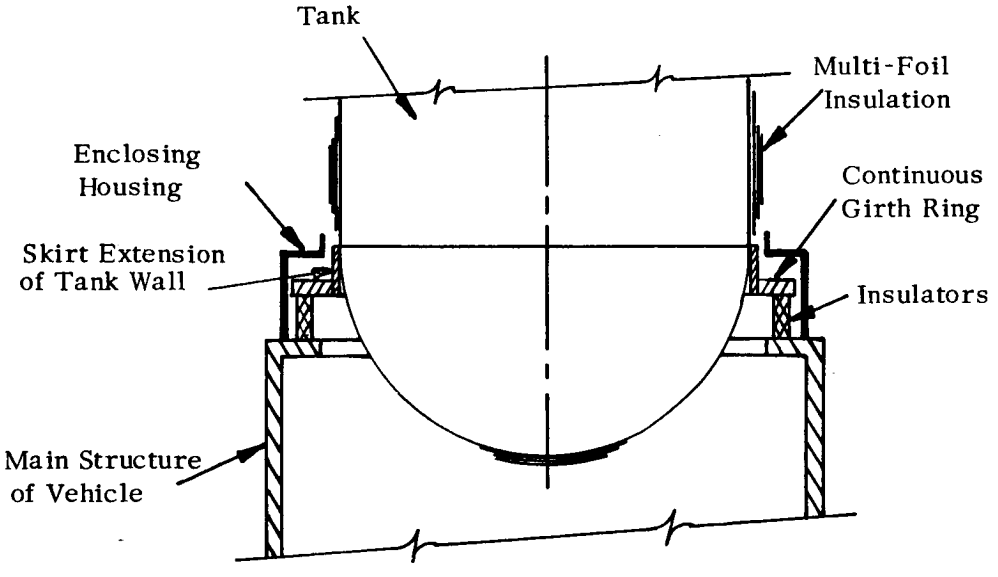

B. SUPPORT ON FLANGED SKIRT

FIGURE C3 TYPICAL POINT SUPPORT SYSTEMS

forces from the shell into a girth ring. Insulating supports are located at a number of points around this girth ring and carry the load to support points on the main structure from which the stresses are distributed to the cylindrical shell of the main structure. This is the point support system used in subsequent comparisons.

3. Support Materials

A number of thermal insulating materials which are capable of supporting loads were investigated for use in both a continuous support system and a point support system. Initial screening of candidate materials was done by deriving a figure of merit to indicate the lowest weight isolator for the specified loading and heat leak, and final material selection was made by comparing several support system designs incorporating different isolating materials.

In the continuous support system, the thermal isolator is a thin cylindrical shell subjected to an axial load uniformly distributed around its circumference. The most critical condition from a design standpoint is when this load is compressive, under which condition the mode of failure is local buckling of the cylindrical shell. A figure of merit has been derived for an isolator loaded in this manner. This derivation shows that the isolator portion of the support system will have a minimum weight when the isolator is made of the material for which the parameter $\frac{k\rho}{E}$ is a minimum; where k is the thermal conductivity, ρ is the density, and E is Young's modulus for the material in question. This factor of

merit serves when the loading, temperature difference, heat leak, and cylinder diameter are the same for all materials.

Table C-II shows a comparison of a number of materials which were considered for use in the continuous support system. As may be seen from this table, fiber glass reinforced plastic will give the lightest support for this system, Mylar will give a slightly heavier one, and Micarta will give a considerably heavier one.

In a point support system the thermal isolator is a prismatic member subjected to axial loads. In an actual design these isolators would be located so that the loads would be nearly axial, even under transverse loading of the tank and, therefore, material comparisons considered only axial loading. All the materials considered are able to sustain both tensile and compressive loads. The sole exception to this is the stacked stainless steel washer type of support, which is able to sustain only compressive loads. Therefore, for the point support configuration, the most critical load is the one which will cause tensile or compressive yielding of the isolator. Analysis shows that the isolator portion of a point support system will be the lightest when the isolator is made of a material for which the parameter $\frac{k\rho}{\sigma^2}$ is a minimum. In this parameter, k is the thermal conductivity, ρ, is the density and σ is the yield strength of the material in question. For all materials except stainless washers, σ is taken as either the tensile or compressive yield strength, whichever is lower. For the stainless washers, σ is taken as the compressive yield

TABLE C-II

COMPARISON OF THERMAL ISOLATING MATERIALS

Material	k Thermal Conductivity Btu-in/hr ft^2 °F	ρ Density lb/ft^3	E Young's Modulus, lb/in^2	σ Yield(1) Strength lb/in^2	FIGURE OF MERIT Buckling $\frac{k\rho}{E}$ Btu-in^3 / hr ft^5 °F	FIGURE OF MERIT Yielding $\frac{k\rho}{\sigma^2}$ Btu-in^5 / lb hr ft^5 °F
Stacked Stainless Steel Washers	.130	500	-	60,000	(2)	7.25×10^{-8}
Fiber Glass Reinforced Plastic	2.0	140	3.3×10^6	18,000	$.849 \times 10^{-4}$	119×10^{-8}
Mylar	1.05	86.6	1.0×10^6	20,000	$.909 \times 10^{-4}$	23.7×10^{-8}
Micarta	2.0	84.1	1.0×10^6	35,000	1.68×10^{-4}	12.8×10^{-8}
Rigid Polyvinyl-chloride	0.70	87.0	0.35×10^6	6,000	1.74×10^{-4}	169×10^{-8}
Nylon	1.33	71.0	0.40×10^6	20,000	2.36×10^{-4}	23.6×10^{-8}
Stainless Steel	87.6	500	30×10^6	60,000	14.6×10^{-4}	1220×10^{-8}
Titanium	55.2	276	16×10^6	120,000	9.52×10^{-4}	106×10^{-8}

(1) Tensile or compressive yield, whichever is lower.

(2) This material not applicable to this support configuration.

strength and the entire parameter is multiplied by four to account for the fact that each compressive support will have to be opposed by a duplicate compressive support, and each of these opposing supports must have a heat leak of one half the comparable support with tension-bearing capabilities. This method of comparison assumes the same load, temperature difference, and heat leak for each material. As shown in Table C-II comparisons of support materials on the basis of tensile or compressive yielding of the support indicates that for a point support system the stacked stainless steel washers will give the lightest isolator. A Micarta isolator will be about twice as heavy, and a Nylon or Mylar isolator will be approximately four times as heavy. Actually, projected designs of actual point support assemblies show that a point support using stacked stainless steel washers will weigh about the same as one using Micarta as the thermal isolator because of the extra weight required by the double-opposed construction of the stainless washer assembly. It may be seen on the basis of weight, that stainless steel and titanium are poor support material choices even though they have high strength, because of their high thermal conductivity and density compared to other materials. The titanium skirt on the tank has a negligible insulating effect.

4. Comparison of Support Designs

Selection of the support system configuration and isolator material was made after comparing the weights of several comparable support systems. Several similar continuous support designs using different isolating materials were projected to check the figure-of-merit approach to material

selection, several point support assemblies were projected for the same reason, and the continuous support system design was compared with the point support system. All comparisons were made on the basis of weight for a system to withstand the loads indicated in Figure C-2 and with a heat leak of 7 watts. All systems investigated were required to be compatible with a multi-foil tank insulation system.

Table C-III compares a continuous support thermal isolator made of the two most promising materials for this type of support, fiber glass reinforced plastic and Micarta. The support system is of the type shown in Figure C-1.

TABLE C-III

COMPARISON OF CONTINUOUS SUPPORT ISOLATOR MATERIALS

Material	Fiber Glass Reinforced Plastic	Micarta
Thickness	.110 in.	.190 in.
Total length	13.5 "	20.75 "
Weight	37 lb.	69 lb.
Figure of merit for local buckling (Table C-II)	$.849 \times 10^{-4}$	1.68×10^{-4}

The ratio of the weight of the fiber glass reinforced plastic isolator to that of the Micarta isolator is .537, and the ratio of the figures of merit is .505, indicating that the figure-of-merit approach to material selection is valid for a given configuration, and that the fiber glass reinforced plastic is the best continuous support material.

Designs were projected for the thermal isolating portion of a point support system of the type shown in Figure C-3B. These designs included mounting brackets in addition to the isolator, and showed that the total weight of the isolating assemblies was about five pounds for isolators using either stacked stainless steel washers or Micarta. Table C-IV compares the best continuous support system with what appears to be the best point support system.

TABLE C-IV

COMPARISON OF WEIGHTS OF SUPPORT SYSTEMS

Continuous Support System		
Titanium Skirt on Tank		35 lbs.
Fiber glass reinforced plastic insulator		37
Misc. hardware		1
	Total:-	73 lbs.
Point Support System		
Titanium Skirt on Tank		35 lbs.
Titanium girth ring on tank skirt	more than	45
Insulator assemblies		5
Titanium girth ring on vehicle structure	more than	45
Misc. hardware		1
Total:-	more than	131 lbs.

The calculations for the girth rings on the point support system were made using simplifying assumptions which give a ring size smaller than would actually be required, hence the notation on the ring weights in the table.

Note that the weight of the continuous support system is considerably less than that for the point support system in spite of the fact that the isolator in the continuous system is much heavier. It is evident from these figures that the weight of structure required to collect all the loads at one point far overbalances the weight advantage gained by using a very light insulator.

A useful generalization concerning support systems might be made here. It has been seen that for a support system with an allowable heat leak which is not too restrictive, as in the present case, a continuous support system will be lighter in weight than a point support system, even though the thermal isolator in the latter is considerably lighter than in the former. However, if the allowable heat leak were much less, as it would be for extended space voyages during which there was no withdrawal of hydrogen from the tank, other factors come into play which would require the use of the point support system. The point support system can be extended to very low heat leak values because it is able to utilize the extremely effective stacked washer type of thermal insulator. Requiring extremely low heat leaks through a continuous type support system, means that the thermal isolator becomes longer and thinner. As the allowable heat leak is decreased, eventually the design reaches the point where either the increasing weight of the isolator more than offsets the weight of the added structure required by the point support system, or the length-to-thickness ratio set by thermal requirements is so large that it is outside the area of practical designs which will fulfill the strength

requirements of local buckling. In either event it would be necessary to accept the heavier point support design in order to meet heat leak requirements.

REFERENCES

C1. Fung, Y. C., and Sechler, E. E., "Buckling of Thin-Walled Circular Cylinders Under Axial Compression and Internal Pressure", Jour. of Aeronautical Sciences, V. 24, N. 5, p. 351, May 1957.

C2. Harris, L. A. et al, "The Stability of Thin-Walled Unstiffened Circular Cylinders Under Axial Compression Including the Effects of Internal Pressure", Jour. of the Aeronautical Sciences, V. 24, N. 8, p. 587, August 1957.

C3. Peterson, G. P., "Properties of High Modulus Reinforced Plastic", Soc. Plastics Engineers Jour., January 1961.

C4. Pfluger, A., Elementary Statics of Shells, F. W. Dodge Corp., 1961.

C5. Gibbs and Cox, Inc. Marine Design Manual of Fiberglass Reinforced Plastics, McGraw Hill, 1960.

C6. Roark, R. J., Formulas for Stress and Strain, McGraw Hill, 1954.

C7. Seide, P., "Calculations for the Stability of Thin Conical Frustrums Subjected to External Uniform Hydrostatic Pressure and Axial Load", Jour. of the Aerospace Sciences, V. 29, N. 8, p. 951, August 1962.

C8. Timoshenko, S., Strength of Materials, Parts I and II, Van Nostrand, 1940.

C9. Timoshenko, S., Theory of Elastic Stability, McGraw Hill, 1936.

C10. Timoshenko, S., Theory of Plates and Shells, McGraw Hill, 1940.

APPENDIX D

THE METEOROID HAZARD TO THE HYDROGEN STORAGE TANK

A. INTRODUCTION

In order to estimate the hazard that meteoroids pose to space vehicles, it is necessary to have a description of the flux of meteoroids in space, their velocity and mass distributions, and their composition. It is also necessary to know to what extent a meteor particle can penetrate a surface which it will encounter. A large uncertainty now exists in the available information and this results in a commensurate uncertainty in the prediction of the hazard. Our own examination and interpretation of the available information on the meteoroid hazard results in estimates of penetrating encounters with meteoroids that vary by a factor of 1000 for a given material and thickness. The major factor contributing to the uncertainty is our lack of knowledge on the meteoroid population, particularly regarding its mass flux distribution. Lack of knowledge on the penetrating phenomena also contributes, but to a lesser extent.

The meteoroid environment and the potential hazard of its interaction with space vehicles has been discussed at length in the selected references listed at the end of this report. It is not our purpose to repeat here the background of information already presented in the literature; rather, we intend to derive from it the meteoroid hazard to the hydrogen storage tank and the basis for defining its protection requirements. The design approach to the meteoroid protection system which we will take is extremely

simple. We do this because the uncertainty of the data relating to design is so large at the present time that a more sophisticated attack is not warranted. More realistic or near optimum designs must await the results of both the analytical and experimental work on the meteoroid hazard that is in progress.

B. THE METEOROID HAZARD

The liquid hydrogen vessel will be approximated as a thin-wall, 114-inch diameter by 90-inch long cylinder with hemispherical ends. The heads have a combined exposed area of 284 square feet and the cylindrical portion has an exposed area of 224 square feet. The minimum wall thickness, that is the thickness required to withstand internal pressure only, is 0.010 inch or,0.026 inch for the head and 0.019 inch or 0.053 inch for the shell, depending on whether the tank is fabricated of high strength stainless steel or aluminum. A tank made of a titanium alloy would have wall thicknesses close to that of a stainless steel fabrication. If the unprotected hydrogen vessel were exposed to the meteoroid environment for one hundred and twenty days, we estimate that the number of penetrating encounters would be in the amounts given in Table D-I. Table D-II gives the skin thicknesses required to raise the probability of no penetrating encounters to within an acceptable range.

From the data shown in these tables, we conclude that a hydrogen vessel with walls of minimum thickness needs protection against meteoroids and that to provide this protection by the sole means of increasing the wall thickness leads to an unacceptable weight penalty. The meteoroid

TABLE D-I

EXPECTED NUMBER OF PENETRATIONS FOR UNPROTECTED HYDROGEN VESSEL

Material	Thickness (in.)	Expected Number of Penetrations*		
		Estimated Upper Limit	Intermediate Estimate	Estimated Lower Limit
Aluminum	.026 (head)	17,000	610	21
	.053 (shell)	1,700	61	2
Stainless	.010 (head)	51,000	1,800	63
	.020 (shell)	5,100	180	6

*Calculated on basis given in Reference D-1.

TABLE D-II

THICKNESS VS. PROBABILITY OF PENETRATING ENCOUNTERS FOR UNPROTECTED HYDROGEN VESSEL

Material	Probability of No Penetrating Encounters	Thickness (in)* Estimated Upper Limit	Intermediate Estimate	Estimated Lower Limit
Stainless	99	2.07	0.65	0.23
Aluminum	99	3.90	1.22	0.43
Stainless	90	0.94	0.29	0.10
Aluminum	90	1.77	0.55	0.20

*Calculated on basis given in Reference D-1.

bumper, a concept introduced by Whipple, promises protection at a reduced weight penalty; therefore, we will adopt this concept and apply it to our purposes.

C. METEOROID PROTECTION

Because of weight limitations it is not feasible to design a system to protect against the larger meteoroids which might impact. Protection is provided for meteors having masses less than a specified upper bound and one accepts a certain probability of failure of the mission due to a chance encounter with a meteoroid larger than that for which protection is given. Fundamentally, the design of the meteoroid protection system is established by the degree of risk which is considered tolerable. This point is illustrated by Figure D-1.

Figure D-1 stems from Whipple's description of the meteoroid population. In this description, the number of meteoroids larger than mass m, hitting a given surface in a given period of time is assumed to be inversely proportional to m. Current estimates of the integrated meteoroid flux in the upper range of masses for which protection can be afforded are spanned by assigning a mass of one gram (as a minimum) or thirty grams (as a maximum) to the zero magnitude visual meteor.

We will consider designs for meteoroid protection against masses up to 10^{-3} or 10^{-2} grams. Protection for masses up to 10^{-3} grams tacitly assumes the willingness to accept a 50 or 2.5 percent probability of failure of the mission due to the chance encounter with a larger meteoroid. The two values of probability reflect the currently accepted uncertainty in the integrated

FIGURE D1 NOMOGRAM FOR DETERMINATION OF SIZE OF DESIGN METEOR

mass flux distribution. Protection for masses up to 10^{-2} grams reduces the risk of failure to 6 or 0.2 percent. In the present concept, the structural system for meteoroid protection will consist of:

1. A thin skin, referred to as the bumper, which is easily penetrated by the largest (design) meteoroid but whose purpose is to generate such a strong shock wave in the impacting meteoroid that it will be fragmented into tiny pieces or, possibly, even vaporized.
2. A space to allow dispersion of the disintegrated meteoroid and bumper material.
3. A second skin capable of absorbing the dispersed material without failure. This second skin can, at the designers discretion, be the tank wall or an outer layer of insulation or a structural skin.

In order to define the physical aspects of the protection system, we assume a bumper sufficient to disintegrate the largest design meteoroid and that all of the momentum of the meteoroid passes through the bumper and is impulsively transferred to the second skin. The separation of the bumper and second skin is made sufficient to spread this momentum over enough area on the second skin so that the latter is not seriously damaged. The second skin is designed so that under impulsive loading it is not stressed to failure.

A detailed analysis of the fragmentation process or detailed stress analysis of the second skin under the conditions postulated is beyond the

scope of this work. Such analyses are in process by Arthur D. Little, Inc., under Contract No. NAS 5-664. For our purposes we must at this time make some further simplifications in order to arrive at some engineering design criteria. The resultant criteria must be viewed as tentative, for data in hand is not sufficient to lend its uncontested support.

It appears from calculations and experiments[D2] [D3] that a bumper having a mass to projected surface area equal to 10 percent of the mass per unit of projected area of a projectile will be more than adequate to cause the complete breakup of the projectile even at low meteoric velocities.* Table D-III summarizes calculations relating to bumpers designed in accordance with the above criterion.

We note from Table D-III that a fairly appreciable bumper is required to break up the 0.01 or 0.001 gram design meteors if they are iron-like, while a reasonably thin bumper should pulverize the dust ball type. It is generally believed that by far the greatest number of meteoroids in the mass ranges of significance to the protection system design are of the dust ball type with perhaps 10 percent being of the iron type. This means that the probability of zero hits from iron meteoroids greater than 0.001 grams

---

*This is a gross simplification of the results predicted by hypervelocity impact analysis.

TABLE D-III

BUMPER DESIGN PARAMETERS

Meteoroid Mass (grams)	Meteoroid Density (gm/cc)		Bumper Mass/ Unit Area (gms/cm^2)	Bumper Thickness (mils) Mylar	Aluminum	Steel
0.01	8	(iron like)	0.0712	20.0	12.0	4.0
0.001	8		0.0328	9.2	5.6	1.8
0.0001	8		0.0152	4.2	2.6	0.8
0.01	1.0	(stone like)	0.0179	5.0	3.0	1.02
0.001	1.0		0.0083	2.4	1.4	0.46
0.01	0.1	(dust balls)	0.00286	1.08	0.64	0.22
0.001	0.1		0.00178	0.50	0.30	0.10

is about the same as the 0.01 gram or larger dust ball (namely, greater than ninety percent) and we will not protect against them. On the other hand, the probability of zero hits from iron-like meteoroids greater than 0.0001 grams may lower to near 50 percent (depending on assumption of meteoroid flux density and the fraction of all meteoroids that are iron) and the bumper should be sufficient to fragment meteoroids of this or smaller mass. From a similar argument applied to the stone-like meteoroids one concludes that protection against those having masses of 0.001 grams or smaller deserves consideration but the risk of hits from larger ones is tolerably small. To summarize, a 4 to 5 mil thickness of mylar or equivalent should serve the bumper function.

As a failure criterion for the second skin we assume that its impact area can be impulsively accelerated to a maximum average velocity of 100 feet per second.* To place this criterion in perspective, we note that a unit mass of steel stressed to 200,000 psi stores an elastic strain energy equivalent to the kinetic energy of this unit mass traveling at 112 feet

---

*This criterion has its origins in a preliminary analysis carried out under NASA Contract No. NAS 5-564, of the stresses induced on a large thin elastic plate by an impulsive load having an axisymmetric gaussian distribution. This work to be published under NAS 5-664.

per second. Therefore, if momentum and energy is conserved in the impact process on the second skin and if this skin in the impact region deforms as a uniformly stressed elastic membrane, the 100 feet per second average velocity bound limits the stress to something less than 200,000 psi. Actually, one does not expect one hundred percent conversion of kinetic energy to strain energy and one expects an area of the second skin greater than the impact area to store energy so that the failure criterion is conservative in these respects. On the other hand, one does not expect the second skin to be uniformly stressed in the impact zone and the failure criterion is not conservative in this regard.

Combining the second-skin failure criterion with our assumption of conservation of momentum, we get

$$\rho_s A_s t_s V_s = mV \qquad (1)$$

where:

ρ_s = density of second skin

A_s = impact area at second skin

t_s = thickness of second skin

V_s = maximum average velocity of impact portion of second skin, set equal to 100 feet per second

m = mass of largest meteor to be defeated

V = velocity of largest meteor to be defeated

The velocity of meteoroids in the vicinity of the earth are estimated to vary between about 33,000 feet per second and 260,000 feet per second

with a number-mean velocity of about 120,000 feet per second. Using the number-mean velocity for the meteoroid, Equation (1) reduces to:

$$\rho_s A_s t_s = 1200 \text{ m} \qquad (2)$$

and from Equations (1) and (2) we see that the weight of the second skin is proportional to the impact area, A_s.

The appropriate impact area depends on the uniformity and divergence of the spray from the meteor exploding at the bumper and the bumper-to-second skin spacing. The uniformity and divergence of the spray depends on many factors including structure and composition of the meteoroid and bumper, meteoroid velocity, angle of incident of meteoroid with bumper, etc., and predictions based on present information are tenuous.

From an elementary theory[D2], one expects that the spray from a normal impact at the bumper would be confined to a cone whose half angle is mainly determined by the meteor velocity and the ratio of the meteor mass to the mass of bumper material intercepted by the meteor. Some experimental data at the relatively low impact velocities now obtainable give a measure of support to this theory.

On the other hand, more advanced theoretical considerations[D3] of the impact of pellets having impact energies commensurate with meteoroids on thin plates predict spray angles much larger than predicted by the elementary theory and realized from hypersonic range firings. Awaiting a more precise definition of the expected spray angle, we estimate that the divergence of the spray for the meteoroid-bumper combinations considered here will be greater than 10 degrees. In other words, the assumption of a

spray having a semi-vertex angle of 10 degrees is intended to be conservative. Factoring this assumption into Equation (2), we arrive at an expression for the minimum mass per unit area, M_a, of the second skin necessary to defeat the design meteor.

$$M_a = \rho_s t_s = \frac{12{,}300\ m}{\delta^2} \tag{3}$$

where δ is the bumper-to-second skin distance.

Table D-IV shows the results of calculations based on Equation (3).

In interpreting Table D-IV it may be well to reiterate that the need to defeat the 0.01 gram dust ball or the 0.001 stone-like type meteors remains questionable. If the zero magnitude visual meteor can be taken as 1 gram, the probability of hits from these or larger meteors of like kind is a fraction of one percent. In this event it appears that a bumper that is the equivalent of 5 mils of mylar spaced a few inches from a second skin that is the equivalent of a mil or so of high strength steel would provide acceptable protection. On the other hand, to defeat the 0.01 gram dust ball meteor would require either a separation distance of the order of two feet or a heavier second skin.

As the second skin is expected to absorb a good deal of energy upon impact without fracture, it is necessary that it not be highly stressed at times of meteor exposure. As the inner hydrogen containing tank wall is highly stressed it should not be made to serve as the second skin. It may be that the thermal insulation would serve as a second skin, but the mechanical characteristics of typical types bear little resemblance to the

TABLE D-IV

ESTIMATED SECOND-SKIN DESIGN REQUIREMENTS

Mass of Meteor (grams)	Mass/Unit Area, M_a (gram-cm^2)	Thickness of Steel Second-Skin (cm)	Standoff Distance, δ for 1 mil Thick Steel Second Skin (cm)
0.0001	$1.20/\delta^2$	$0.15/\delta^2$	7.6
0.001	$12.0/\delta^2$	$1.50/\delta^2$	24.4
0.01	$120/\delta^2$	$15.0/\delta^2$	76.3

second skin model that we have postulated and any predictions of its performance cannot be justified on the basis of available information.

The bumper material must not produce fragments having appreciable penetrating power. We have observed fragments from 5 mil steel bumpers penetrate 30 mil steel second skins. Therefore, we recommend that the bumper not be made of a structural metal but suggest rather a plastic film, a fiberglass cloth, or a resin filled fabric. In addition, as the bumper acts as the outermost thermal shield its outward facing surface should be highly reflective to incoming radiation (mostly sunlight) and highly emissive in the IR band, and it is desirable for its inward facing surface to have a low emissivity in the IR band.

D. CONCLUSIONS

Information that is presently available does not provide a sound foundation on which to base the design of a meteoroid protection system.

Uncertainty in the data regarding integrated meteoroid flux densities translates to an uncertainty in the probability of being hit by a damagingly large meteor. This in turn leaves the question of whether the hydrogen tankage should be protected from meteors having masses up to 0.01 grams or just 0.001 grams somewhat open. A less cautious position would hold that protection only against meteors up to 0.001 grams would involve an acceptable risk.

Lack of information on the behavior of protection systems based on the bumper concept makes the specification of design very tenuous at this time. The simplified evaluations which have been carried out herein must be

accepted in this light. Nevertheless, it does appear that adequate protection can be provided for the hydrogen tank without a large weight penalty. A light-weight, deployable, non-metal bumper backed by a mil or so of stainless steel or its equivalent (maybe the multi-foil thermal insulation would serve) should be adequate. A more definitive design of the meteoroid protection system must await the generation of more information on the meteoroid environment and on the behavior of bumper systems.

REFERENCES

D1. Wiederhorn, N. M. et al, "Liquid Propellant Losses During Space Flight", Third and Fourth Quarterly Report, NASA Contract No. NAS 5-664, November 1961.

D2. Wiederhorn, N. M. et al, "Liquid Propellant Losses During Space Flight", Second Quarterly Progress Report, NASA Contract No. NAS 5-664, May 1961.

D3. Bull, G. V., "On the Impact of Pellets with Thin Plates-Theoretical Considerations", - Part 1, Technical Report No. 63270-03-01, NASA Contract No. NAS 5-664, January 1962.

D4. Beard, D. B., Astrophysical Journal 129 pp 496-506 (1959).

D5. Bjork, R. L., "Effects of Meteoroid Impacts on Steel and Aluminum", The Rand Corp., Paper P-1662 (1958).

D6. Bjork, R. L., "Meteoroids Versus Space Vehicles", Rand Report P-1963, April 1960.

D7. Henderson, R. E., and Stanley, P., "The Effect of Micrometeorites on Reflecting Surfaces", 1960 Proceedings of the Institute of Environmental Sciences.

D8. Kornhauser, M., "Prediction of Cratering by Meteoroid Impacts", Advances in Astronautical Sciences, Volume 2, (Proceedings of the Fourth Annual Meeting of the AAS, December 1957), Plenum Press, Inc., New York, 1958.

D9. McKinley, D. W. R., Astrophysical Journal 113 p. 225 (1951).

REFERENCES (2)

D10. Olshaker, A. E., "An Experimental Investigation in Lead of the Whipple Meteor Bumper", Thesis for M.S. Degree M.I.T., 1960.

D11. Ovenden, M. W., "Meteor Hazards Beyond the Atmosphere" in Space Research and Exploration edited by D. R. Bates, pp 102 to 120 (1957).

D12. Pereira, J., "The Effects of Meteorites on the Structural Design of Space Vehicles", Republic Aviation Corp., Report RDSR-7, June 1, 1960.

D13. Whipple, F. L., in Between The Planets, edited by F. G. Watson (1956).

D14. Whipple, F. L., "Meteoritic Phenomena and Meteorites" in Physics and Medicine of the Upper Atmosphere edited by C. S. White and O. O. Benson (1952).

D15. Whipple, F. L., Nature 189 127 (1961).

D16. Whipple, F. L., "The Particulate Content of Space", presented at the Third Symposium on the Medical and Biological Aspects of the Energies of Space.

APPENDIX E

ESTIMATES OF THE THERMAL RADIATION INCIDENT ON HYDROGEN TANK DURING THE TRANSFER TRAJECTOR

A. INTRODUCTION

The design of the insulation system for the hydrogen tank requires, as a first step, that the incident thermal flux to the insulated vessel be evaluated at all times during the mission. This report is addressed to the evaluation of the thermal radiation incident on the vessel during the transfer of the payload from a 500 nautical mile initial orbit to a 22,400 nautical mile, twenty-four hour synchronous, equatorial orbit.

During the transfer trajectory portion of the mission there are three major sources of heat input to the hydrogen vessel: 1) thermal radiation from the space environment, 2) thermal radiation from other portions of the space vehicle (the power plant radiator is the most important source), and 3) gamma heating due to the neutron flux emanating from the nuclear power plant.

B. THERMAL RADIATION FROM THE SPACE ENVIRONMENT

For purposes of this evaluation the hydrogen vessel is approximated as a cylindrical vessel ten feet in diameter with hemispherical ends. The cylindrical portion has an axial length of 7.5 feet. The cylindrical portion and aft hemispherical end of the tank is exposed to the thermal environment of space. These portions are assumed to be completely exposed to the space environment, that is, they are not shadowed by other portions of the vehicle. The forward hemispherical end is enclosed in structure that

attaches the tank to the payload. Heat inleakage through this end is not considered here.

The space vehicle containing the hydrogen tank is assumed to be launched eastward from Cape Canaveral to the 500 nautical mile initial orbit. The acute angle between the earth-sun line and the plane of the initial orbit depends on the time of launch - both hour and day of year - and can vary between 5 and 52 degrees. If the initial orbital plane is inclined at 52 degrees to plane of the ecliptic, we can have at one extreme a near-twilight orbit; if the initial orbital plane is inclined at 5 degrees to the plane of the ecliptic, we can have at the other extreme a near-noon orbit. Each of these extremes gives rise to different amounts of reflected and direct solar radiation intercepted by the tank. In the near-noon orbit the average direct sunlight is reduced to a minimum because of the tank shape factor and because the space vehicle spends a maximum amount of time in the earth's shadow. On the other hand, the incident flux due reflected solar radiation is a maximum. In the near-twilight orbit the incident direct sunlight is a maximum and the incident albedo is a minimum. One can show that the total incident thermal radiation is less in the near-noon orbit (about 10 percent less than in the near-twilight orbit) and the near-noon initial orbit will be assumed.

The inclination of the orbital plane with the ecliptic plane will vary during transfer, depending on the thrust vector control of the arc-jet engine. For purposes of this evaluation, a transfer in the plane of the ecliptic will be assumed. At altitudes where earth shadow and reflected

solar radiation effects are important, this is nearly the case; at higher altitudes the effect of orbital plane inclination is small. In addition, the estimates of incident thermal radiation from the space environment which follow assume that a single orbit around the earth is circular.

Familiar paths have been followed in the calculation of planetary thermal emission, reflected solar, and direct solar radiation to the hydrogen vessel. Data published in Reference E1 were helpful in making these computations.

Table E-I summarizes the results of calculations.

C. THERMAL RADIATION FROM THE MAIN POWER PLANT RADIATORS

That portion of the thermal radiation emitted from the radiators of the main power plant incident on the hydrogen tank is given by the expression

$$q_R = F_{12} A_1 \epsilon_1 \sigma T_1^4 \qquad (1)$$

where:

F_{12} = radiator-to-tank configuration factor

A_1 = surface area of the power plant radiators

ϵ_1 = total hemispherical emissivity of the radiator surfaces

σ = Stephan-Boltzmann constant

T_1 = temperature of the radiator surfaces

The products $A_1 \epsilon_1 \sigma T_1^4$ must be approximately 300 KW for the SNAP-8 power supply. About four hundred square feet of radiator surface with an ϵ of 0.8 and operating at $1200^{\circ}R$ is required to dissipate this amount of energy. If the radiator is divided into two panels and if these panels

TABLE E-I - THERMAL RADIATION INCIDENT ON HYDROGEN TANK FROM SPACE ENVIRONMENT

Altitude (Nautical miles)	Earthshine (watts)		Average Reflected Solar Radiation (watts)		Average Direct Solar Radiation (watts)	
	cylindrical portion	hemispherical portion	cylindrical portion	hemispherical portion	cylindrical portion	hemispherical portion
500	1310	785	1080	610	3480	3370
1000	975	560	833	480	3640	3615
4000	320	174	220	150	4640	4300
8000	133	71	85	50	5320	4600
10000	96	51	66	33	5500	4675
20000	33	16	28	14	6200	5100

are deployed in the vicinity of the tank much like wings, then F_{12} will be of the order of 0.10. Accordingly, about 30,000 watts of thermal energy will be incident on the hydrogen tank.

This energy is in IR wave bands and to obviate its deleterious effect one is faced with the difficult problem of devising a coating for the external surface of the insulation which will effectively reflect this radiation ($1200^{\circ}R$, black-body) and sunlight and still be a good emitter at its own operating temperature (about $500^{\circ}R$). On the other hand, deployment of the power plant together with its radiators to a location more remote from the tank* will greatly reduce the factor F_{12} and provides an effective solution to the problem of thermal emission from the power plant radiators. In addition, remote deployment makes the use of shadow shields very attractive and eases the problem of gamma heating.

In order to assess quantitatively the influence of radiator deployment, computations of F_{12} were carried out for two basic arrangements of the radiators in respect to the tank. These arrangements together with results are illustrated in Figures E-1 and E-2. The calculations of configuration factors were made with the aid of published data[E1][E3] and graphical methods employing physical models.

---

*This idea has been presented previously in Reference E2.

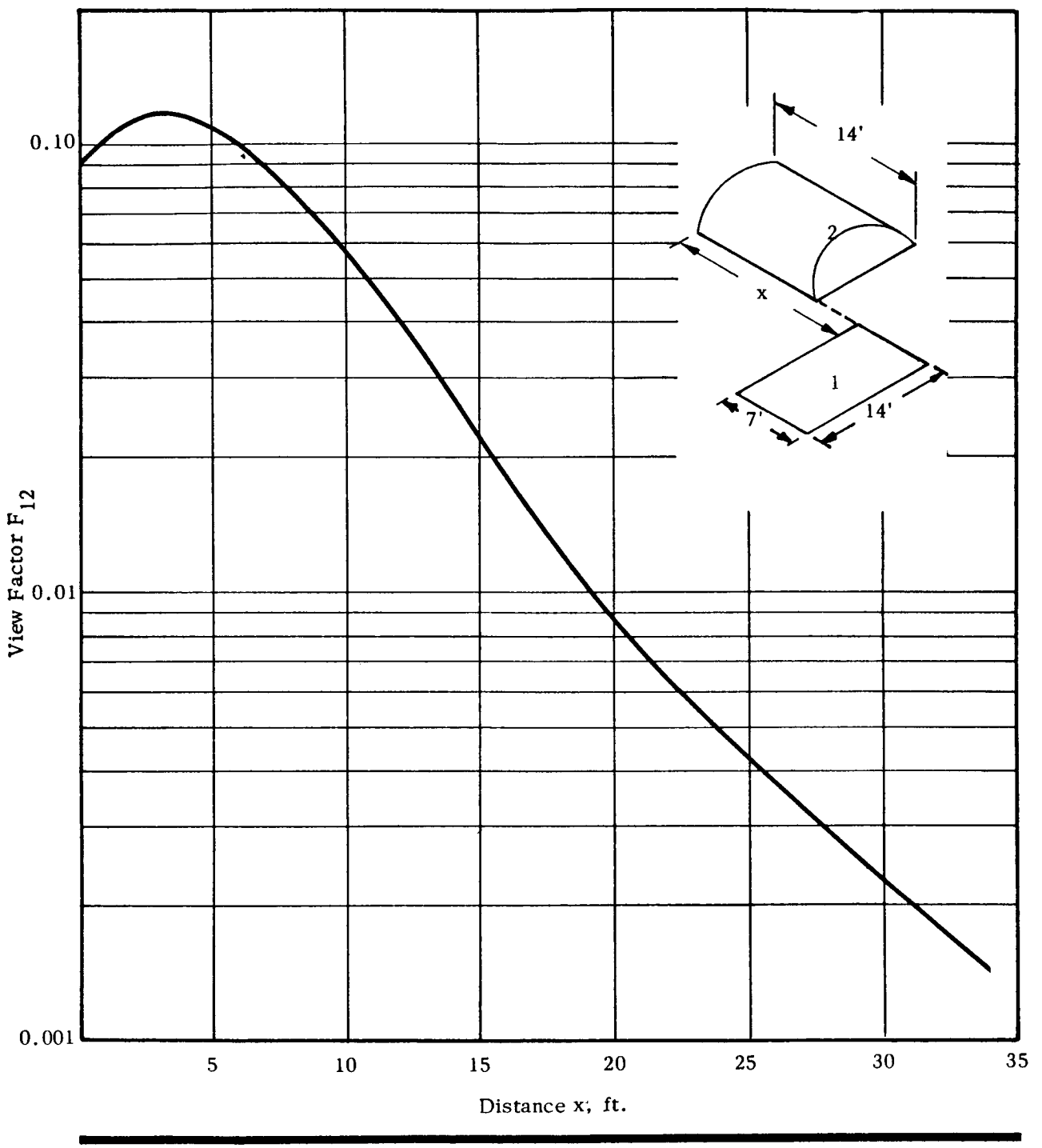

FIGURE E1 RADIATOR-TO-TANK CONFIGURATION FACTOR (Arrangement No. 1)

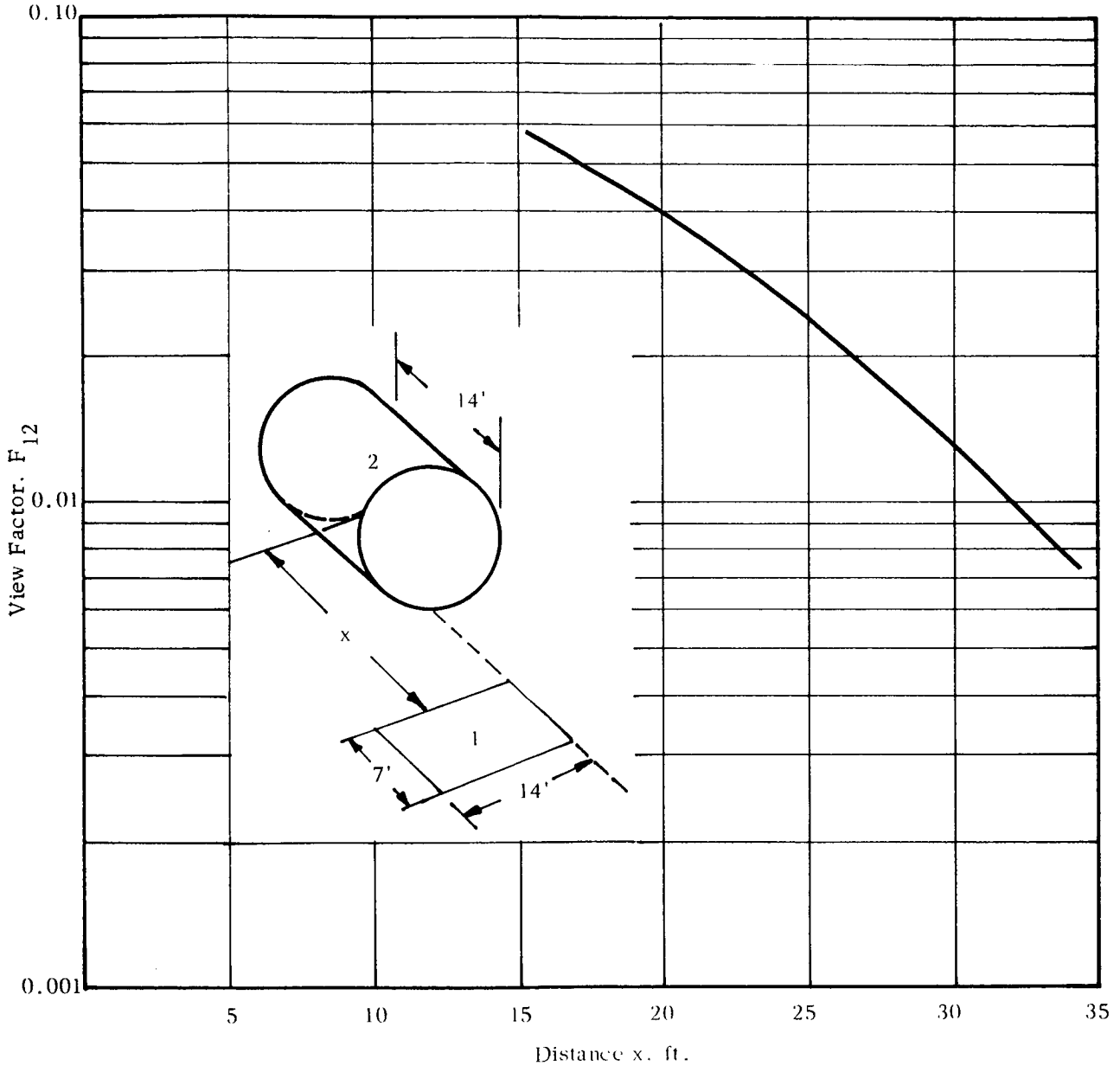

FIGURE E2 RADIATOR-TO-TANK CONFIGURATION FACTOR (Arrangement No. 2)

In all the computations of configuration factor, the hydrogen tank was approximated as a 9.5-foot diameter cylinder having an axial length of fourteen feet and the SNAP-8 power plant radiators were approximated as two 14 by 7 foot rectangular panels.

Figure E-3 translates the effect of radiator deployment in terms of the total heat flux leaving the power plant radiators that is intercepted by the hydrogen tank. These results show the superiority of arrangement 1 over arrangement 2, but either arrangement can be utilized to reduce the intercepted flux an order of magnitude or more. One can also show that a few radiation shields located in the near vicinity of the power plant radiators are sufficient to reduce the thermal input to the hydrogen tank from this source to a negligible amount.

D. GAMMA HEATING

The nuclear reactor in the SNAP-8 power plant will emit energy in the form of electromagnetic radiation and sub-atomic particle radiation. In the absence of specific data about this radiation, we have made a preliminary investigation using general "rules-of-thumb" and simplifications to gain a rough understanding of the thermal effects of the radiation on the hydrogen tankage and to determine if further analysis is necessary. The following is a discussion of the results of this investigation.

The energy emitted from the reactor is predominantly gamma radiation. Since this is the most difficult to shield against it was the only radiation considered in detail. Its effect on liquid hydrogen is the same as thermal radiation, i.e., it causes heating, so that precautions

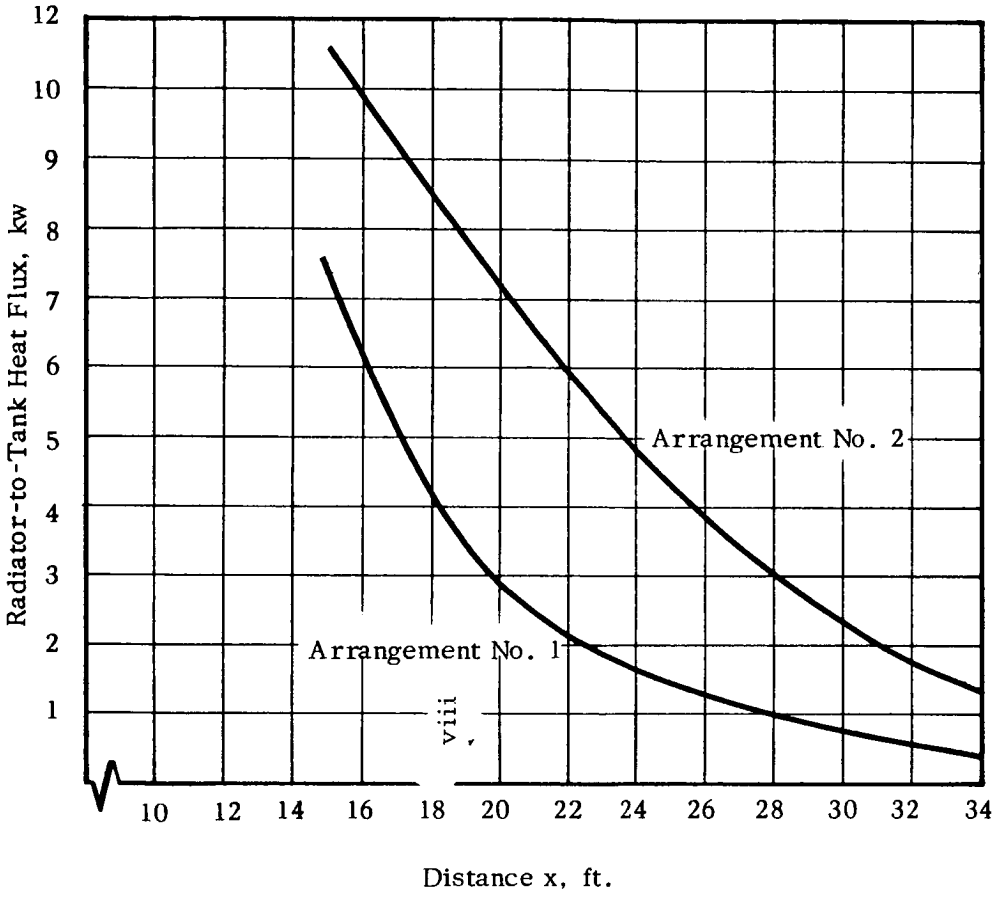

FIGURE E3 POWER PLANT RADIATORS-TO-HYDROGEN TANK HEAT FLUX (No Shadow Shields)

must be taken to limit the amount of this radiation absorbed by the hydrogen. Generally we can expect 1 to 5 percent of the useful power output of the nuclear reactor to be emitted as gamma radiation. Using the higher figure, 1500 watts will be radiated and will be evenly distributed over a spherical surface. The radiation incident upon the hydrogen tank is merely the amount contained in the solid angle of this spherical surface subtended by the tank diameter and will decrease as the reactor is moved farther from the tank. Figure E-4 is a plot of the gamma radiation incident upon the hydrogen tank as a function of the distance between the tank and the center of the reactor for a total quantity of radiation of 1500 watts.

In order to determine the amount of the incident gamma radiation which is absorbed by the tank walls and the hydrogen itself, the complete radiation spectrum must be known (i.e., the intensity of radiation at all radiating frequencies must be known) since the amount of radiation absorbed is a function of frequency. In the absence of this frequency-intensity data, we have assumed all the radiation is monochromatic at an arbitrarily selected energy level of .34 Mev, an energy level at which the absorption of energy is fairly high. Under these conditions, 1 percent of the gamma energy incident upon the tank will be absorbed by the aft head of the hydrogen tank and the balance will pass through it into the hydrogen. If the tank is full of liquid hydrogen, 99.94 percent of the energy incident upon the liquid will be absorbed by the liquid and converted to heat. Thus, for all practical purposes, all of the gamma radiation incident upon the tank will go into heating the hydrogen. This means that

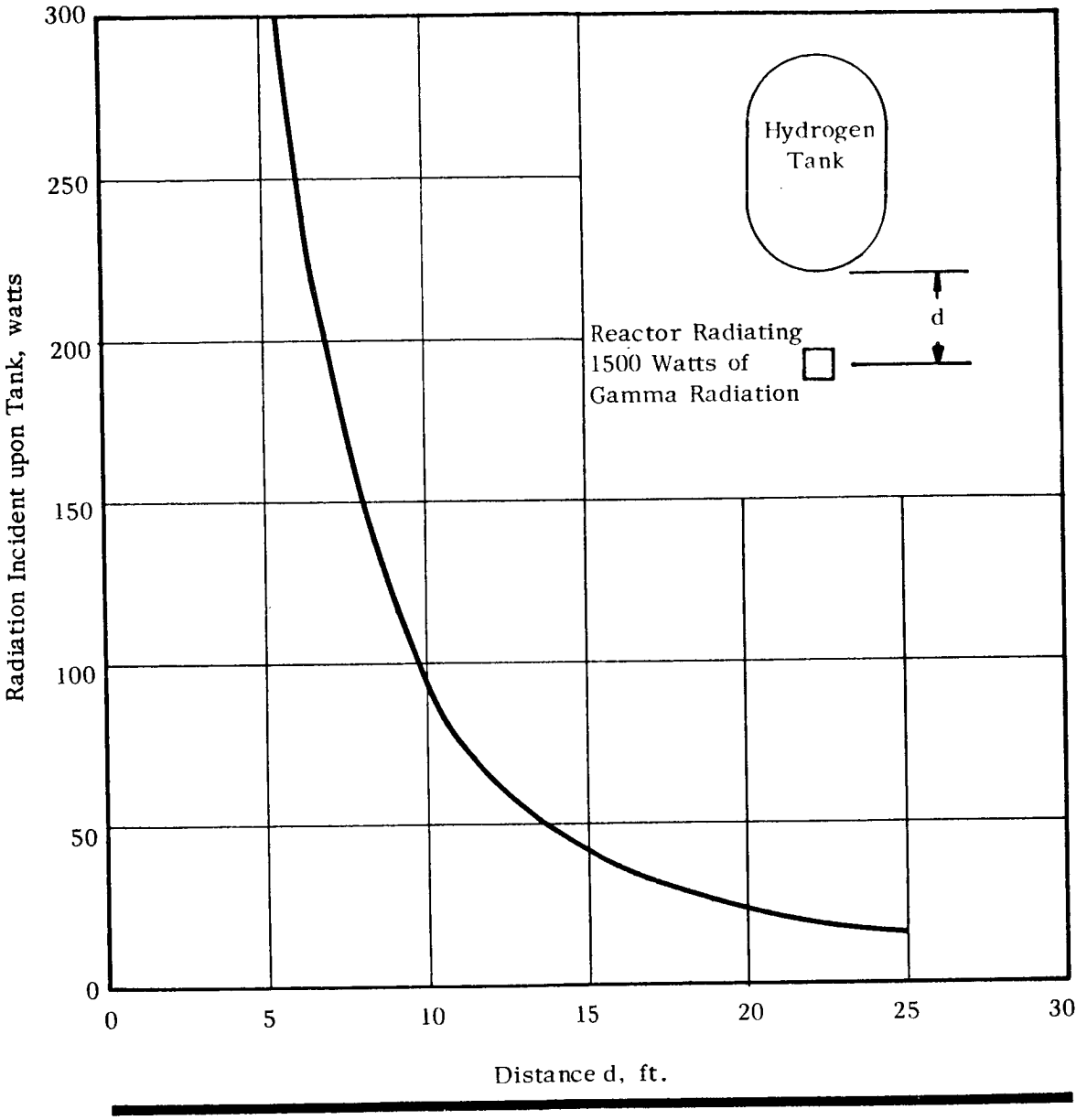

FIGURE E4 ESTIMATED GAMMA RADIATION INCIDENT UPON HYDROGEN TANK

the reactor will have to be placed far enough from the tank so the incident radiation is at an acceptable level or shielding will have to be introduced. In setting target heat leaks, about 20 watts of heating can reasonably be allotted to gamma radiation, thus unless additional shielding is provided, it will be necessary to deploy the reactor 20 to 25 feet aft of the hydrogen tank, as may be seen from Figure E-4.

E. CONCLUSIONS

1. A transfer from an initial orbit near the plane of the ecliptic results in minimum thermal input to the hydrogen vessel. However, differences between this and less favorable initial orbits are small.

2. The thermal flux to the hydrogen tank from the SNAP-8 power plant must be limited. Deployment of the power plant together with its radiators to a location 10 to 20 feet from the hydrogen vessel and the use of shadow shields can provide the means for reducing the thermal input to the hydrogen tank from this source to a negligible amount.

3. Deployment of the power plant to a location remote from the hydrogen vessel is an effective means for limiting the gamma heating of the tank's contents. Preliminary estimates indicate that locating the power plant 20 feet from the hydrogen vessel should limit the gamma heating of the hydrogen to a value which can be considered tolerable. Estimates of gamma heating require refinement.

REFERENCES

E1. Stevenson, J. A., and Grafton, J. C., "Radiation Heat Transfer Analysis for Space Vehicles", ASD Technical Report 61-119, Part I, Contract AF 33(616)-7635, December 1961.

E2. Yarymovych, M. I., et al, "Feasibility of Arc Jet-Propelled Spacecraft", ASTRONAUTICS, June 1962.

E3. Hamilton, D. C., and Morgan, W. R., "Radiant-Interchange Configuration Factors", NACA TN 2836, December 1952.

APPENDIX F

THERMAL PROTECTION SYSTEM FOR THE LIQUID HYDROGEN STORAGE VESSEL

A. INTRODUCTION

The liquid-hydrogen storage vessel should be thermally isolated to the degree necessary to preserve the propellant without loss from the moment of launch until it reaches its final twenty-four hour synchronous orbit. For this to be possible requires the use of a highly effective evacuated multi-foil radiation shield type of insulation sometimes referred to as "super" insulation. The insulation system must be compatible with all requirements imposed by operational conditions during all phases of the mission: ground handling, ascent, forty-eight hour orbit, and transfer.

For purposes of thermal analysis the liquid-hydrogen tank is approximated as a 10-foot diameter cylinder, 7.5 feet long with hemispherical ends. Construction details of this tank and its thermal insulation is given in the main body of this report.

B. REQUIREMENTS FOR GROUND HANDLING

1. General

On the ground, the thermal protection system must function reliably to limit the heat transfer to the hydrogen tankage to some acceptable value. This acceptable value is determined by what may be termed reasonable technical and economic solutions to the problems of filling the hydrogen tank, keeping it filled during the ground hold period, and disposing of the hydrogen boil-off. Past experience with similar vehicle systems indicate a heat inleakage rate

of about 100,000 Btu/hr (29,300 watts) corresponding to a boil-off rate of roughly 500 pounds of hydrogen per hour would be acceptable. To provide this degree of protection we anticipate that a system patterned after the design concept to be discussed in the paragraphs immediately following, would, with development, prove adequate.

2. Design Concept

A 1/2-inch layer of a honeycomb reinforced isocyanate foam would be bonded to the outer surface of the tank. This foam layer would not be continuous but rather will be put on in panels, with narrow intervening spaces left between panels. The honeycomb may well be made of a phenolic glass-cloth and the reinforced foam panels may be bonded to the tank wall with an epoxy adhesive. The foam would be of closed-cell type, blown with either carbon dioxide or freon. The reinforced foam layer would have an apparent mean thermal conductivity of .025 Btu/hr-ft-^{o}F. It would have a density of about 5 pounds/cu. ft. for a total weight of 100 pounds.

The super insulation required for thermal protection in space would be placed on top of the foam layer and the whole insulating system would be encapsulated in a flexible plastic bag. This bag may be made of one of a number of promising candidate materials; for instance, Mylar, Teflon, fabric-plastic composites, etc. The insulation package would be sealed by the use of mechanical clamps (perhaps with O-rings) and vacuum sealants such as silicone vacuum grease.

On the ground, the multi-foil insulation would be compressed by an atmosphere of 15 psi. The insulation must be able to recover to give nearly its full thermal performance upon release of the pressure load. Insulations made of aluminum foil with fibre glass paper spacers have demonstrated an ability to recover satisfactorily. Crinkled aluminized Mylar insulations do not have this capability. Inserting fibre glass paper spacers between the aluminized Mylar sheets may be necessary in order for this type of insulation to recover satisfactorily after compression.

As an operational procedure we anticipate that the multi-foil insulation system would be purged with carbon dioxide prior to filling the hydrogen tank. As the tank is filled the insulation space will be evacuated by the cryo-pumping action of the exposed portions of the cold tank wall. Perforating the foils to have a hole fraction of about one percent, provides a path of reasonable conductance for the migration of the carbon dioxide. Subsequent to the initial evacuation process, the pressure within the insulating space will gradually rise due to the influx of non-condensable gases (mainly hydrogen) due to leakage from the tank, outgassing from the foils and permeation through the plastic outer skin. For instance, a hydrogen inleakage of 1/2 lb/year would result in a pressure rise of about 20 torr/day.

In the absence of any non-condensable gases leaking from the tank or through the collapsible plastic outer skin into the insulating space, the pressure within the multi-foil insulation would be reduced to a level

commensurate with satisfactory operation at the ground. For instance, in its evacuated, compressed state, one expects that a representative aluminum multi-foil insulation will have a density five times and a heat inleakage (at a pressure of 10^{-4} torr or less) one hundred and twenty times greater than in its uncompressed state. These characteristics would be more than satisfactory for ground operations but questions remain as to what interstitial gas pressure can be tolerated before excessive heat leakage takes place and whether the required pressure (vacuum) within the insulation can be maintained practically. Because presently available data are insufficient to answer these questions, we have postulated the use of a foam layer which can limit the heat inleakage to 100,000 Btu's without any benefit from the compressed multi-foil layer. Under these circumstances the outer surface of the plastic bag will operate at about $-100^{\circ}F$. As a result of further developments through experimentation we may find that an acceptable vacuum can be maintained within the multi-foil insulation, in which case the foam layer can be dispensed with.

C. REQUIREMENTS DURING ASCENT

1. General

The effects of acceleration and vibration, aerodynamic heating, and decompression during the boost phase must be accounted for in the design of a satisfactory thermal protection system. Each of these effects and design techniques to accommodate them will be considered briefly.

2. Acceleration and Vibration

The thermal protection system must withstand the "g" loading and vibration accompanying boost. In the system proposed the foam layer is bonded to the exterior tank wall. The multi-foil over-layer must be held in place by other means.

At the time of launch we expect that the insulation system will be under a partial vacuum and the collapsed outer skin will help hold the multi-foil in place; however, this action is only effective for a period between filling and an early stage of ascent. To hold the insulation in place during ground-handling operations and for the latter phases of ascent and space flight, we propose the scheme outlined in the discussion to follow.

The multi-foil layer would be encased first in a "fish net". This net might be made of metal, glass or plastic - a number of promising materials are available. The net would be sewed together to form a bag and, in addition, it may be anchored to the foam at selected points by low conductivity threads. The collapsible plastic outer sheath would be placed immediately outside this interior net and an exterior net tied down by cinch bands* with explosive disconnects would finish the bale. The cinch bands and exterior net would be released automatically after the period of severe acceleration and vibration .

---

* Some experiments on an aluminum multi-foil insulation system that is similarly supported are discussed in Reference F1.

Obviously, at any time prior to release, the pressure difference across the plastic outer bag should not exceed the pressure retention capabilities of the restraining system. As the pressure of the environment at the altitude of release is likely to be only a few torr, the strength of this restraining system sets a maximum allowable pressure within the insulation at launch estimated to be about 20 torr.

3. Ascent Heating

During the ascent phase the shroud surrounding the hydrogen vessel (the existence of a shroud during ascent is fundamental to the proposed thermal protection system) is aerodynamically heated. Heat is transferred from the shroud to the insulation via the principal mechanisms of convection and radiation. In the early stages of ascent convection is predominant; later radiation becomes most important. The thermal transient in the insulation is governed principally by its thermal inertia and by conduction in the interstitial gas. The temperature history in the insulation treated as a semi-infinite slab results from a solution to the fourier equation:

$$\frac{dT}{d\Theta} = \frac{K}{\rho C_P} \frac{\partial^2 T}{\partial x^2} \qquad (1)$$

where:

T = temperature at location, x, at time, Θ

K = apparent thermal conductivity of the insulating slab

ρ = apparent density of the insulating slab

with the boundary conditions:

$$\text{at } \theta = 0,\ T = f(x)$$

$$\text{at } \theta = \theta, \text{ the flux to the outer surface, } x = 0, \text{ is:}$$

$$\phi = E\,\sigma\,(T_o^4 - T_1^4) + h_c\,(T_o - T_1) \qquad (2)$$

where:

ϕ = heat flux to the outer surface of the insulation

E = radiation exchange factor between the shroud and the outer surface of the insulation

σ = Stefan-Boltzmann constant

T_o = temperature of the shroud, $T_o = f(\theta)$

T_1 = temperature of the outer surface of the insulation, $T_1 = f(\theta)$

h_c = convective heat transfer coefficient appropriate to gas layer between the shroud and the outer surface of the insulation

Figure F-1 illustrates a solution to a model problem involving ascent heating of a multi-foil insulation. This solution was carried out by numerical methods using a machine program available at Arthur D. Little, Inc., through work in other programs. The assumptions inherent to this example are:

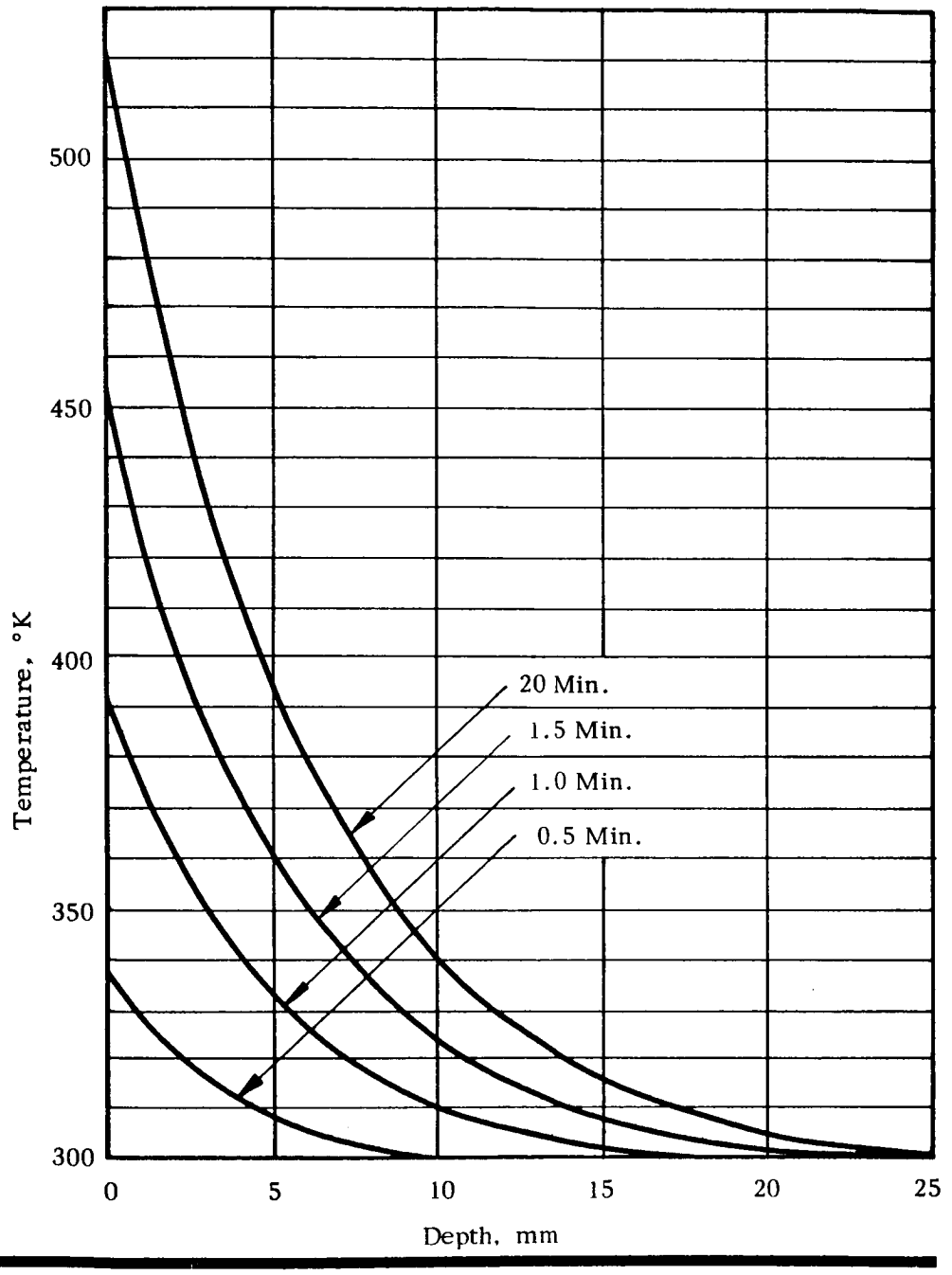

FIGURE F1 TEMPERATURE TRANSIENT IN MULTI-FOIL INSULATION PANEL

1) The multi-foil insulation is 1-inch (25mm) thick.

2) T_o is a ramp function going from 80^oF to 880^oF (300^oK to 745^oK) in two minutes.

3) At the start the temperature of the multi-foil layer is constant at 80^oF (300^oK).

4) At all times the temperature at the internal boundary of the insulation is fixed at 80^oF (300^oK).

5) The thermal diffusivity of the insulation is 0.023 ft^2/hr (typical of either the aluminized Mylar or aluminum-foil types).

6) $E = 0.1$

7) $h_c = 1 \sqrt{a}$ Btu/hr = ft^2, with a, the pressure in atmospheres, being determined by a representative flight plan of altitude versus time.

The results illustrated in Figure F-1 can be regarded only as representative, for the conditions and assumptions inherent to the model are typical rather than actual. However, they show that, unless precautions are taken, serious deleterious effects on the insulation may take place as a result of heating. The peak temperature of 520^oK (475^oF) reached by the outermost foil after two minutes is almost certainly in excess of that tolerable. The aluminum-foil type of super insulation may tolerate such temperatures but it will be seriously weakened and the emittance of the foils will be increased. The aluminized Mylar type of insulation would disintegrate at such temperatures. The assumed maximum temperature of 880^oF for the shroud may be high and the assumed starting temperature

of $80^{o}F$ for the foils is certainly high ($-100^{o}F$ is more nearly correct), therefore the predicted peak temperature is most likely higher than that which will be actually experienced. Nevertheless, the results suggest that greater shielding of the insulation from the shroud will be necessary either by interposing additional radiation shields or by the use of ablative materials at the internal surfaces of the shroud.

The actual heat absorbed by the insulation during the two-minute transient is only about 8 Btu/ft^2 of insulation or about 4000 Btu's for the whole hydrogen tank. Only a fraction of this will be transferred to the tank for part will be re-radiated to space after the shroud is blown off. In any event, the heat absorbed by the hydrogen during the ascent phase presents no particular problem.

3. Decompression

During ascent the pressure of the interstitial gas within the multi-foils will eventually exceed the pressure of the environment. As stated in a previous paragraph (C-2), the cinch bands and net holding the plastic outer sheath will be released automatically at a predetermined altitude. The pressure of the environment at this altitude is expected to be only a few torr; therefore, upon release, the plastic bag will balloon outward to take a shape fixed by its original form.* As it balloons it will expose some holes which were located internal to the sealed outer skin when all the cinch bands were

---

* In its extended shape the plastic skin also provides the function of a meteoroid bumper.

in place. These holes will communicate the multi-foil insulation to the environment and the interstitial gas pressure will bleed through the perforations in the foils to space. Because of strength restrictions on the insulation envelope (see paragraph C-2), the maximum pressure within the insulation at launch is limited to 20 torr; hence this is the maximum pressure loading which the interior fish net must retain. The pressure across any individual foil would be less than this value. As the individual foils support each other while transferring their pressure loads to the supporting net, we believe the problem of decompression can be met by this proposed scheme.

D. REQUIREMENTS FOR FORTY-EIGHT HOUR ORBIT AND ORBIT TRANSFER

1. General

After injection into parking orbit the cylindrical portion and the aft hemispherical end of the tank is exposed to the thermal environment of space. The forward hemispherical end is enclosed in structure that attaches the tank to the payload structure. The outer surface of the insulation capping the enclosed forward end is assumed to be in thermal equilibrium with "viewed" surfaces at $540^{\circ}R$. The arc-jet and SNAP-8 power supply together with its radiators are deployed about 20 feet aft of the liquid-hydrogen vessel. At this location the gamma heating of the stored liquid should be reduced to about 20 watts and the thermal radiation from the deployed package to the tank is negligible compared to that received from the space environment. The advisability of deploying the SNAP-8 power supply is established in Appendix E.

Prior to the time of injection into the 500 nautical mile orbit thermal events are controlled so that the fluid in the tank is at a lower temperature and pressure than during normal operation during transfer. During the forty-eight hour orbit period, as a result of heat inleakage to the tank, the pressure and temperature of its fluid contents approach normal operating design conditions. The heat capacity of the contents of the tank is so large that it can be shown that a vessel insulated to the degree required for the transfer period will experience a tolerable pressure rise without venting or withdrawal during a two-day period.

During transfer to the twenty-four hour synchronous orbit a controlled steady feed of hydrogen vapor is withdrawn from the tank by virtue of the operation of the expulsion and flow control system. To maintain a constant pressure within the hydrogen tank (a feature of the feed system proposed) requires a steady heat input of 100 watts. A significant fraction of this heat can be allowed to come through the insulation system and hence the design of this insulation system becomes more tractable. The remaining fraction of the 100 watts would be supplied by a heater in the tank in order to exercise the desired degree of control over tank pressure. A set of target heat leaks established for the transfer period as a reasonable guide for design are listed below:

Heat inleakage through insulating blanket	-	20 watts
Heat inleakage through pipes and supports	-	14
Gamma Heating	-	16
Controlled electric heating	-	50
Total:-		100 watts

2. Thermal Analysis

The real thermal problem associated with the use of a typical multi-foil insulation introduces many factors which complicate analysis:

1) Variations of the incident heat flux with location and time.
2) Anisotropic nature of the insulation.
3) Temperature-dependent thermal properties of the insulation.
4) Interruptions in the insulating blanket caused by pipes, supports and seams.

Techniques for dealing with these complications are advanced in Reference F2; however, the application of these techniques in a detailed thermal analysis is beyond the scope of this work.

For this work the basis for the specification of the thermal insulation requirements for the transfer period is given in Appendix E. Figure F-2 shows results applied to the hydrogen tank.

As a first step in determining the insulation required we treat the insulation as a homogeneous blanket with an isothermal outer surface and with a thermal resistance sufficiently high to be considered an adiabatic wall. Neglecting the effects of discontinuities, this treatment gives rise to a computation of heat inleakage greater than actual as shown in Reference F2.

Then

$$(\bar{W}_D + \bar{W}_A)\,\alpha_s + \bar{W}_E\alpha_E = \epsilon\sigma A T^4 \qquad (3)$$

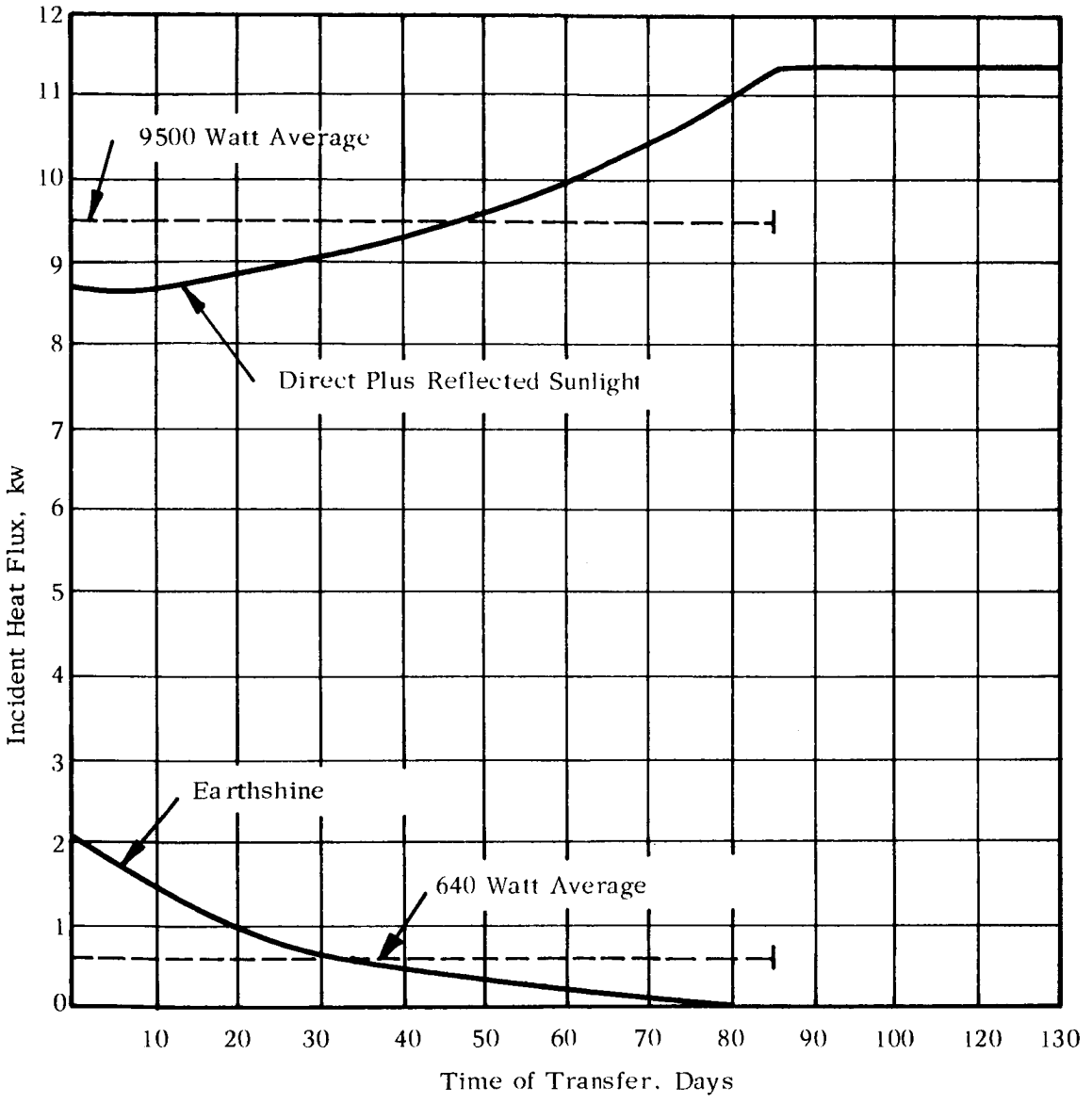

FIGURE F2 INCIDENT HEAT FLUX FROM SPACE TO EXPOSED SURFACES OF LIQUID HYDROGEN TANK

where:

$\bar{W}_D$ = average thermal incident power due direct sunlight

$\bar{W}_A$ = average thermal incident power due reflected sunlight

$\bar{W}_E$ = average thermal incident power due earthshine

A = exposed area of tank

α_s = absorptance of outer surface of insulation to sunlight

α_E = absorptance of outer surface of insulation to earthshine

ϵ = emittance of outer surface of insulation

σ = Stefan-Boltzmann constant

T = temperature of outer surface of insulation

With $\alpha_s = 0.2$, $\alpha_E = 0.8$, $\epsilon = 0.8$, A = 393 ft^2 and substituting the data of Figure F-2, the average value of T during transfer is computed to be $350^{\circ}R$. During the forty-eight hour orbit period and at the end of the transfer the average value of T is computed to be $380^{\circ}R$ and $344^{\circ}R$, respectively.

Assuming an insulating blanket of the highly effective multi-foil radiation-shield type with a thermal conductivity of 2.0×10^{-5} Btu/ft-hr-$^{\circ}R$, a layer of 0.64-inch thick on the exposed surface will reduce the average heat inflow to the liquid-hydrogen tank from space sources during the transfer period to 13.3 watts. A 0.82-inch thickness of insulation applied to the enclosed hemispherical end will result in an additional heat inflow of 6.7 watts for a total of 20 watts.

Under the assumed conditions the above-listed division of allowable heat flux through the insulation at the exposed and enclosed areas of the tank results in a minimum total weight of insulation; however, this weight is not sensitive to the division. The weight of the insulating blanket is estimated to be one hundred and sixty pounds based on an insulation density of 5 lbs/ft^3.

An apparent thermal conductivity of 2.0×10^{-5} $Btu/ft\text{-}hr\text{-}^oR$ is typical of values measured between room and liquid-hydrogen temperatures on carefully prepared samples of "super" insulation. One expects a lower (nearly twice as low) apparent thermal conductivity for the insulation operating with the hot side at 350^oR. In this sense the calculations of required insulation thickness are conservative. On the other hand, this conservatism is offset to a degree by the fact that discontinuities in the insulating blanket at seams and necessary penetrations give rise to additional heat inflow unaccounted for by the simple blanket concept.

3. Some Design and Operational Considerations

The high vacuum of outer space provides the pumping required to keep the insulation evacuated to the degree required for peak performance. Introduction of gas internal to the foils due to leakage from the hydrogen tank or outgassing from the insulation acts to reduce the performance of the insulation by raising the interstitial gas pressure. By perforating the foils one can provide a means for escape of the interstitial gas without an unacceptable pressure build-up within the foils. Calculations based on the work of Reference F3 indicate that foils having a hole

fraction of one percent should allow the passage of about 1/2 pound of hydrogen per year to space and still provide acceptable thermal protection. To place this figure of 1/2 pound per year in perspective, it might be of interest to note that it would take about thirty 32-inch diffusion pumps to pump this flow at 10^{-7} torr. Stated in other terms, this flow is 600 to 700 times the smallest leak which can be detected by the soap bubble technique applied to vacuum vessels.

The payload radiator will probably require a surface area of some 300 sq. ft. It may be convenient to wrap this radiator about the hydrogen tank. This arrangement is satisfactory provided that the outward facing surface of the radiator is treated to have a low absorptance to sunlight and a high emittance in the infrared band. Of course, this radiator cannot and should not be utilized during the transfer trajectory.

E. SUMMARY

The proposed thermal protection system is a composite made up of a layer of honeycomb-reinforced closed-cell, isocyanate foam followed by an over-layer of perforated multi-foil super-insulation. The foam layer is bonded to the exterior wall of the hydrogen tank in panels with narrow spaces left between panels. The multi-foil layer is held in place with a net.

For ground operations and for a portion of the ascent, the foam and multi-foil are encapsulated in a sealed plastic skin. At a predetermined altitude the plastic skin is automatically deployed to serve as a meteoroid bumper and to communicate the insulation to the vacuum of space. Prior to

launch the insulation system within the sealed plastic skin is purged with carbon dioxide and, upon filling the tank with hydrogen, the insulation is evacuated by the cryopumping action of the cold wall.

Table F1 summarizes some important characteristics of the thermal protection system.

F. CONCLUSIONS

There is little doubt that the most formidable technical problem attendent to the design of the hydrogen feed system is the definition of a suitable thermal protection system for the hydrogen tank. This point is amplified by the full discussion of the development status of thermal protection systems for liquid hydrogen tanks given in Reference F4. There is not enough information available on which to base an optimum light-weight design whose workability under all conditions of ground-hold, launch, ascent, and orbit transfer can be predicted with confidence. The system proposed draws on the body of information now available in support of the design of highly effective and light-weight insulation systems but a great deal more experimentation with the application and performance of these systems is needed before a final specification of the thermal protection system can be made.

TABLE F-I

SOME CHARACTERISTICS OF THE THERMAL PROTECTION SYSTEM

Item	Material	Thickness (in)	Density (lbs/ft^3)	Weight (lbs)
Foam sub-layer	Honeycomb-reinforced closed-cell isocyanate foam	0.50	5	100
Multi-foil layer	Super insulation	0.64 (exposed surfaces) 0.82 (facing payload)	5	160
Net (two)	Metal, plastic, or glass weave	--	--	40
Plastic Sheath	Mylar, Teflon, others	0.005		30
Miscellaneous				20
			Total Weight:-	350 lbs.

Heat Inleakage to Hydrogen Tank During Ground Operations: $\backsim$ 30,000 watts

Heat Inleakage to Hydrogen Tank During Orbit Transfer:

Through insulating blanket $\backsim$ 20 watts

Through pipes and supports $\backsim$ 14 watts

Gamma Heating $\backsim$ 16 watts

REFERENCES

F1. Matsch, L. C., "Advances in Multi-Layer Insulation", Advances in Cryogenic Engineering, K. D. Timmerhaus, ed., Vol. 7, Plenum Press, Inc., (New York 1961), p. 413.

F2. Bonneville, J. and Gabron, F. "A Guide to the Computation of Heat Flow in Insulated Cryogenic Storage Vessels in the Space Environment", Report No. 63270-13-01, Contract No. NAS 5-664, September 1962.

F3. Emslie, A. G., "Gas Conduction Problem with Multi-Layered Radiation Shields", Report No. 63270-04-01, Contract No. NAS 5-664, April 1961.

F4. Glaser, Peter E., "Thermal Protection Systems for Liquid Hydrogen Tanks", Report No. 65008-3, Contract No. NAS 5-664, November 1962.

F5. Knox, R. E., "Insulation Properties of Fluorocarbon Expanded Rigid Urethane Foam", ASHRAE Journal, Vol. 4, October 1962, p. 89.

F6. Kropschot, R. H., Schrodt, J. E., Fulk, M. M., and Hunter, B. J., "Multiple-Layer Insulation" Advances in Cryogenic Engineering, K. D. Timmerhaus, ed., Vol. 5, Plenum Press, Inc., (New York, 1960).

F7. Hnilicka, M. P., "Engineering Aspects of Heat Transfer in Multi-Layer Reflective Insulation and Performance of NRC Insulation", Ibid.

F8. Riede, P. M. and Wang, D. I-J., "Characteristics and Applications of Some Superinsulations", Ibid.

REFERENCES (2)

F9. Wang, D. I-J., "Multiple-Layer Insulations", Proceedings Aerodynamically Heated Structures, P. E. Glaser (ed.), Prentice-Hall, Inc., (Englewood Cliffs, New Jersey, 1962), p. 95.

APPENDIX G

ROTARY-PHASE SEPARATING HEAT EXCHANGER

The major piece of equipment associated with the general approach of flashing the discharge stream to a lower pressure and exchanging heat with the fluid remaining in the tank so as to vaporize the discharge is the heat exchanger. The heat transfer rate to vaporize a flow of 5×10^{-4} lb/sec, assuming that the fluid withdrawn from the tank is all liquid, would be 370 Btu/hr. The surface area required to effect this transfer is given by

$$A = \frac{q}{U_o \triangle T}$$

where A = heat transfer area, ft^2

q = heat transfer rate, Btu/hr

U_o = over-all heat transfer coefficient, Btu/hr ft^2-^oF

$\triangle T$ = over-all temperature differential, ^oF

The pressures of the stored fluid and the discharge stream would be controlled so that the temperature differential between them would be about 5^oF. Achievable values of the over-all heat transfer coefficient, U_o, depend on the nature of the fluid films on both the hot and cold sides of the primary heat transfer surface. In the phase-separating exchanger, vaporization is occurring on the cold (low pressure) side while condensation is occurring on the warm (high pressure) side. With these conditions high values of U_o could be obtained in a 1 g acceleration field. For example, for hydrogen a value of U_o of 70 Btu/hr-ft^2-^oF would not be unusual and using the figures above for q and $\triangle T$ in the present case, a heat transfer area of only 1.06 sq. ft. would be required. Thus, a phase-separating heat exchanger for hydrogen to operate in a one g environment could be rather small.

The absence of an appreciable acceleration field may have a profound effect on the required heat transfer area. Under zero g conditions no natural mechanism exists for the removal of condensed liquid from the warm side of the heat exchanger and a thick, stagnant film of liquid may develop. Convection will be absent and heat will only be transferred by conduction. The thermal conductivity of liquid hydrogen is very low, and the heat transfer coefficients that obtain in the presence of thick, stagnant liquid films are orders of magnitude lower than those which are realized in a one g environment. Based on our previous work* a heat transfer area of about 1000 ft^2 would be required for the vaporization of 5×10^{-4} lb/sec of hydrogen. The large area is a direct result of the poor heat transfer through the condensed-liquid film on the warm side. Since the fluid in the discharge tube is in motion and is boiling, good heat transfer would be expected on the cold side; were this the only limitation, extremely high values of U_o would be achievable. Provision of the large heat transfer surface area stated above would add a substantial structure and considerable weight to the hydrogen storage vessel (probably close to 100 pounds additional).

The area required for heat transfer might be considerably reduced if motion could be induced in the liquid which collects on the warm side. If the liquid were made to flow over the heat transfer surface with a velocity

---

* Fowle, A. A., et al, "Investigations of Propellant Feed Systems for Electrothermal Engines," Final Report, Phase I, Contract No. NAS8-1695, NASA Marshall Space Flight Center, Huntsville, Alabama, October 1961.

of only a few feet per second, over-all heat transfer rates order of magnitude higher than those that prevail with a thick, stagnant film present, could be achieved. The savings in structural complexity and weight that might result, particularly in the case of hydrogen, led us to investigate means for inducing motion. It appears that suitable fluid motion can be induced with a fairly simple device that will be relatively small and lightweight, can be made to operate reliably, and may be pre-tested on the ground in a one g environment. The device as envisioned for use with hydrogen is shown in Figure G-1. It consists of a stationary housing of generally circular shape, and a rotating disc containing wedge-like vanes. It would be placed inside the storage vessel, centered near one end with its axis of rotation coincident with the vessel axis.

Fluid from the vessel would pass through a pressure-reducing valve into the discharge tube, which is spiral-wound and connected to the primary heat transfer surface of the phase-separating device, as indicated by the figure. The fluid would enter at the outer periphery, spiral inward on one side of the exchanger, pass to the outer periphery of the tube spiral on the other side, and again flow inward through the spiral in a second pass. Finally, after being completely vaporized it discharges. The spiral-like flow path of the low-pressure fluid will induce a radial acceleration field which can be made comparable to one g. Liquid droplets in this two-phase flow would tend to be flung radially outward to the walls of the tube so that the excellent heat transfer associated with liquid boiling would prevail. Calculations indicate that the resistance to heat transfer of the fluid on the low-pressure side would be small compared to that on the high-pressure side.

Fluid motion across the heat transfer surface on the high-pressure side is induced by the rotation of the vaned impeller. The radial acceleration field established in the constant-flow-area channels in the disc will centrifuge either liquid or gas radially outward and will maintain a controlled fluid velocity adjacent to the primary heat transfer surface. By this means it appears that a warm side heat transfer coefficient of 90 to 100 Btu/hr-ft^2-^{o}F may be sustained. With the $\triangle$ T of 5^{o}F, only about one square foot of actual heat transfer area is required. An over-all diameter of approximately twenty inches (as shown in the figure) would provide the necessary area. Our analysis has indicated that the major resistance to heat transfer on the high-pressure (warm) side of the exchanger will be due to the condensed liquid film which might accumulate in the clearance between the rotor and the primary heat transfer surface (indicated in Figure G-1 as the rotor clearance). Consequently, it will be important to maintain this clearance at a small value, something on the order of 0.005 inch.

The flow through the low-pressure discharge tube will be essentially isothermal since vaporization will be occurring. The flow through the high-pressure side of the exchanger may be made essentially isothermal if it is so large that the temperature drop of the fluid is small compared to the 5^o $\triangle$ T. If the fluid entering the high-pressure side were all gas, heat would be provided to the low-pressure stream by condensation of this gas on the primary heat transfer surface. If the thickness of the condensed liquid film exceeds the rotor clearance, liquid would be centrifuged radially outward

by the impeller. Continued flow of gas through the device would maintain heat transfer through the liquid film in the rotor clearance as gas condensed on the film surface exposed to the flow channels. Something less than 2 lbs/hr of condensing gas would provide sufficient heat release to vaporize the low-pressure stream. If the fluid entering the high-pressure side of the exchanger were all liquid, a flow rate on the order of 300 lbs/hr with a temperature rise of only 0.5°F would provide sufficient heat release to vaporize the discharging fluid. With liquid flowing through the impeller, the high heat transfer coefficients associated with liquid flow would be realized at the primary heat transfer surface.

Our analysis indicates that to achieve the above flow rates with the device such as shown in the figure, the rotational speed of the disc would be in the range of 100 to 200 rpm. At these low rotational speeds and considering the light loads that will prevail, the use of ball-bearings appears feasible. The required operating life of 2,880 hours appears to be achievable with a high degree of reliability. The power required to drive the rotor at these rotational speeds is expected to be very low, something on the order of 2 to 3 watts. A convenient drive for this low rotational speed and power level can be fashioned by using the rim of the impeller as an eddy current rotor of an induction motor. The arrangement shown in Figure G-1 is similar to that used in the common household watt-hour meter. By using several closely spaced stator poles at the rim of the impeller, a very low rotational speed can be produced, even when the stator is supplied with 400-cycle power. With proper design the over-all efficiency of this motor would be expected to exceed

50 percent. Thus, the power input to the fuel storage tank associated with the rotary phase-separating heat exchanger is expected to be between 5 and 10 watts. This power input incurs no fuel loss since the sum of the heat leak through the insulation into the tank and the power input to the exchanger will be less than the heat input required to maintain tank pressure constant when vapor is being withdrawn at the prescribed rate. To maintain constant pressure, the difference between the power input and that required will be made up by the pressure stabilizing heaters shown in the figure. They are placed near the discharge of the impeller, where fluid motion across their surfaces will insure good heat transfer.

A rotary phase-separating heat exchanger is preferable to the large-surface-area static heat exchanger required for hydrogen, and would form the basis of an active expulsion system. The advantages to be gained by its use with ammonia are much less distinct, and we do not propose its use with that fluid.

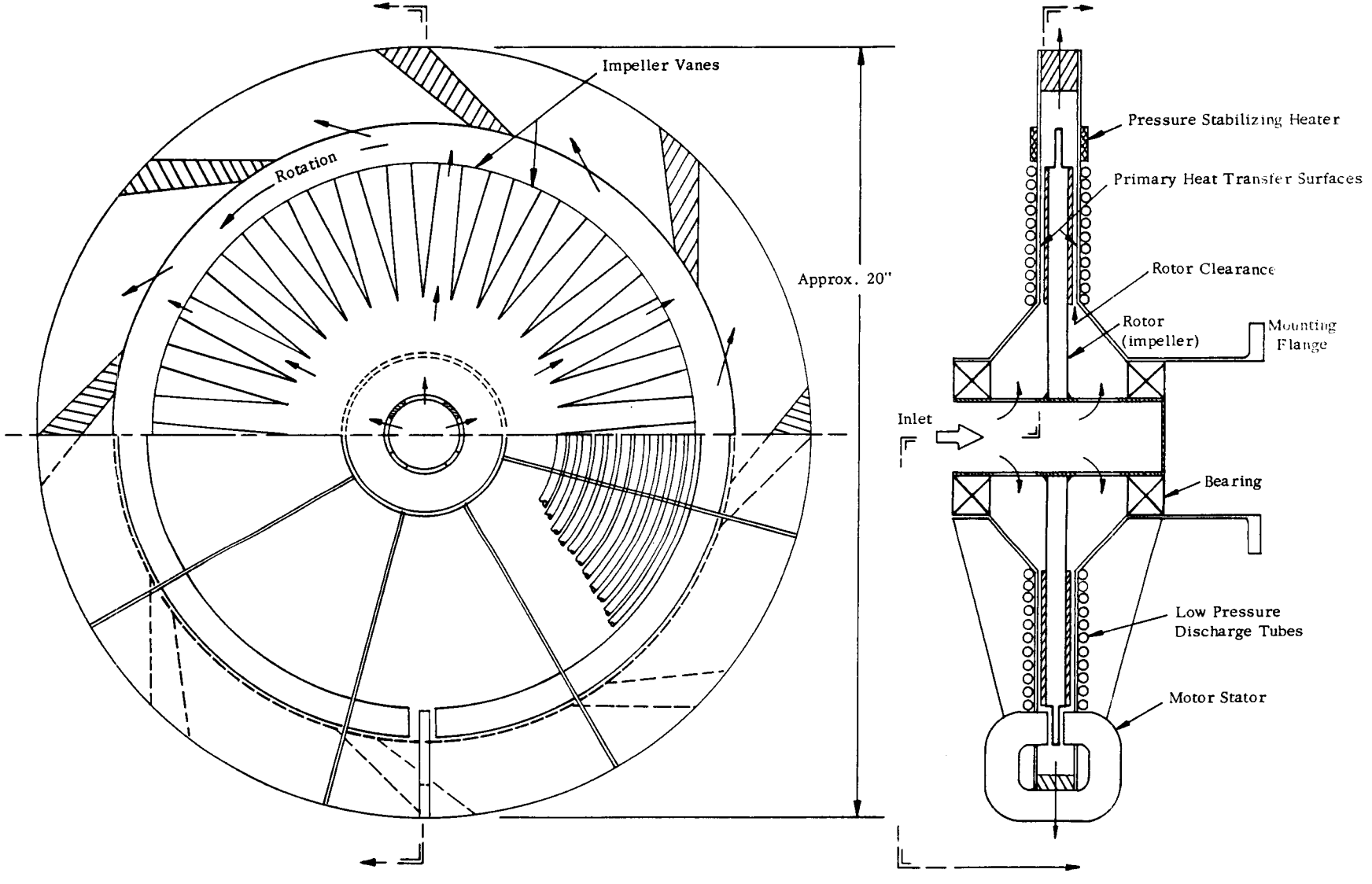

FIGURE G1 ROTARY PHASE - SEPARATING HEAT EXCHANGE

APPENDIX H

DESIGN OF FLOW CONTROLLER FOR HYDROGEN FEED

A. DESCRIPTION OF OPERATION

The configuration of the proposed flow controller is shown schematically in Figure H-1. Gas at constant temperature and pressure (preconditioned) enters the controller through the inlet, flows through the metering orifice, and leaves the controller through the control orifice. The flow rate through the control orifice, and thus through the controller, depends upon area of the control orifice A_c. The area A_c is changed by moving a plug which is connected to the piston.

As gas flows through the metering orifice, its pressure decreases. The difference in pressure between the upstream and downstream sides of the metering orifice also appears on the two sides of the piston. The pressure differential acting on the piston develops a force which tends to close the control orifice and so decreases the flow of gas. The piston continues to decrease the gas flow until the pressure drop through the metering orifice balances a control force F_c from the force motor which tends to open the control orifice.

B. ANALYSIS

1. General

The detail analysis of the flow controller which follows is based upon two assumptions. First, the gas flowing through the controller is a perfect gas. Second, the flow through the metering orifice is incompressible.

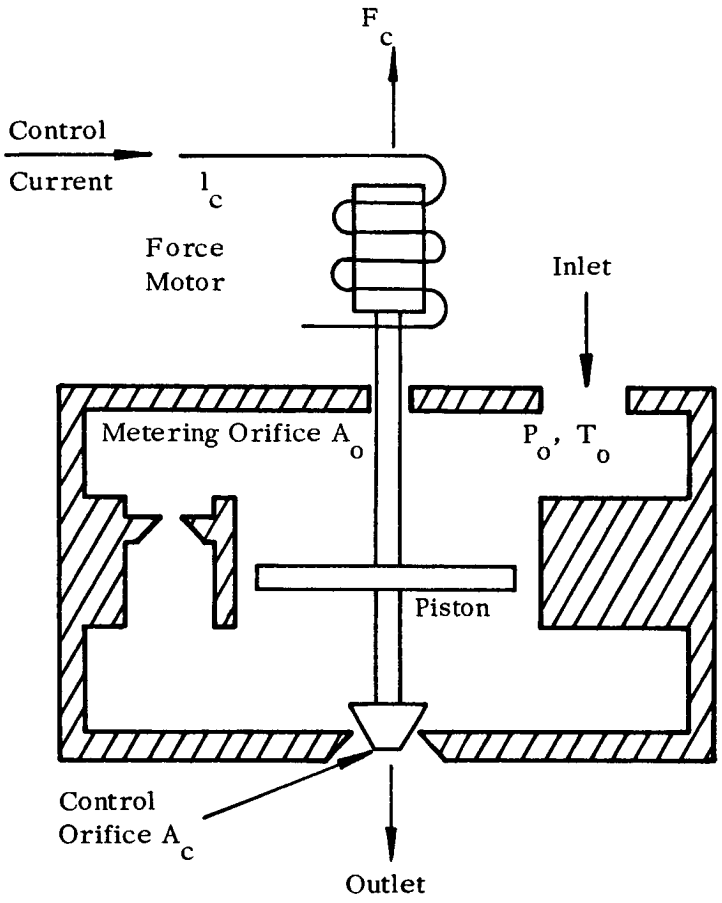

FIGURE H1 SCHEMATIC DIAGRAM OF FLOW CONTROLLER

These two assumptions allow the use of simplified equations relating flow rate to pressure drop through an orifice. The assumption that hydrogen is a perfect gas at the temperatures and pressures present at the controller introduces negligible uncertainty in the analysis. The approximations inherent to the assumption of incompressibility yield answers which are within one percent of the correct answer if the pressure drop through the orifice is less than two percent of the inlet pressure. This assumption places a design constraint on orifice size.

The equation describing incompressible flow through the metering orifice is given in Equation (1).

$$\dot{W} = A_o \, k_o \, \sqrt{2 \rho \triangle P \, g} \tag{1}$$

$\dot{W}$ = weight rate of flow, (lbm/sec.)

A_o = area of the metering orifice, ft^2

k_o = discharge coefficient of A_o

g = gravity acceleration constant, $\frac{lbm - ft}{sec^2 - lbf}$

ρ = density of fluid (lbm/ft^3)

$\triangle P$ = pressure drop through orifice A_o, lbf/ft^2

The density of the gas in terms of the inlet temperature and pressure is given by the equation of state for a perfect gas.

$$\rho = \frac{P_o}{R\,T_o} \tag{2}$$

P_o = inlet pressure (lbf/ft^2)

T_o = inlet stagnation temperature, ^oF

R = particular gas constant, $\frac{ft - lbf}{lbm - {}^oF}$

Substituting Equation (2) for ρ in Equation (1) gives an expression for the weight rate of flow in terms of measurable quantities.

$$\dot{W} = A_o\, k_o \sqrt{\frac{2\,g\,P_o \Delta P}{R\,T_o}} \tag{3}$$

The control orifice A_c operates at or near choked flow. Choked operation was chosen because this mode of operation is insensitive to different engine characteristics. A plot of flow characteristics for the engine and control orifices operating choked as a function of engine pressure, P_e, (controller outlet pressure) is shown in Figure H-2. The intersection of an engine characteristic curve with an orifice curve gives the flow rate for a given engine pressure and the orifice opening required for the combined engine-control orifice system. From Figure H-2, the cross plot of Figures H-3 and H-4 are obtained. Figure H-3 is a plot of propellant flow as a function of control orifice area. The choked orifice exhibits a linear characteristic while flow for the unchoked orifice is quite insensitive to changes in area at flow rates near full flow. The insensitivity of flow through a choked control orifice to changes in engine characteristics is illustrated in Figure H-4 where flow rate is plotted as a function of the engine flow constant K_e.

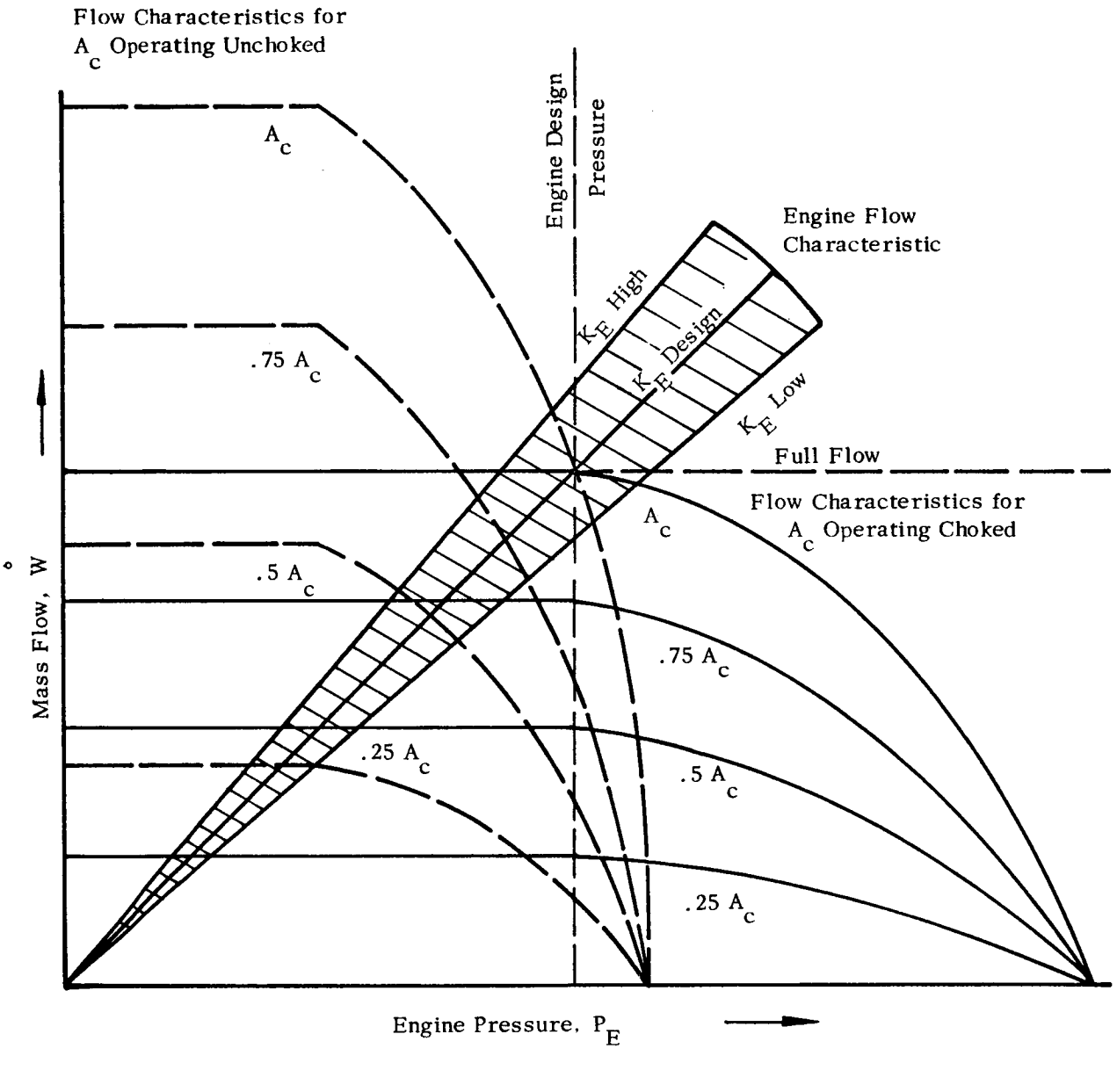

FIGURE H2 FLOW CHARACTERISTICS FOR ENGINE WITH CONTROL ORIFICE OPERATING CHOKED AND UNCHOKED

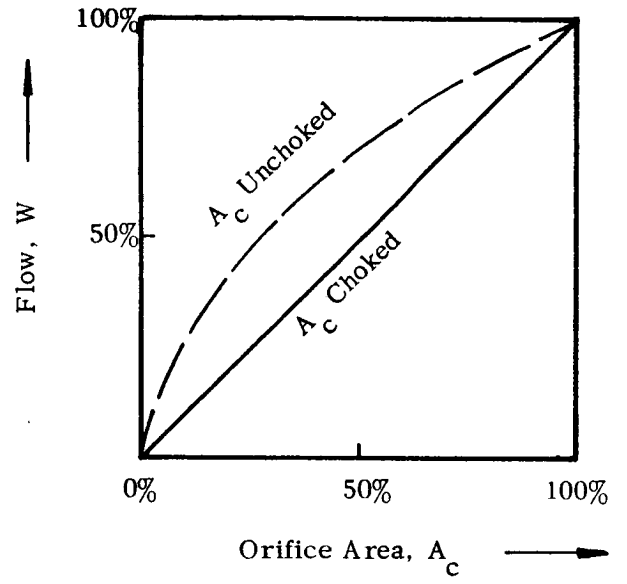

FIGURE H3 CONTROL CHARACTERISTICS OF COMBINED ENGINE AND CONTROL ORIFICE

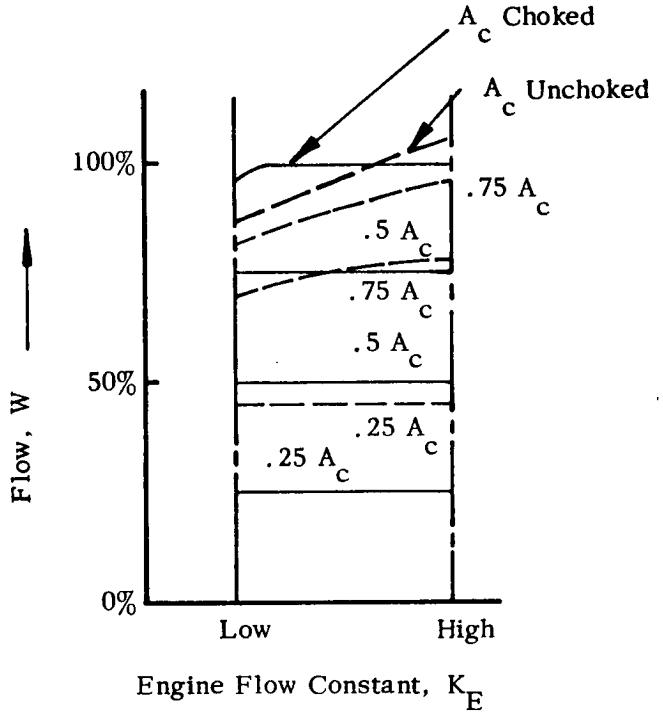

FIGURE H4 EFFECT OF ENGINE FLOW CHARACTERISTICS ON FLOW CONTROL

The equation describing weight flow rate through a choked control orifice is

$$\dot{W} = A_c k_c g \frac{P_o - P}{\sqrt{T_o}} \sqrt{\frac{k}{g R} \left(\frac{2}{k+1}\right)^{\frac{k+1}{k-1}}} \qquad (4)$$

A_c = area of control orifice

k_c = discharge coefficient of A_c

T_o = stagnation temperature of gas

$P_o - \Delta P$ = pressure upstream of control orifice

k = ratio of specific heats for gas

The square root involving k, R, and g is a constant which depends only upon the gas used, so for convenience, let

$$C_g = \sqrt{\frac{k}{g R} \left(\frac{2}{k+1}\right)^{\frac{k+1}{k-1}}}$$

Equation (4) is then simplified to

$$\dot{W} = A_c k_c g \frac{P_o - \Delta P}{\sqrt{T_o}} \cdot C_g \qquad (5)$$

Flow through the engine is similar to choked flow through an orifice, and the flow can be expressed as being in proportion to the engine pressure, P_e.

$$\dot{W} = K_e P_e$$

However, since the control orifice will be operated choked, the back pressure on the controller due to the engine will have no effect on flow rate. The engine characteristics can, therefore, be neglected for the purposes of this analysis.

The flow controller operates by balancing the force due to pressure drop through the metering orifice A_o against a command or control force F_c. The controller can be described as a simple mechanical system having an effective mass, M, an effective spring constant, K_s, and a viscous friction coefficient, B. The equation describing the motion of the system is

$$F_c - A_b \Delta P = M \frac{d^2 x}{dt^2} + B \frac{dx}{dt} + K_s x \tag{6}$$

x = displacement from relaxed spring position

A_b = area of piston

F_c = control force

Assume that the control orifice area varies linearly with x

$$A_c = C_c x \tag{7}$$

Then substituting Equations (3), (5), and (7) into Equation (6), the relationship between control force and flow rate becomes

$$F_c - \frac{R T_o}{(A_o k_o)^2 2g P_o} A_b \dot{W}^2 = \frac{\sqrt{T_o}}{C_c k_c C_g P_o} \left[M \frac{d^2}{dt^2} \left(\frac{\dot{W}}{1 - \frac{R T_o}{2g (A_o k_o)^2} \dot{W}^2} \right) \right.$$

$$+ B \frac{d}{dt}\left(\frac{\dot{W}}{1 - \frac{R T_o}{2g (A_o k_o)^2 P_o^2}\dot{W}^2}\right)$$

$$+ K_s\left(\frac{\dot{W}}{1 - \frac{}{2g (A_o k_o)^2 P_o^2}\dot{W}^2}\right)\Bigg] \qquad (8)$$

2. Steady-State Behavior

Consider first the steady-state conditions, i.e., $\dot{W}$ = const.

Equation (8) reduces to

$$F_c = \frac{R T_o}{(A_o k_o)^2 2 g P_o} A_b \dot{W}^2 + K_s \frac{\sqrt{T_o}}{C_c k_c g C_g P_o}\left(\frac{\dot{W}}{1 - \frac{R T_o}{2g (A_o k_o)^2 P_o^2}\dot{W}^2}\right) \qquad (9)$$

Notice that from Equation (3)

$$\frac{R T_o}{2g (A_o k_o)^2 P_o^2}\dot{W}^2 = \frac{\Delta P}{P_o}$$

and $\frac{\Delta P}{P_o}$ is always less than 0.02 by the requirement for incompressible flow through A_o. This can be neglected in comparison with one, so Equation (9) is simplified to

$$F_c = \frac{R\,T_o}{(A_o\,k_o)^2\,2g\,P_o}\,A_b\,\dot{W}^2 + K_s\,\frac{\sqrt{T_o}}{C_c\,k_c\,g\,C_g\,P_o}\,\dot{W} \tag{10}$$

Rearranging (10) the equation describing steady-state flow through the controller is obtained.

$$\dot{W} = \frac{A_o\,k_o}{\sqrt{A_b}}\left[\frac{2g\,P_o}{R\,T_o}\cdot F_c\cdot\left(1 - \frac{\delta F_c}{F_c}\right)\right]^{1/2} \tag{11}$$

$$\text{where}\quad \delta F_c = \frac{\sqrt{T_o}}{g\,k_c\,C_g\,P_o}\,\frac{K_s}{C_c}\,\dot{W} \tag{12}$$

$$\text{or by Equation (5)}\quad \delta F_c = K_s\,\frac{A_c}{C_c}$$

Equation (11) shows that steady-state flow through the flow controller is proportional to the square root of the control force. The term $\frac{\delta F_c}{F_c}$ represents the normalized deviation from the ideal equation due to the spring constant of the suspension system. Any friction or hysteresis effects present in the mechanical system would be added to Equation (12).

To insure accurate control $\frac{\delta F_c}{F_c}$ must be made very small. Ideally, the ratio should be zero which would be the case in the absence of any spring forces ($K_s = 0$) or friction forces. Since accurate flow control is most important at maximum flow, a design equation can be written in terms of maximum flow conditions.

$$\left(\frac{\delta F_c}{F_c}\right)_{\text{max flow}} = \frac{K_s\ (A_c)\ \text{max flow}}{C_c\ A_b\ (\triangle P)\ \text{max flow}} \tag{13}$$

If the flow controller is designed so that $(\frac{\delta F_c}{F_c})$ is negligibly small, Equation (11) reduces to

$$\dot{W} = A_o\ k_o \sqrt{\frac{2g\ P_o}{R\ T_o}\ \frac{F_c}{A_b}} \tag{14}$$

Equation (14) is the basic equation governing the flow of gas through the controller. Equation (14) is identical to Equation (3) because

$$\frac{F_c}{A_b} = \triangle P.$$

3. Dynamic Behavior

In addition to the steady-state behavior of the flow controller, the dynamic behavior also must be considered. Because the flow controller is merely required to regulate flow at a given set point, or, at most, follow a slowly varying input, it is only necessary to inquire into the stability of the flow about a given set point.

In Equation (8) apply the approximation used in (10) and let

$$y = \frac{\sqrt{T_o}}{C_c\ k_c\ g\ C_g\ P_o}\ \dot{W}$$

$$K_f = \frac{R\ C_g^{\,2}\ C_c^{\,2}\ K_c^{\,2}\ g\ P_o\ A_b}{2\ (A_o\ k_o)^2}$$

then the equation becomes

$$\ddot{y} + \frac{B}{M}\dot{y} + \frac{K_s}{M}y + \frac{K_f}{M}y^2 - \frac{F_c}{M} = 0 \qquad (15)$$

Equation (15), a nonlinear differential equation, is difficult to solve. However, because the flow controller is to regulate flow to a given set point, it is sufficient to investigate the behavior of the controller for small perturbations about the set point. To do this, let

$$y = u_o + u \qquad u << u_o$$

where u_o represents the conditions at the set point, and u represents the perturbation from set point.

Then

$$\dot{y} = \dot{u}$$

$$\ddot{y} = \ddot{u}$$

Equation (15) becomes

$$\ddot{u} + \frac{B}{M}\dot{u} + \frac{K_s}{M}u + \frac{2K_f}{M}u_o u + \frac{K_f}{M}u^2 + \frac{K_f}{M}u_o^2 + \frac{K_s}{M}u_o - \frac{F_c}{M} = 0 \qquad (16)$$

If u_o is chosen so that

$$\frac{K_f}{M}u_o^2 + \frac{K_s}{M}u_o - \frac{F_c}{M} = 0$$

u_o can be written as

$$u_o = \left[\frac{F_c}{K_f} \cdot \left(1 - \frac{K_s}{F_c}u_o\right)\right]^{1/2} \qquad (17)$$

It can be shown that each term in Equation (17) corresponds to a like term in Equation (11), i.e.,

$$\frac{K_s u_o}{F_c} \sim \frac{F_c}{F_c}$$

$$\sqrt{\frac{F_c}{K_f}} \sim \frac{A_o k_o}{\sqrt{A_b}} \sqrt{\frac{2g P_o}{R T_o}} \cdot F_c$$

so u_o is indeed the steady-state value of $\dot{W}$ multiplied by an appropriate constant.

Choosing u_o as discussed above reduces Equation (16) to an equation for perturbations about the set point. Terms involving u^2 are neglected because the perturbations are defined as being small so their squares are negligible.

$$\ddot{u} + \frac{B}{M} \dot{u} + \frac{(K_s + 2 K_f u_o)}{M} u = 0 \qquad (18)$$

Equation (18) is a linear second order differential equation whose solution is a damped sinusoid if B is positive. This means that $\dot{W}$ is stable but may oscillate about the set point with natural frequency

$$W_n = \sqrt{\frac{K_s + 2 K_f u_o}{M}} = \sqrt{\frac{K_s + \frac{R C_c C_g K_c A_b \sqrt{T_o}}{(A_o k_o)^2} \dot{W}_o}{M}}$$

and per unit damping

$$\delta = \frac{B}{2\sqrt{M}\sqrt{K_s + 2K_f u_o}} = \frac{B}{2\sqrt{M}\sqrt{K_s + \frac{R C_c C_g K_c A_o \sqrt{T_o}}{(A_o k_o)^2}}} \cdot W_o$$

From the foregoing linearized analysis, it can be concluded that the controller is stable for small perturbations about the set point for all set points. However, the relative stability and the frequency of oscillation frequency will increase, and the system damping decreases.

Damping of the system cannot be predicted at present. It is expected that the residual friction and viscous forces in the controller will provide sufficient damping. If this does not prove to be the case in practice, it will be necessary to add additional damping in the form of a viscous or magnetic damper. To make the most of the residual damping forces, it must be a mechanical design objective to make the effective mass of the moving parts as low as is consistent with strength requirements.

4. Static Error Analysis

The static accuracy of the flow controller depends upon maintaining the inlet temperature and pressure at the correct values as well as making the unwanted mechanical forces small. Equation (19) gives the per unit variation in flow rate in terms of the per unit variations in pressure, temperature, and undesirable mechanical forces when these variations are known.

$$\frac{\partial \dot{W}}{\dot{W}} = \frac{1}{2}\frac{\delta P_o}{P_o} - \frac{1}{2}\frac{\delta T_o}{T_o} - \frac{1}{2}\frac{\delta F_c}{F_c} \tag{19}$$

In general, the variations are not known exactly, but limits are placed on the maximum allowable variation of each parameter. The worst possible error in flow rate is the sum of the absolute values of the maximum variations in the parameters.

$$\left(\frac{\delta \dot{W}}{\dot{W}}\right)_{\text{worst case}} = \frac{1}{2}\left|\frac{\delta P_o}{P_o}\right| + \frac{1}{2}\left|\frac{\delta T_o}{T_o}\right| + \frac{1}{2}\left|\frac{\delta F_c}{F_c}\right| \tag{20}$$

The parameters discussed above are those which are most likely to vary. The other quantities in Equation (11) are functions of the geometry of the controller or of the propellant gas. Any variations in these quantities should be insignificant.

C. DESIGN OF CONTROLLER

The detail analysis of the flow controller described the operation of the flow controller and presented the equations governing its operation. Some of the equations involved approximations which become design restrictions. These restrictions were stated in the analysis. From the equations and design restrictions given in the analysis, the major features of the flow controller can be determined. These features are summarized in Table H-I.

The following characteristics are required of the controller:

TABLE H-I

DESIGN PARAMETERS OF FLOW CONTROLLER FOR HYDROGEN GAS

Quantity	Value
Flow Rate, Maximum	5×10^{-4} lb/sec full scale
Accuracy of Control	$\pm$ 10 percent of full scale
Inlet Pressure, P_o	32.2 ± 1.6 psia
Inlet Temperature, T_o	540 ± 5 deg. R
Outlet Pressure, P_e	Approximately 1 atm.
Maximum Control Orifice Area, A_C	3.95×10^{-3} in^2
Metering Orifice, A_o	1.68×10^{-2} in^2
Piston Area, A_B	4 in^2

1) Maximum flow, $\dot{W} = 5 \times 10^{-4}$ lb/sec

2) Accuracy of control $\pm$ 10 percent full scale

3) Outlet Pressure, P_e = approximately one atmosphere

The characteristics of the gaseous hydrogen propellant are:

1) Temperature, $T_o = 540^{\circ}R$

2) Gas constant, $R = 767 \frac{ft - lbf}{lbm - {}^{\circ}R}$

3) Ratio of specific heats, $k = 1.4$

The equation for the control orifice operating with choked flow is given by Equation (5)

$$\dot{W} = A_c K_c g \frac{P_o - \Delta P}{\sqrt{T_o}} C_g \tag{5}$$

$$C_g = \sqrt{\frac{k}{g R}\left(\frac{2}{k+1}\right)^{\frac{k+1}{k-1}}} = 4.36 \times 10^{-3} \frac{\text{sec} - {}^{\circ}R^{1/2}}{ft}$$

For an orifice to operate with choked flow, its upstream pressure must be at least twice the exhaust pressure. From this requirement and the requirement for a one atmosphere engine pressure, the pressure upstream of the control orifice is determined.

$$P_o - \Delta P = 2 P_e = 30 \text{ psia}$$

Then by arrangement of (5), the maximum control orifice area is:

$$A_c k_c = \frac{\dot{W}\sqrt{T_o}}{g\,(P_o - \triangle P)C_g} = 1.92 \times 10^{-5}\ ft^2$$

$$= 2.77 \times 10^{-3}\ in^2$$

Assume a discharge coefficient $k_c = 0.7$

$$A_c = 3.95 \times 10^{-3}\ in^2$$

A_c corresponds to a hole 0.0709 in. dia.

The area of the metering orifice is determined by the application of Equation (3).

$$\dot{W} = A_o k_o \sqrt{\frac{2 g P_o \triangle P}{R T_o}} \qquad (3)$$

The assumption of incompressible flow through A_o limits the value of $\triangle P$ to less than two percent of P_o, a convenient value of $\triangle P$ which satisfies this requirement at full flow is:

$$\triangle P = 0.5 \text{ psi}$$

The inlet pressure required for the flow controller to operate satisfactorily must be such that the pressure downstream of the metering orifice $(P_o - \triangle P)$ is always at least 30 psia. This must take into account any variation in inlet pressure. If a five percent variation about the nominal inlet pressure is allowed, P_o can be determined from the following relationship:

$$.95\ P_o - \triangle P = 30 \text{ psia.}$$

$$P_o = 32.2 \pm 1.6 \text{ psia}$$

Using the values of P_o and ΔP just arrived at, the metering orifice area can be calculated

$$A_o k_o = \dot{W}\sqrt{\frac{R T_o}{2 g P_o \Delta P}}$$

$$= 6.99 \times 10^{-5} \text{ ft}^2$$

$$= 1.01 \times 10^{-2} \text{ in}^2$$

Assume the discharge coefficient $k_o = 0.6$

$$A_o = 1.68 \times 10^{-2} \text{ in}^2$$

which is a hole

$$D_o = 0.146 \text{ in. dia.}$$

Both the control and metering orifices are of the sharp-edged type.

The choice of piston area A_b depends upon the control force F_c and the magnitude of the disturbing forces in Equation (11) due to friction and spring deflections. These disturbing forces, δF_c, cannot be predicted, but some upper limit can be assigned to the forces.

Specify: δF_c 0.1 lb

$\frac{\delta F_c}{F_c}$ 0.05

Then the maximum control force required is

$$F_c = 2 \text{ lb.}$$

Since $F_c = A_b \Delta P$, the effective area of the piston must be:

$$A_b = 4 \text{ in}^2$$

Limits of variation have been assigned to the inlet pressure and perturbing mechanical forces in the controller. A limit must also be

assigned to the allowable temperature variation of the gas. A regulation of one percent represents a variation in temperature of approximately $5^{\circ}R$ and should present no control problem. The inlet temperature is then specified as

$$T_o = 540 \pm 5^{\circ}R$$

The effect of the allowable variations in major parameters on the accuracy of control may now be computed. The worst case per unit deviation from ideal is determined by evaluating Equation (20).

$$\left|\frac{\delta \dot{W}}{\dot{W}}\right|_{\text{worst case}} = \frac{1}{2}\left|\frac{\delta P_o}{P_o}\right| + \frac{1}{2}\left|\frac{\delta T_o}{T_o}\right| + \frac{1}{2}\left|\frac{\delta F_c}{F_c}\right| \tag{20}$$

where

$$\frac{\delta P_o}{P_o} = 0.05$$

$$\frac{\delta T_o}{T_o} = 0.01$$

$$\frac{\delta F_c}{F_c} = 0.05$$

$$\left|\frac{\delta \dot{W}}{\dot{W}}\right|_{\text{worst case}} = 0.055 \text{ (5.5 percent)}$$

The allowable error for $\dot{W}$ is ten percent of full scale, so the worst case error expected for the tolerances assigned is within the specification.

D. FORCE MOTOR

The force motor which provides the control force, F_c, for the flow controller is an electromagnet. A dc electromagnet produces a force which is proportional to the square of the current flowing through the winding. Propellant flow rate through the flow controller is proportional to the square root of the control force. The electromagnet force motor provides a linear relationship between control current and propellant flow rate.

In addition to the square relation for the force and input current of the force motor, the force produced must be independent of magnet armature position. Changes in force with armature position would contribute to the $\frac{\delta F_c}{F_c}$ term in Equation (11). The force exerted by most configurations of electromagnets depends strongly upon armature position (usually the inverse square of the gap length). The basic magnetic configuration of Figure H-5, in which the lines of flux are perpendicular to the armature motion, develops a force which is independent of armature position when fringing is neglected. This configuration is less efficient in terms of force developed than other magnet configurations, but independence of position is of major importance for this application.

A modification of the configuration of Figure H-5 which locates the working air gap more conveniently and reduces the weight of the moving armature is shown in Figure H-6. The magnetic flux is still perpendicular to the direction of armature motion, so force is independent of armature position.

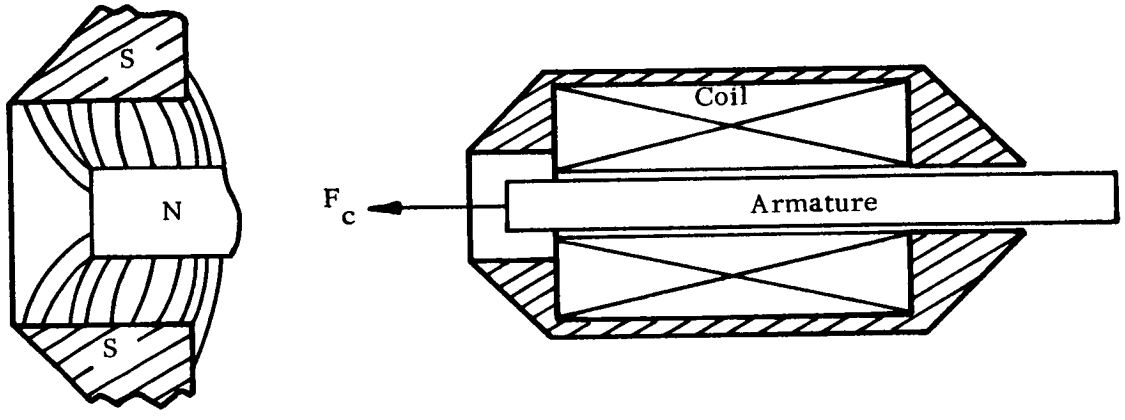

FIGURE H5 BASIC ELECTROMAGNET CONFIGURATION

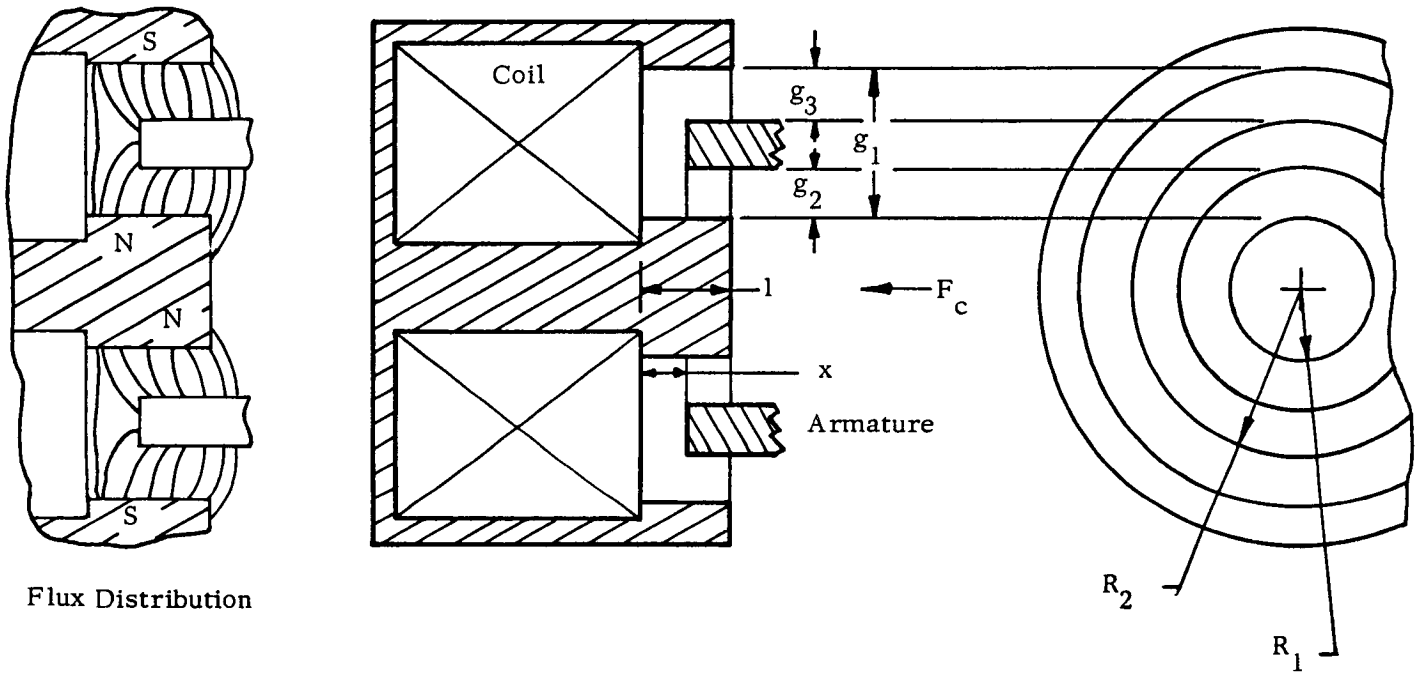

FIGURE H6 COAXIAL ELECTROMAGNET CONFIGURATION

1. Analysis

Using the notation of Figure H-6 the equations for force produced by the electromagnet can be developed. The analysis which follows neglects fringing of the magnetic field at the poles. To keep fringing from affecting the force produced by the magnet, the armature must always be inside the poles and should not approach the open end. It is also assumed that the characteristics of the iron in the magnetic circuit will have little effect on the performance of the electromagnet.

This is usually valid because the permeability of unsaturated iron is so much greater than the permeability of air that the energy stored in the air gap is much greater than in the iron.

The force exerted by a magnet is such that the energy stored in the magnetic field will tend to be reduced. Using the notation of Figure H-4

$$F_c = \frac{dW}{dx} \tag{21}$$

where W is the energy in the magnetic field

$$W = 1/2\, \mathcal{F} \phi \tag{22}$$

$\mathcal{F}$ = mmf (ampere turns)

ϕ = magnetic flux (webers)

To find the force exerted by a magnet, evaluate Equation (22) and then differentiate with respect to x. Since the permeability of iron is very high compared to air, it is only necessary to calculate the energy stored in the air gap. The total energy stored in the air gap (neglecting fringing) is the sum of the energies stored in gaps g_1, g_2, and g_3. Thus

$$W = W_1 + W_2 + W_3 \tag{23}$$

W_1 = energy in air gap g_1

W_2 = energy in air gap g_2

W_3 = energy in air gap g_3

By applying Kirchoff's laws for magnetic circuits and neglecting mmf drops in iron, the following relations are obtained

$$\mathcal{J}_1 = \mathcal{J}_2 + \mathcal{J}_3 = \mathcal{J} \tag{24}$$

$$\phi_2 = \phi_3 \tag{25}$$

$$\phi = \phi_1 + \phi_2 \tag{26}$$

Applying Equations (22), (24), (25), and (26) to Equation (23), an expression for total energy is obtained.

$$W = \frac{1}{2}\left[\mathcal{J}\phi_1 + (\mathcal{J}_2 + \mathcal{J}_3)\ \phi_2\right] \tag{27}$$

All three air gaps are of similar geometric construction differing only in size so one basic formula suffices for energy calculations. The energy stored in the air gap between cylindrical poles may be calculated as follows:

$$\mathcal{J} = \int_R^{R+g} H(r)\, dr \tag{28}$$

R = radius of inner pole (in)

g = length of air gap (in)

$H(r)$ = magnetic intensity $\frac{\text{ampere turns}}{\text{in.}}$ at radius r.

$B(r) = \frac{\phi}{2\pi r y}$

$B(r)$ = flux density $\frac{\text{webers}}{\text{in}^2}$ at radius r

y = width of poles (in)

$H(r) = \frac{B(r)}{\mu_o}$

μ_o = permeability of air gap

$$\mathcal{J} = \int_R^{R+g} \frac{\phi}{2\pi \mu_o y} \frac{dr}{r}$$

$$= \frac{\phi}{2\pi \mu_o y} \log_e \left(1 + \frac{g}{R}\right) \tag{29}$$

When the gap length, g, is small compared with R, Equation (29) can be approximated by Equation (30)

$$\mathcal{J} = \frac{\phi}{2\pi \mu_o y} \frac{g}{R + \frac{g}{2}}, g << R \tag{30}$$

Using Equation (29), the energy in air gap g_1 is calculated as

$$W_1 = \frac{1}{2} \mathcal{J} \phi_1$$

$$W_1 = \frac{\pi \mu_o \mathcal{J}_x^2}{\log_e \left(1 + \frac{g_1}{R_1}\right)} \tag{31}$$

The air gaps g_2 and g_3 are smaller than R_1 and R_2 respectively, so Equation (30) may be used.

$$\mathcal{J}_2 = \frac{\phi_2 g_2}{2\pi\mu_o (l - x)(R_1 + \frac{g_2}{2})} \tag{32}$$

$$\mathcal{J}_3 = \frac{\phi_2 g_3}{2\pi\mu_o (l - x)(R_2 + \frac{g_3}{2})} \tag{33}$$

$$\mathcal{J}_2 + \mathcal{J}_3 = \mathcal{J} = \frac{\phi_2}{2\pi\mu_o (l - x)}\left[\frac{g_2}{(R_1 + \frac{g_2}{2})} + \frac{g_3}{(R_2 + \frac{g_3}{2})}\right] \tag{34}$$

$$\phi_2 = \frac{2\pi\mu_o \mathcal{J}(l - x)}{\frac{g_2}{R_1 + \frac{g_2}{2}} + \frac{g_3}{R_2 + \frac{g_3}{2}}} \tag{35}$$

$$\frac{1}{2}(\mathcal{J}_2 + \mathcal{J}_3)\phi_2 = \frac{\pi\mu_o \mathcal{J}^2 (l - x)}{\frac{g_2}{R_1 + \frac{g_2}{2}} + \frac{g_3}{R_2 + \frac{g_3}{2}}} \tag{36}$$

Combining the energies stored in the individual air gaps, the total energy is obtained.

$$W = \pi\mu_o \mathcal{J}^2 \left[\frac{x}{\log_e\left(1 + \frac{g_1}{R_1}\right)} + \frac{(l - x)}{\frac{g_2}{R_1 + \frac{g_2}{2}} + \frac{g_3}{R_2 + \frac{g_3}{2}}}\right] \tag{37}$$

To obtain the force exerted by the magnet differentiate (37) with respect to x.

$$F_c = \frac{dW}{dx} = \pi \mu_o \mathcal{J}^2 \left[\frac{1}{\log_e \left(1 + \frac{g_1}{R_1}\right)} - \frac{1}{\frac{g_2}{R_1 + \frac{g_2}{2}} + \frac{g_3}{R_2 + \frac{g_3}{2}}} \right] \tag{38}$$

Equation (38) shows that the force exerted by the magnet is proportional to the square of the magnetomotive force across the air gap and independent of armature position. Because the permeability of iron is very high compared with the air gap, the mmf across the air gap is substantially the magnetomotive force developed by the magnet winding. That is

$$\mathcal{J} = N I_c \tag{39}$$

2. Force Motor Design

Using Equation (38), a design for the magnetic force motor can be calculated. The major characteristics of the design are summarized in Table H-II and Figure H-7. The requirements for the force motor are as follows:

Maximum Force : 2 lbs

Maximum Stroke : 0.25 in.

Force constant over full stroke

Current Required for Maximum Force

: 10 ma.

The permeability of air is

TABLE H-II

MAJOR CHARACTERISTICS OF FORCE MOTOR

Maximum Force:	2 lbs.
Maximum Input Current:	10 ma.
Winding Resistance at 20°C:	2270 ohms
Residual Force after Removal of Maximum Input Current:	approx. 0.00729 lbs.
Approximate Weight:	4.9 lbs.

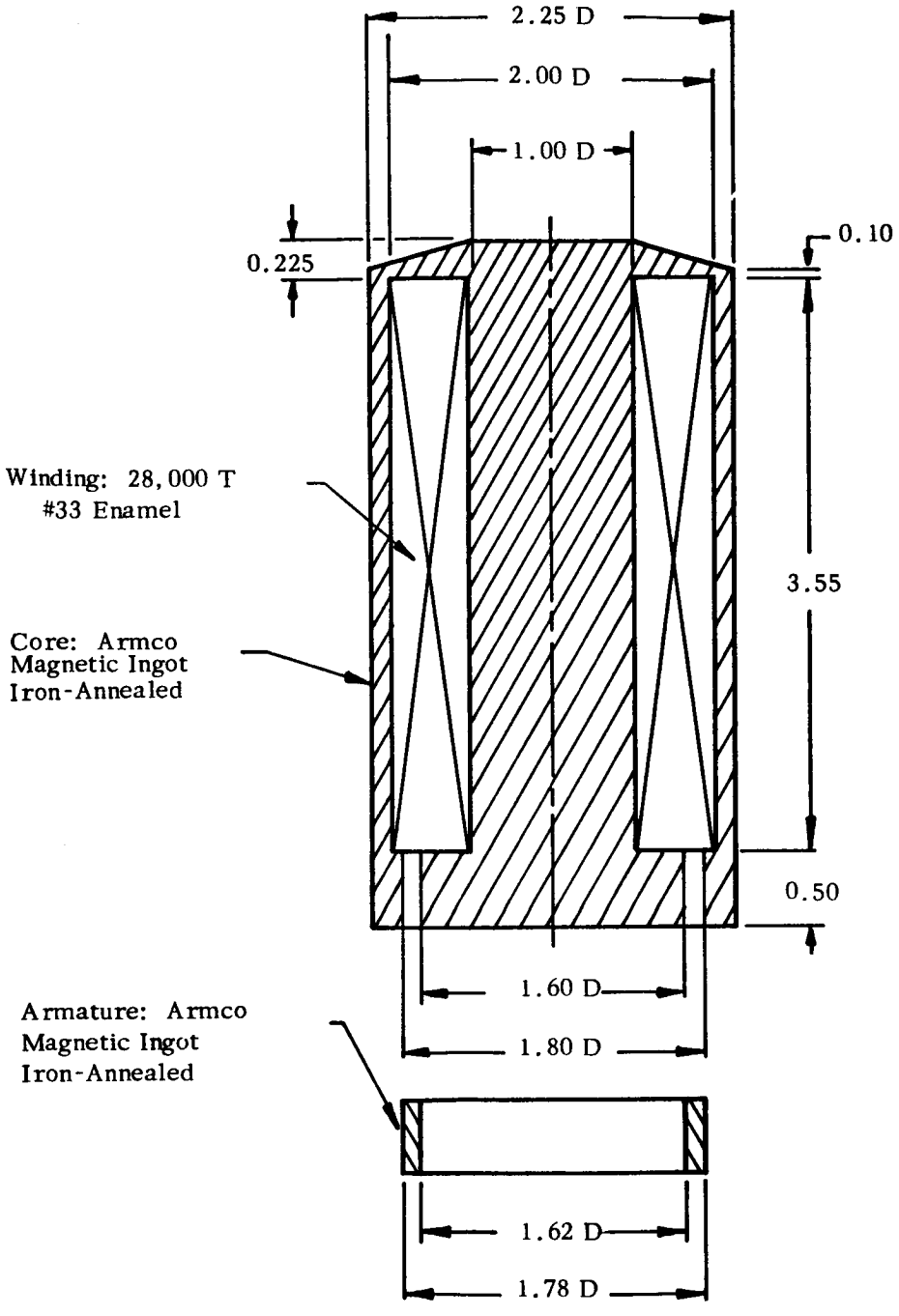

FIGURE H7 ELECTROMAGNET FORCE MOTOR

$$\mu_o = 4\pi \times 10^{-7} \frac{\text{weber}}{\text{amp. turn meter}}$$

$$= 2.83 \times 10^{-7} \frac{\text{lb.}}{\text{amp.}^2 \text{ turn}^2}$$

The force developed by the magnet is a function of the pole dimensions chosen. From several trial designs the following air gap dimensions were selected as being nearly optimal:

$R_1 = 0.80$ in.

$g_1 = 0.10$ in.

$g_2 = 0.01$ in.

$g_3 = 0.01$ in.

$R_2 = 0.89$ in.

$\mathcal{F} = 256$ ampere turns.

The dimensions of the iron parts of the magnetic circuit are determined primarily by the maximum allowable flux density in the iron. The maximum flux density is determined by requiring operation in a relatively linear portion of the B-H curve.

The material chosen for the magnetic circuit is Armco Magnetic Ingot Iron annealed at 1700°F. The maximum allowable flux density for the iron parts is set at

$$B_{max} = 1 \frac{\text{weber}}{\text{meter}^2} = 6.55 \times 10^{-4} \frac{\text{weber}}{\text{in}^2}$$

The total flux flowing in the magnetic circuit is

$$\phi = \frac{2W}{\mathcal{J}_1} = \pi\mu_o \left[\frac{1}{\log_e \left(1 + \frac{g_1}{R_1}\right)} - \frac{1}{\frac{g_2}{R_1 + \frac{g_2}{2}} + \frac{g_3}{R_2 + \frac{g_3}{2}}} \times \right.$$

$$\left. + \frac{\ell}{\frac{g_2}{R + \frac{g_2}{2}} + \frac{g_3}{R_2 + \frac{g_3}{2}}} \right] \mathcal{J}_1 \qquad (40)$$

Because x is constrained by fringing considerations to no less than about 0.25ℓ, the maximum flux for this design will be

$$\phi_m = 8.82 \times 10^{-4} \ell \text{ webers}$$

The value ϕ_m is useful for determining the cross-section areas of most portions of the magnetic structure where the flux density is fairly uniform. However, in the vicinity of the poles flux densities may become quite high in some locations. First compute the flux density at the surface of the inner pole piece included in the region $(\ell - x)$.

$$B_{(\ell - x)} = \frac{\phi_{(\ell - x)}}{A_{(\ell - x)}} = \frac{\mu_o \mathcal{J}_1}{\left(\frac{g_2}{R_1 + \frac{g_2}{2}} + \frac{g_3}{R_2 + \frac{g_3}{3}}\right) R_1} \qquad (41)$$

$$= 2.18 \times 10^{-4} \frac{\text{webers}}{\text{in}^2}$$

The value of $B_{(\ell - x)}$ is less than the maximum allowable value, so the value of R_1 chosen will not cause saturation of that portion of the pole

piece. Radius R_1 is the radius at which the greatest flux density will occur.

Because $B_{(\ell - x)}$ is independent of x the value of ℓ can be chosen to make fringing very small. It was specified that the maximum stroke must be

$$x_{max} - x_{min} = 0.25 \text{ in}$$

x_{max} and x_{min} are chosen from fringing considerations to be

$$x_{max} = 0.75\,\ell$$

$$x_{min} = 0.25\,\ell$$

$$x_{max} - x_{min} = 0.50\,\ell$$

$$\ell = 0.50 \text{ in} \tag{42}$$

From this, the maximum total flux in the magnetic circuit will be

$$\phi_m = 4.41 \times 10^{-4} \text{ webers} \tag{43}$$

From the maximum flux and maximum allowable flux density, the minimum area for any iron part with a fairly uniform flux distribution can be calculated.

$$A_m = \frac{\phi_m}{B_{max}} = \frac{4.41 \times 10^{-4}}{6.65 \times 10^{-4}} = 0.673 \text{ in}^2 \tag{44}$$

All magnetic parts must have a cross-sectional area perpendicular to the flux path which is greater than A_m for good operation. This is the criterion used for sizing the parts of the magnetic circuit. The over-all length of the electromagnet is determined by the space required for the winding. The number of ampere turns required across the air gap is

$$\mathcal{F} = 256 \text{ amper turns.} \tag{45}$$

To take care of leakage flux fringing and the reluctance of the iron portion of the magnetic circuit add ten percent to $\mathcal{F}$ making

$$NI_c = 280 \text{ ampere turns.} \tag{46}$$

The value of I_c to achieve $\mathcal{F}$ was specified as 10 ma. so

$$N = 28{,}000 \text{ turns.} \tag{47}$$

The mean turn length obtained by finding the average circumference of the winding space is

$$L_{AV} = 4.71 \text{ in.} \tag{48}$$

If 250 milliwatts dissipation in the coil is allowed, the coil resistance is

$$R_c = \frac{P}{I^2} = \frac{2.5 \times 10^{-1}}{10^{-4}} = 2500 \text{ ohms.} \tag{49}$$

The total length of wire in a winding is

$$NL_{AV} = 2.8 \times 10^4 \times 4.71 = 1.32 \times 10^5 \text{ in.} \tag{50}$$

The resistance per unit length of wire to be used is

$$\rho = \frac{R_c}{NL_{AV}} = 1.89 \times 10^{-2} \text{ ohms/in.} \tag{51}$$

From a wire table #33 copper wire at $20^{\circ}C$ has a resistance of 17.24 ohms/1000 in. Using #33 copper wire, the coil resistance is about

$$R_c = 2270 \text{ ohms} \tag{52}$$

and the power dissipated in the coil at full current is

$$P = 227 \text{ mw.} \tag{53}$$

The winding space required by #33 enamel wire can be calculated from the turns density which is taken from a table (Reference 1, p. 172) as

$$N_s = 17{,}000 \frac{\text{turns}}{\text{in}^2} \tag{54}$$

N_s includes a winding space factor.

The winding cross-sectional area required for 28,000 turns is

$$A_W = \frac{N}{N_s} = 1.65 \text{ in}^2 \tag{55}$$

The length of winding space required for the coil can be calculated from the required winding cross section and winding thickness to be 3.3 inches. Add 0.25 in. for insulation at the ends of the winding.

The total coil length is then

$$L_c = 3.55 \text{ in.} \tag{56}$$

Figure H-7 is a sectional view of the electromagnet which shows the major dimensions based on the design criteria discussed above.

Using the dimensions of Figure H-7, the approximate weight of the magnet can be computed. The density of iron is 0.28 lb/in^3. The density of copper is 0.32 lb/in^3. The total weight of the magnet is computed to be 4.9 lbs. The total weight of the armature is 0.054 lb.

The hysteresis properties of magnetic materials result in a residual flux remaining in the material after the exciting mmf has been removed. This residual flux produces a force on the armature after the control current is turned off. The size of this residual force must be calculated.

To calculate the value of the residual force, the iron and air gap are considered as a magnetic circuit in which the mmf giving rise to the residual flux in the iron is balanced by the mmf drop in the air gap due to the residual flux in the air gap. From the mmf in the air gap, the residual force can be calculated. The determination of residual mmf in the air gap is best done graphically by plotting the total flux versus total mmf in the iron and the total flux versus mmf in the air gap. The intersection of the two curves gives the residual mmf and flux in the air gap.

Using the hysteresis of Armco Magnetic Ingot Iron for a peak induction of 1 weber/m^2, the demagnetization curve for the magnetic circuit of Figure H-7 is plotted in Figure H-8. The following average values for the geometry were used.

Mean Magnetic Path Length : 9.61 in.

Mean Cross-sectional Area : 0.743 in^2.

Maximum Air Gap Permeance : 1.71×10^{-6} $\frac{\text{webers}}{\text{ampere turn}}$

From the intersection of the demagnetization curves for the air gap and iron, the following residual quantities are obtained:

$$\phi_r = 0.26 \times 10^{-4} \text{ webers}$$

$$\mathcal{F}_r = 15.6 \text{ ampere turns}$$

The values of $\mathcal{F}_r$ and ϕ_r are maximum for any allowable position of the armature, and so reflect the worst case.

Evaluating Equation (38) for $\mathcal{F}_r$ the residual magnet force is obtained.

$$F_{cr} = 7.29 \times 10^{-3} \text{ lbs.}$$

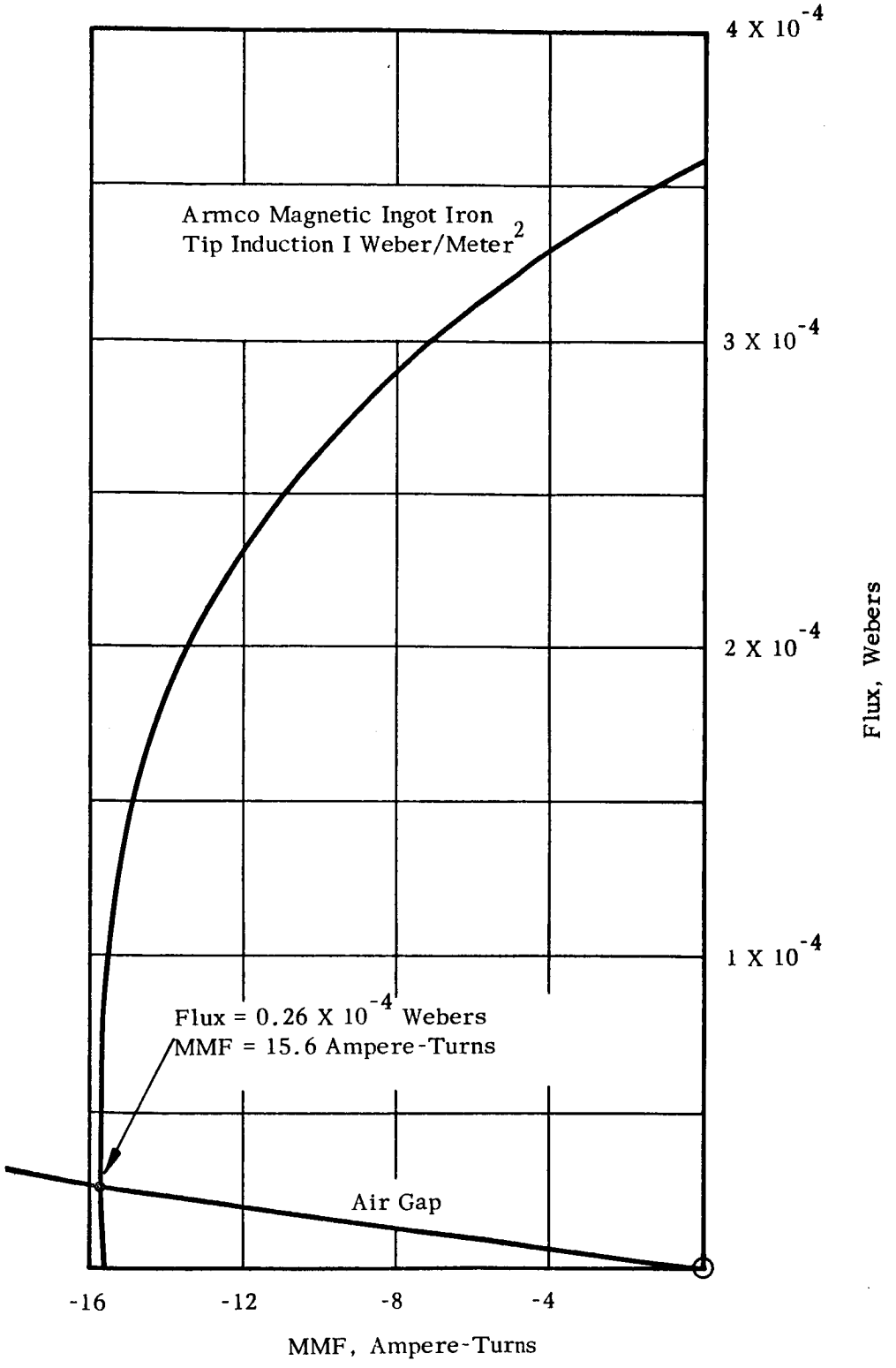

FIGURE H8 DEMAGNETIZATION CURVE FOR MAGNETIC CIRCUIT OF FIGURE H7

Though small, this residual force must be taken into consideration in the final design for the flow controller.

REFERENCES

H1. Roters, H. C., Electromagnetic Devices, John Wiley and Sons, New York, 1944.

H2. Shapiro, Ascher H., The Dynamics and Thermodynamics of Compressible Fluid Flow, Vol. 1, The Ronald Press Company, New York, 1954.

E-2498 NASA-Langley, 1964

ERRATA

NASA Contractor Report CR-60

CRYOGENIC PROPELLANT FEED SYSTEMS FOR
ELECTROTHERMAL ENGINES

Prepared by Arthur D. Little, Inc.
Cambridge, Massachusetts
May 1964

Pages 6 to 12 were incorrectly numbered and assembled. The following re-arrangement will provide the correct sequence:

Page 9 should be page 6
Page 6 should be page 12.

NASA-Langley, 1964

Issue date: 6-10-64